Study on Molecular Miscibility and Domain Formation in Adsorbed Monolayer and Lipid Bilayer

平城, 慎也

Study on Molecular Miscibility and Domain Formation in Adsorbed Monolayer and Lipid Bilayer

Shinya Hiraki

Laboratory of Soft Interface Chemistry

Department of Chemistry

Graduate School of Science

Kyushu University

Abstract

The nanoscopic domain called “raft” is expected to exist in a biological membrane. Despite of the fact that mesoscopic domains have been observed in the monolayer and bilayer composed of several lipids, the principle of domain formation with a various shape and size in a complicated matter is still unclear mainly because of a lack of data on structure and molecular miscibility in domains. Thus, in this study, we investigated the effect of molecular miscibility on domain formation in two binary adsorbed films at hexane/water interface on the basis of “line tension”, which arises the domain boundary and is dominant for domain morphology. The molecular miscibility such as composition and intermolecular interaction and molecular arrangement inside and outside of domains were quantitatively evaluated by coupling interfacial tensiometry and X-ray reflectometry (XR). The effect of molecular mixing on domain morphology was examined by Brewster angle microscopy (BAM).

In Chapter 2, *n*-tetradecyl phosphocholine (C14PC) and Cholesterol (Chol) mixed system was adopted as a simple model of biological membrane. The adsorbed film took four kinds of film states; gaseous (G), expanded (E), liquid condensed (LC), and condensed (C) ones, depending on the molality of C14PC in the aqueous and that of Chol in the hexane solutions. The phase diagram of adsorption, the activity coefficient in the film, and the electron density profile showed that the arrangement of C14PC molecules was changed from staggered to parallel as mixing of Chol with C14PC because the favorable interaction between C14PC and Chol overcomes the electrostatic repulsion between PC groups of C14PC. Furthermore, BAM observation demonstrated that the circular domain with E state was dispersed into the C film at just above the E – C phase transition point and that the domain size reduced with increasing the C14PC compositions

inside and outside of domains, suggesting that a correlation between molecular miscibility and line tension.

In Chapter 3, methyl palmitate (MePa) – Chol mixed system was adopted in order to examine the effect of molecular mixing on line tension in more detail. The adsorbed film exhibited the phase transitions from G to C at low and from G to C via E states at high Chol composition in the hexane solution. In each state, the film was very rich in Chol because of a loss of effective packing between hydrophobic parts competing with hydrogen bonding between their hydrophilic parts of MePa and Chol molecules. As well as the former system, the circular domain with the G (or E) state was confirmed in the C film at just above the G or E – C phase transition point by BAM and by domain fitting analysis of XR data. The domain size reduced with small decreasing the Chol compositions in domains. Judging from the calculated line tension value as well as the electron density profile and activity coefficient, MePa molecule adding into domains reduces the thickness mismatch between domains and adsorbs at the domain boundary, both of which promote the reduction of contact energy associated with the contact of C domain and surrounding hexane solvent, shrinking the total length of domain boundary.

The purpose in Chapter 4 is to measure the line tension in giant unilamellar vesicle (GUV). Adopting distearoyl phosphatidylcholine (DSPC)/dioleoyl phosphatidylcholine (DOPC)/Chol and brain sphingomyelin (bSM)/DOPC/Chol mixed systems, we observed the domain formation by fluorescence microscopy and measured the line tension at a different tie lines which connect the lipid compositions of coexisting domains by Fourier analysis on thermally fluctuating domain contour called flicker spectroscopy. The line tension reduced from 1.1 pN to 0.4 pN for DSPC- and from 0.8 pN to 0.44 pN for bSM-containing systems as tie line becomes closer to critical point. The line tension was further

calculated from the equation of elastic energy due to the lipid deformation around domain boundary, into which the published structural and elastic properties of domains were substituted. The theoretical value was much higher but depended on the lipid composition of GUVs, indicating that the molecular miscibility inside and outside of domains affect the line tension by changing molecular arrangement or elastic property even in lipid bilayer. In the perspective section, the appropriate method to measure the line tension in monolayer at the liquid/liquid interface was discussed.

Contents

Chapter 1. General Introduction

1-1. *General Introduction*

Studies on soft interfaces including molecular films at gas/liquid and liquid/liquid interfaces, emulsion, foam, and biological membrane provide us useful information on structure and property of them available for development of sophisticated materials in applied science as well as for understanding structure – function relation of living cells in basic science. One of the current issues in biochemistry and biophysics is heterogeneity of soft interfacial films which is closely related to high performance of biological membrane of eukaryotic cells.

In the end of 20th century, Simons and Ikonen have proposed "raft" hypothesis that the biological membrane is regarded as a heterogeneous bilayer in which nanoscopic liquid ordered domains are surrounded by fluid phase region and is responsible for the function of several membrane proteins and plays crucial role in signaling, membrane transferring, and virus infection[1–7]. Although many researchers have explored the role and principle of raft formation from the viewpoints of not only biology such as lipid metabolism and endocytosis but also physical chemistry such as phase separation in membrane, the nanoscopic domains in natural biological membrane has not been detected directly yet because of their extremely small size. In the study of model membrane using lipid vesicle of phospholipid (PL), cholesterol (Chol), and proteins, however, mesoscopic domain was found by a microscopic observation[8–11] and the morphology was examined in terms of lipid composition, membrane rigidity, and line tension at domain boundary.

According to the theories developed by McConnell *et al.*[12] and Kuzmin *et al.*[13], the line tension in monolayer is the sum of contact energy and dipole – dipole repulsive energy at the domain boundary. The former is due to the contact of hydrophobic part of

domain with the surrounding solvent and reduces the total length of the boundary, whereas the latter extends the domain boundary and promotes the formation of many tiny circular or stripe shaped domain. In the case of lipid bilayer (vesicle) dispersed in aqueous solution, because the contact of hydrocarbon chain with water causes the large contact energy, the relatively low energy of elastic deformation such as tilt, splay, and bend takes the place of the contact one (see Chapters 2 and 4 in detail, respectively).

Following the theories, attentions have been directed to an estimation of structural and mechanical properties of domains as well as to a development of the method to quantify line tension. In the researches on lipid monolayer and bilayer of PL – Chol mixture[14–21],the domain properties closely related line tension such as film thickness, molecular density, bending and tilt moduli, and spontaneous curvature were determined experimentally or estimated theoretically and found to be dependent on film composition, suggesting that the structure and property of heterogeneous film are affected appreciably by the mutual interaction between the molecules at the soft interfacial films[22–25]. Thus, disclosing the quantitative relation of molecular miscibility to structural and mechanical properties inside and outside of domains is one of key issues to elucidate the principle of domain formation with a diversity of morphology in the complicated molecular organized system such as biological membrane, from the viewpoint of line tension.

A main purpose in this thesis is to examine the effect of molecular mixing on domain formation form the viewpoint of physical chemistry. Thus, a study on the monolayer and bilayer of mixed component systems were adopted, and molecular miscibility and microscopic structure of the films as well as the domain formation were examined by coupling the thermodynamic strategy based on interfacial tensiometry with microscopic one on Synchrotron X-ray reflectometry (XR)[26,27]. Brewster angle microscopy (BAM)

was also adopted to visualize the domain morphology and to calculate the line tension[12].

In Chapter 2, we adopted binary single-chain PL (*n*-tetradecyl phosphocholine; C14PC) – Chol system as a simple model of biological membrane. It was confirmed that the adsorbed film of the pure Chol system was a heterogeneous in which dilute circular domains are dispersed into condensed phase region. Furthermore, a dilute domain size decreased as mixing of C14PC molecule inside and outside of domain due to hydrogen bonding and van der Waals interactions between C14PC and Chol, suggesting the influence of molecular mixing on line tension and domain size.

In Chapter 3, methyl palmitate (MePa) was used instead of C14PC. As well as the mixed C14PC – Chol system, a dilute domain size decreased with slight increase of MePa in the adsorbed film. In this case, it was suggested that MePa molecule is less miscible with Chol in domains because of the ineffective packing between hydrocarbon chain and sterol ring, whereas it adsorbs at the domain boundary due to the hydrogen bonding between methyl ester and hydroxyl groups and reduces the line tension, such as a surfactant adsorbs at the interface and reduces the interfacial tension[28].

In Chapter 4, line tensions was determined in lipid bilayers of two ternary mixtures; (i) distearoyl phosphatidylcholine (DSPC)/dioleoyl phosphatidylcholine (DOPC)/Chol and (ii) brain-sphingomyelin (bSM)/DOPC/Chol ones by flicker spectroscopy. This method is a shape analysis of thermal fluctuation of domain boundary by Fourier series[14,28–32]. The measured value was compared with that calculated from elastic theory into which the published structural, compositional, and mechanical values[16–19,29,33–35] were substituted. Then, it was verified that the molecular and domain structures are dominant for line tension Furthermore, we discussed on the appropriate method to measure the line tension in adsorbed film at soft interface including liquid/liquid one.

1-2. *References*

[1] R.M. Epand, *Biochim. Biophys. Acta - Biomembr.*, 1778, **2008**, 1576–1582.

[2] D.A. Brown, J.K. Rose, *Cell*, 68, **1992**, 533–544.

[3] M.J. Aman, K.S. Ravichandran, *Curr. Biol.*, 10, **2000**, 393–396.

[4] K. Simons, E. Ikonen, *Nature*, 387, **1997**, 569–572.

[5] P. Gonnord, C.M. Blouin, C. Lamaze, *Semin. Cell Dev. Biol.*, 23, **2012**, 154–164

[6] S. Mañes, E. Mira, C. Gómez-Moutón, R.A. Lacalle, P. Keller, J.P. Labrador, C. Martínez-A, *EMBO J.*, 18, **1999**, 6211–6220.

[7] P. Scheiffele, A. Rietveld, T. Wilk, K. Simons, *J. Biol. Chem.*, 274, **1999**, 2038–2044..

[8] H.M. McConnell, *Annu. Rev. Biophys. Biomol. Struct.*, 32, **2003**, 469–492.

[9] G.W. Feigenson, *Biochim. Biophys. Acta - Biomembr.*, 1788, **2009**, 47–52.

[10] G.W. Feigenson, *Nat. Chem. Biol.*, 2, **2006**, 560–563.

[11] E. London, *Biochim. Biophys. Acta*, 1746, **2005**, 203–220.

[12] H.M. McConnell, V.T. Moy, *J. Phys. Chem.*, 92, **1988**, 4520–4525.

[13] P.I. Kuzmin, S.A. Akimov, Y.A. Chizmadzhev, J. Zimmerberg, F.S. Cohen, *Biophys. J.*, 88, **2005**, 1120–1133.

[14] S.L. Keller, A.R. Honerkamp-Smith, P. Cicuta, M.D. Collins, S.L. Veatch, M. den Nijs, M. Schick, *Biophys. J.*, 95, **2008**, 236–246.

[15] G. Pabst, N. Kučerka, M.P. Nieh, M.C. Rheinstädter, J. Katsaras, *Chem. Phys. Lipids*, 163, **2010**, 460–479.

[16] G. Khelashvili, B. Kollmitzer, P. Heftberger, G. Pabst, D. Harries, *J. Chem. Theory Comput.*, 9, **2013**, 3866–3871.

[17] F.A. Heberle, R.S. Petruzielo, J. Pan, P. Drazba, N. Kuc, *J. Am. Chem. Soc.*, 135,

2013, 6853–6859.

[18] B. Kollmitzer, P. Heftberger, M. Rappolt, G. Pabst, *Soft Matter*, 9, **2013**, 10877–10884.

[19] P. Heftberger, B. Kollmitzer, A.A. Rieder, H. Amenitsch, G. Pabst, *Biophys. J.*, 108, **2015**, 854–862.

[20] J. V. Bleecker, P.A. Cox, S.L. Keller, *Biophys. J.*, 110, **2016**, 2305–2308.

[21] W.C. Tsai, G.W. Feigenson, *Biochim. Biophys. Acta - Biomembr.*, 1861, **2019**, 478–485.

[22] B.P. Binks, MODERN ASPECTS OF EMULSION SCIENCE, Royal Society of Chemistry, CambridgeLondon, **1998**.

[23] T. Takiue, T. Fukuda, D. Murakami, H. Sakamoto, H. Matsubara, M. Aratono, *J. Phys. Chem. B*, 113, **2009**, 14667–14673.

[24] J.N. Israelachvili, Intermolecular and Surface Forces, 3rd ed., Academic Press, **2011**.

[25] S. Hiraki, T. Goto, H. Tanida, K. Nitta, T. Ina, T. Uruga, H. Matsubara, M. Aratono, T. Takiue, *Colloids Surfaces A Physicochem. Eng. Asp.*, 482, **2015**, 454–463.

[26] R. Fukuhara, H. Tanida, K. Nitta, T. Ina, T. Uruga, H. Matsubara, M. Aratono, T. Takiue, *J. Phys. Chem. B*, 118, **2014**, 12451–12461.

[27] S. V. Pingali, T. Takiue, G. Luo, A.M. Tikhonov, N. Ikeda, M. Aratono, M.L. Schlossman, *J. Phys. Chem. B*, 109, **2005**, 1210–1225.

[28] I. Sriram, D.K. Schwartz, *Surf. Sci. Rep.*, 67, **2012**, 143–159.

[29] R.D. Usery, T.A. Enoki, S.P. Wickramasinghe, M.D. Weiner, W.C. Tsai, M.B. Kim, S. Wang, T.L. Torng, D.G. Ackerman, F.A. Heberle, J. Katsaras, G.W. Feigenson, *Biophys. J.*, 112, **2017**, 1431–1443.

[30] B.L. Stottrup, A.M. Heussler, T.A. Bibelnieks, *J. Phys. Chem. B*, **2007**, 11091–11094.

[31] C. Esposito, A. Tian, S. Melamed, C. Johnson, S.Y. Tee, T. Baumgart, *Biophys. J.*, 93, **2007**, 3169–3181.

[32] M.C. Heinrich, I. Levental, H. Gelman, P.A. Janmey, T. Baumgart, *J. Phys. Chem. B*, 112, **2008**, 8063–8068.

[33] J. Lipfert, L. Columbus, V.B. Chu, S.A. Lesley, S. Doniach, *J. Phys. Chem. B*, 111, **2007**, 12427–12438.

[34] T.M. Konyakhina, J. Wu, J.D. Mastroianni, F.A. Heberle, G.W. Feigenson, *Biochim. Biophys. Acta - Biomembr.*, 1828, **2013**, 2204–2214.

[35] R.S. Petruzielo, F.A. Heberle, P. Drazba, J. Katsaras, G.W. Feigenson, *Biochim. Biophys. Acta - Biomembr.*, 1828, **2013**, 1302–1313.

Chapter 2. Molecular Miscibility and Domain Formation in Adsorbed Film of C14PC – Chol Mixture at C6/W Interface

2-1. *Introduction*

Soft interfacial films of surface active such as gas/liquid and liquid/liquid interfaces are strongly affected not only by the structure of the molecules but also by the mutual interaction between adsorbed molecules[1–10], and regarded as a basic structure of more complicated soft matters such as emulsion, foam film, and biological membrane. The investigation of the structure and property of them, therefore, is crucial to clearly understand the structure – function relation of molecular organized systems[11–17].

Since Simons *et al.* have proposed the heterogeneity of biological membrane[18], a lot of efforts have been paid to ascertain the formation of a heterogeneous structure in model membranes composed of phospholipid (PL) and cholesterol (Chol) from both microscopic and macroscopic viewpoints[19–24]. Among others, direct observation of insoluble monolayer and liposome (bilayer) of PL and Chol mixtures by optical method using Brewster angle microscope (BAM) and fluorescence microscope (FM) clearly indicated that the lateral phase separation, in which Chol-rich liquid ordered (Lo) domain with μm order is formed in Chol-poor liquid disordered (Ld) region, takes place depending on the composition of Chol in the mixture[25–29]. The application of Förster resonance energy transfer (FRET) and small angle neutron scattering (SANS) to the lipid liposome enables us to detect Lo domains with tens of nm[27,28,30–34]. In the theoretical studies by McConnell[35] and Kuzmin[36], furthermore, the effect of line tension, which is an excess energy generated on the domain boundary, on the domain morphology has been discussed from the viewpoint of the contact of domain forming molecules and solvent, the dipole – dipole interaction, and the tilt and spray of molecules at the domain boundary.

In our previous study on the adsorbed film of 1H,1H,2H,2H-perfluorodecanol (FC10OH) at the hexane (C6)/water (W) interface by interfacial tensiometry and X-ray reflectometry (XR)[37], it was found that the adsorbed FC10OH film shows an expanded – condensed phase transition detected by a break on the interfacial tension versus concentration and temperature curves, and that the expanded film is heterogeneous structure in which condensed domains with μm order are surrounded by low density gaseous region. The contact of FC10OH with hexane at the domain boundary produces line tension with a few pN (10^{-12} N) orders[38]. Another recent study on the adsorbed film of 1H,1H,10H,10H-perfluorodecane-1,10-diol (FC10diol) and FC10OH mixture[39] demonstrated the appearance of the heterogeneous condensed film where the normal-oriented condensed domain of FC10OH coexists with the parallel-oriented condensed phase of FC10diol, due to the weaker interaction between different molecules than between the same ones. The coverage of domains resulted from XR is consistent with that estimated from film composition evaluated by interfacial tensiometry, indicating that the high reliability for our strategy of quantitative evaluation of molecular miscibility in the adsorbed film by the two techniques.

One of the current issues to be solved on the heterogeneous film in the mixed system is to understand the effect of molecular miscibility on the domain formation because many soft matters including biological membrane generally consists of several components and therefore their structure and property should be closely related to the mixing of molecules both in domain and surrounding phase. However, because of few methods to determine their compositions, a quantitative discussion on the driving force of domain formation as well as the effect of line tension on the domain formation is still unclear.

In this study, we aim at clarifying the effect of molecular mixing on the domain

formation in the adsorbed film of PL and Chol mixture as a simple model for biological membrane. For doing this, we employed the adsorbed film of water soluble single chain PL: *n*-tetradecyl phosphocholine (C14PC) and oil soluble Chol mixture at the C6/W interface, because our thermodynamic strategy for evaluating the film composition, especially those of coexisting two interfacial states, can be applicable to the adsorbed film in order to estimate the compositions of domain and surrounding phase by coupling with the domain coverage determined by BAM images of heterogeneous film. Furthermore, to understand the effect of line tension on the domain formation with the help of these valuable data, the adsorbed film at the C6/W interface was directly observed by BAM. This study is a challenge to estimate quantitatively the compositions of coexisting domains and to elucidate the connection between molecular miscibility – domain formation – line tension by the combination of interfacial tensiometry, XR, and BAM. The interfacial tension γ of the hexane Chol solution against aqueous C14PC one was measured as functions of molality of C14PC and that of Chol at $298.15\,\mathrm{K}$ under atmospheric pressure. The phase diagram of adsorption was constructed and the activity coefficient of a component in an adsorbed film was evaluated in order to examine the molecular miscibility in the adsorbed film from the viewpoint of intermolecular interaction between adsorbed molecules. X-ray reflectivity from the adsorbed film was analyzed to determine the electron density profile normal to the interface in the homogeneous film as well as the domain coverage in the heterogeneous one. The heterogeneity of adsorbed film was also observed by BAM to evaluate the coverage, size and shape of domains.

2-2. *Experimental*

Materials

n-Tetradecyl phosphocholine (C14PC) purchased from Avanti polar Lipid Inc. ($>$ 99 %) was used without further purification. Purity was confirmed by an equilibrium interfacial tension value at the C6/aqueous solution interface. Cholesterol (Chol) purchased from Aldrich Chemical Co. Ltd. ($>$ 99 %) was purified by recrystallization at least twice from ethanol. Purity was checked by gas-liquid chromatography and by the equilibrium interfacial tension value between hexane solution and water phases. Hexane ($99+$ % grade, Aldrich Chemical Co. Ltd.) was distilled once under atmospheric pressure and water was purified by Millipore Milli-Q system.

Interfacial Tensiometry

The interfacial tension γ at the C6/W interface was measured as a function of molality of C14PC in aqueous solution $m_{\mathrm{PC}}^{\mathrm{w}}$ and that of Chol in the hexane solution $m_{\mathrm{Ch}}^{\mathrm{o}}$ at $298.15\ \mathrm{K}$ under atmospheric pressure by the pendant drop method demonstrated in Figure 2-1[40]. Before measurements, both solutions at given $m_{\mathrm{PC}}^{\mathrm{w}}$ and $m_{\mathrm{Ch}}^{\mathrm{o}}$ were mixed in a volumetric flask at $298.15\ \mathrm{K}$ and then allowed to stand for at least 24 hours to separate two transparent phases. For the calculation of an interfacial tension, densities of pure hexane and water were used instead of those of hexane and aqueous solutions at equilibrium, because both solutions are dilute and their mutual solubility was negligibly small. The experimental error of γ value was estimated within $\pm 0.05\ \mathrm{mN\ m^{-1}}$.

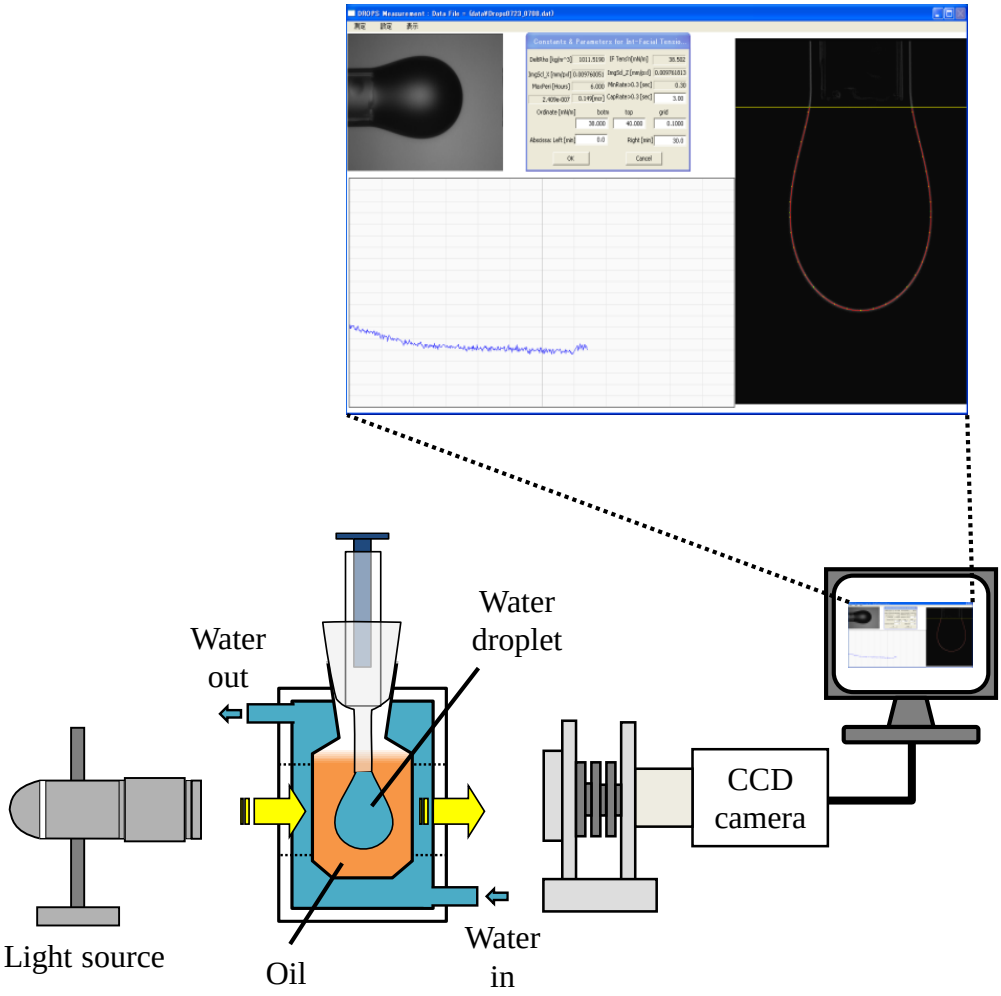

Figure 2-1. A schematic of the equipment for the pendant drop method.

Thermodynamics of Adsorption

Here let us briefly introduce thermodynamic relations used in this study. A total differential of interfacial tension γ is expressed as functions of temperature T, pressure p, $m_{\mathrm{PC}}^{\mathrm{w}}$, and $m_{\mathrm{Ch}}^{\mathrm{o}}$ by[41,42]

$$\mathrm{d}\gamma = -\Delta s \mathrm{d}T + \Delta v \mathrm{d}p - \Gamma_{\mathrm{PC}}^{\mathrm{H}} \left(\frac{RT}{m_{\mathrm{PC}}^{\mathrm{w}}} \right) \mathrm{d}m_{\mathrm{PC}}^{\mathrm{w}} - \Gamma_{\mathrm{Ch}}^{\mathrm{H}} \left(\frac{RT}{m_{\mathrm{Ch}}^{\mathrm{o}}} \right) \mathrm{d}m_{\mathrm{Ch}}^{\mathrm{o}} \ , \qquad (2-1)$$

where Γ_i^{H} $(i = \mathrm{PC}, \mathrm{Ch})$ is the interfacial density of component i and Δy $(\Delta y = s, v)$ is thermodynamic quantity change associated with an adsorption of C14PC and Chol respectively from the aqueous and hexane solutions to the C6/W interface defined by

$$\Delta y = y^{\mathrm{H}} - \Gamma_{\mathrm{PC}}^{\mathrm{H}} y_{\mathrm{PC}}^{\mathrm{w}} - \Gamma_{\mathrm{Ch}}^{\mathrm{H}} y_{\mathrm{Ch}}^{\mathrm{o}} \ . \qquad (2-2)$$

The $\Gamma_{\mathrm{PC}}^{\mathrm{H}}$ and $\Gamma_{\mathrm{Ch}}^{\mathrm{H}}$ values were calculated respectively by

$$\Gamma_{\mathrm{PC}}^{\mathrm{H}} = -\frac{m_{\mathrm{PC}}^{\mathrm{w}}}{RT} \left(\frac{\partial \gamma}{\partial m_{\mathrm{PC}}^{\mathrm{w}}} \right)_{T,p,m_{\mathrm{Ch}}^{\mathrm{o}}} \ , \qquad (2-3)$$

and

$$\Gamma_{\mathrm{Ch}}^{\mathrm{H}} = -\frac{m_{\mathrm{Ch}}^{\mathrm{o}}}{RT} \left(\frac{\partial \gamma}{\partial m_{\mathrm{Ch}}^{\mathrm{o}}} \right)_{T,p,m_{\mathrm{PC}}^{\mathrm{w}}} \ . \qquad (2-4)$$

Then, in order to assign a state of adsorbed film, interfacial pressure π versus mean area per molecules A curves were drawn by using

$$\pi = \gamma^0 - \gamma \ , \qquad (2-5)$$

and

$$A = 1/N_{\mathrm{A}} \Gamma^{\mathrm{H}} \ , \qquad (2-6)$$

where γ^0 is the interfacial tension between pure hexane and water, N_{A} is Avogadro's number, and Γ^{H} is the total interfacial density calculated by $\Gamma^{\mathrm{H}} = \Gamma_{\mathrm{PC}}^{\mathrm{H}} + \Gamma_{\mathrm{Ch}}^{\mathrm{H}}$.

The mixing of C14PC and Chol molecules in the adsorbed film was examined by evaluating the composition of Chol in the adsorbed film $X_{\mathrm{Ch}}^{\mathrm{H}}$ defined by

$$X_{\mathrm{Ch}}^{\mathrm{H}} = \Gamma_{\mathrm{Ch}}^{\mathrm{H}}/\Gamma^{\mathrm{H}} \ . \qquad (2-7)$$

A mutual interaction between C14PC and Chol molecules in the adsorbed film is further evaluated quantitatively by estimating an activity coefficient of component i in the adsorbed film at given γ, defined symmetrically as $f_i^{\mathrm{H}} \to 1$ when $X_i^{\mathrm{H}} \to 1$, by using[43]

$$X_i^{\mathrm{H}} f_i^{\mathrm{H}} = X_i m/m_i^0 \ , \qquad (2-8)$$

where m and X_i are respectively the total molality and the bulk composition of component i defined by

$$m = m_{\mathrm{PC}}^{\mathrm{w}} + m_{\mathrm{Ch}}^{\mathrm{o}} \ , \qquad (2-9)$$

and

$$X_i = m_i^{\alpha}/m \ , \qquad (i = \mathrm{PC}, \mathrm{Ch} \ , \ \alpha = \mathrm{w}, \mathrm{o}) \qquad (2-10)$$

respectively, and m_i^0 is the molality of pure component i at given γ.

X-ray Reflectometry

X-ray reflectivity from the adsorbed film at the C6/W interface was measured at the beamline BL37XU in SPring-8 by using liquid surface spectrometer schematically described in Figure 2-2[44]. The X-ray beam introduced into the experimental hutch is diffracted by a Ge(111) crystal in order to select the energy (25 keV) and adjust the incident angle of the beam. A slit placed in front of the sample cell determines the beam size; the slit gaps were 10 μm in vertical and 200 μm in horizontal. The footprint on the interface is around 2 cm along the beam path. A N_2 gas ion chamber put between the slit and the sample cell measures the incident X-ray flux. The intensity of reflected beam was detected by two-dimensional pixel detector (PILATUS) combined with a copper-aluminum absorber to reduce the X-ray photons to optimum amounts.

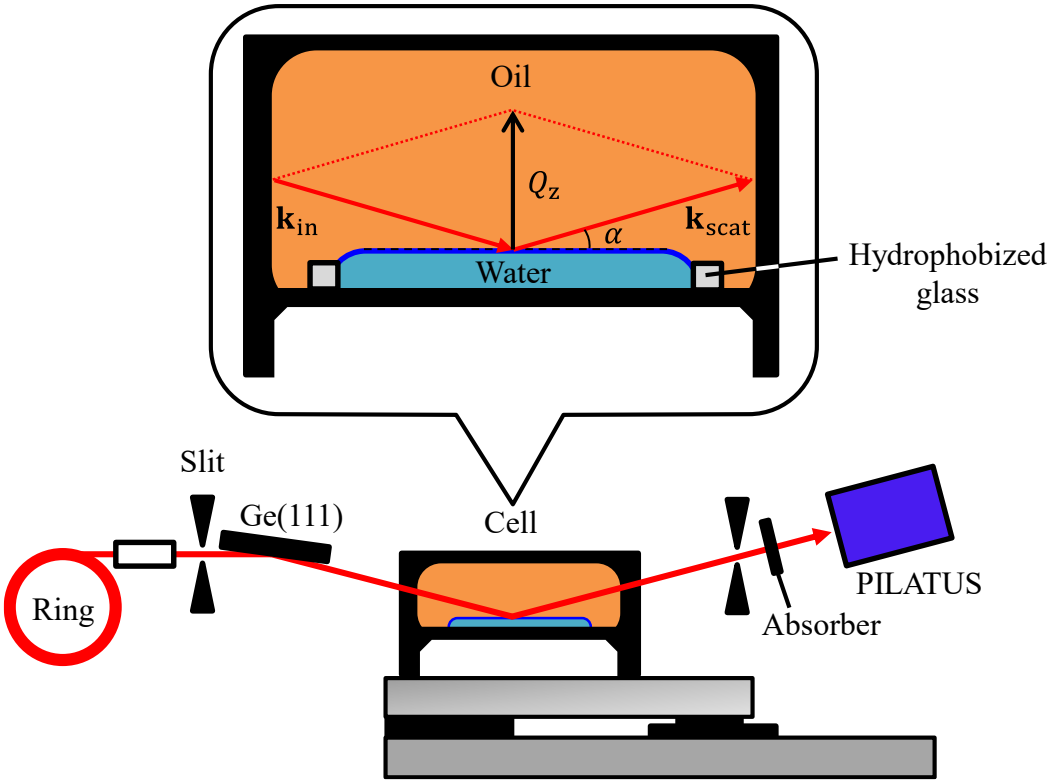

Figure 2-2. The schematic of the equipment for X-ray reflectivity measurement at BL 37 XU in SPring-8. The inset demonstrates kinetics of the reflectivity.

The sample cell is made of stainless steel and equipped with Mylar windows. In specular reflection condition, the scattering vector $\mathbf{Q} = \mathbf{k}_{\mathrm{scat}} - \mathbf{k}_{\mathrm{in}}$ is only in normal to the interface (z-direction) and given by $Q_{\mathrm{z}} = (4\pi/\lambda)\sin\alpha$, where $\lambda\ (= 0.496\ \text{Å})$ is the X-ray wavelength used in the present study, and α is the incident angle. The measurement was carried out at given $m_{\mathrm{PC}}^{\mathrm{w}}$ and $m_{\mathrm{Ch}}^{\mathrm{o}}$ under atmospheric pressure. Temperature was controlled at 298.15 ± 0.1 K by the Peltier device equipped to the cell.

X-ray reflectivity $R(Q_{\mathrm{z}})$ measured as a function of Q_{z} can be interpreted to yield the electron density profile normal to the interface. Under the first Born approximation, Q_{z} is given by[45,46]

$$\frac{R(Q_{\mathrm{z}})}{R_{\mathrm{F}}(Q_{\mathrm{z}})} \approx \left| \frac{1}{\rho_{\mathrm{w}} - \rho_{\mathrm{h}}} \int \frac{\mathrm{d}\langle\rho(z)\rangle}{\mathrm{d}z} \exp(-i\mathrm{Q}_{\mathrm{z}}z)\,\mathrm{d}z \right|^2 , \qquad (2-11)$$

where $\langle\rho(z)\rangle$ is the electron density profile averaged over the interfacial plane along with z-direction which is normal to the interface, ρ_{w} and ρ_{h} are respectively the electron densities of bulk water and hexane phases, and $R_{\mathrm{F}}(Q_{\mathrm{z}})$ is Fresnel reflectivity for an ideally smooth interface expressed as[46,47]

$$R_{\mathrm{F}}(Q_{\mathrm{z}}) \approx \left| \frac{Q_{\mathrm{z}} - Q_{\mathrm{z}}^{\mathrm{T}}}{Q_{\mathrm{z}} + Q_{\mathrm{z}}^{\mathrm{T}}} \right|^2 , \qquad (2-12)$$

where $Q_{\mathrm{z}}^{\mathrm{T}}$ is the z-component of the scattering vector with respect to the lower phase given by

$$Q_{\mathrm{z}}^{\mathrm{T}} = \sqrt{Q_{\mathrm{z}}^2 - Q_{\mathrm{c}}^2} , \qquad (2-13)$$

where the scattering vector at critical angle Q_{c} is calculated by using the difference of bulk densities $\Delta\rho\ (= \rho_{\mathrm{w}} - \rho_{\mathrm{h}})$ as $Q_{\mathrm{c}} \approx 4\sqrt{\pi\Delta\rho r_{\mathrm{e}}}$, where r_{e} is the classical electron radius $r_{\mathrm{e}} = 2.818$ fm.

The adsorbed films at the C6/W interface are modeled by n slabs. Interfaces at the top and bottom of each slab will be fluctuated with thermally exited capillary waves[48,49], which broaden the interface with an error function of interfacial roughness σ. Thus, the electron density for n-slab model is given by

$$\langle \rho(z) \rangle = \frac{1}{2}(\rho_{\mathrm{w}} + \rho_{\mathrm{h}}) + \frac{1}{2}\sum_{i=0}^{n}(\rho_i - \rho_{i+1})\,\mathrm{erf}\left(\frac{z + \sum_{j=0}^{i} L_j}{\sqrt{2}\rho}\right) \qquad (2-14)$$

with

$$\mathrm{erf}(z) = 2\sqrt{\pi}\int_0^z e^{-t^2}\,\mathrm{d}t\ , \qquad (2-15)$$

where ρ_i and L_i are the electron density and thickness of slab i, respectively.

The interfacial roughness σ is usually considered to be the combination of two different contributions; the intrinsic profile width σ_0 and the resolution dependent capillary wave contribution σ_{cap}. In this the hybrid model, σ_{cap} is expressed as

$$\sigma_{\mathrm{cap}}^2 \approx \frac{k_{\mathrm{B}}T}{2\pi\gamma}\left(\frac{q_{\max}}{q_{\min}}\right)\ , \qquad (2-16)$$

where γ is the interfacial tension at the C6/W interface, $k_{\mathrm{B}}T$ is the Boltzmann constant times temperature, $q_{\min} = (2\pi/\lambda)\Delta\beta\sin\alpha$ with the angular acceptance of the detector $\Delta\beta = 6.37 \times 10^{-4}$. $q_{\max}$ is determined by the cut off for the smallest wavelength of capillary waves that the interface can support and given by $q_{\max} = 2\pi/l$ Å^{-1}, where l is an approximate size of hexane molecule (~5 Å).

In the case of laterally heterogeneous interface consisting of the domain and surrounding phase, another analysis of $R(Q_{\mathrm{z}})$ can be applied. If the domain size is much smaller than the spatial coherent length of the X-ray in the plane of the interface the domain size, the X-ray reflected from the domain and surrounding phase interfere nearly

coherently. In this case, the amplitudes of reflected electromagnetic fields should be added, and then, the coherent X-ray reflectivity $R_{\mathrm{coh}}(Q_{\mathrm{z}})$ is given by[37]

$$R_{\mathrm{coh}}(Q_{\mathrm{z}}) = [C_{\mathrm{XR}} r_1(Q_{\mathrm{z}}) + (1 - C_{\mathrm{XR}}) r_2(Q_{\mathrm{z}})]^2 \qquad (2-17)$$

where $r_1(Q_{\mathrm{z}})$ and $r_2(Q_{\mathrm{z}})$ are the reflection amplitudes of the domain and surrounding phase respectively, and C_{XR} is the area coverage of domain 1 in the adsorbed film. On the other hand, if the domain size is much larger than the coherent length of X-ray, the interference between neighboring phases is incoherent. Then, incoherent reflectivity $R_{\mathrm{inc}}(Q_{\mathrm{z}})$ is provided by[37]

$$R_{\mathrm{inc}}(Q_{\mathrm{z}}) = C_{\mathrm{XR}} R_1(Q_{\mathrm{z}}) + (1 - C_{\mathrm{XR}}) R_2(Q_{\mathrm{z}}) \qquad (2-18)$$

where $R_1(Q_{\mathrm{z}})$ and $R_2(Q_{\mathrm{z}})$ are the X-ray reflectivity from the domain and surrounding phase, respectively.

Brewster Angle Microscopy

The observation of the adsorbed film at the C6/W interface was performed with using Brewster angle microscope (BAM), Nanofilm EP4 Imaging Ellipsometer (Acurrion, Goettingen, Germany) constructed by Xenon laser at 658 nm, polarizer, compensator, analyzer, and CCD camera, equipped with 10x 0.21 N.A. objective lens (Nikon, Japan). This setup fixed the pixel size to be $\sim 0.72\ \mu\mathrm{m}$. Both aqueous and hexane solutions were contained in the rectangular quartz glass cell purchased from Starna Scientific Ltd. (Hainault, UK). The cell was placed on a stage which align the cell windows to the beam path as shown in Figure 2-3. Temperature was controlled by circulating thermostated water in the jacket around the cell.

Polarizer, analyzer and compensator were respectively adjusted to be $10°$, $10°$, and $0°$ with $0.04 \sim 0.1$ sec. of exposure time, to acquire an image with enough contrast

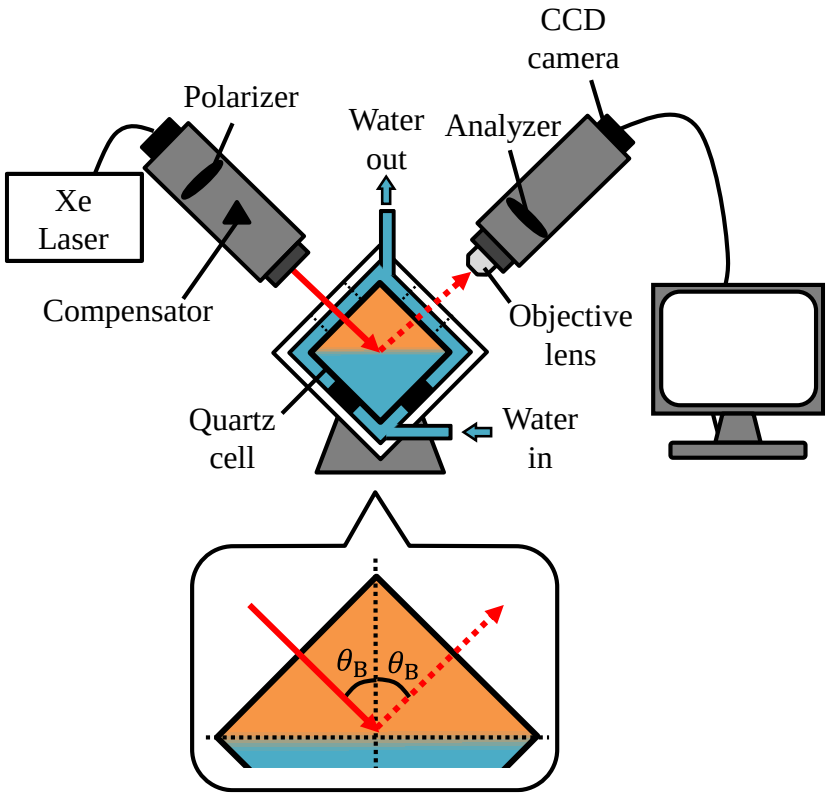

Figure 2-3. The schematic of the equipment of Brewster angle microscope and the optical setup in the inset.

between two coexisting domains. Brewster angle θ_B for pure C6/W interface at 298.15 K, at which no *p*-polarized light is reflected from the interface, was estimated to be $\theta_B = 44.2°$ by $\theta_B = \arctan(n_w/n_o)$, where n_w and n_o are respectively the refractive indexes of water and hexane[3,50,51]. Furthermore, in order to ensure equilibrium film state, thermal annealing was carried out before the observation; the cell was heated and cooled few times, and then was turned to 298.15 K over 1 hour. The contrast of the acquired image was enhanced by using Image J software[52].

Line Tension in Monolayer

In the heterogeneous film, the domain line tension is a crucial factor to determine domain morphology. According to theoretical study by McConnell *et al.*[53], an equilibrium domain size is governed by the line tension τ, which consists of two competitive effects; (i) a contact energy τ_0 associated with the contact of a domain with its surrounding phase, which shrinks the total length of domain boundary, and (ii) the dipole – dipole repulsion between neighboring molecules at domain boundary τ_{el}, which extends the length of domain boundary. The τ_0 value is roughly evaluated by[38]

$$\tau_0 \approx \gamma^{DS} \times \Delta L \ , \qquad (2-19)$$

where γ^{DS} is the interfacial tension between the domain and its surrounding phase and ΔL is contact length between coexisting phases. For nonpolar compounds, the γ^{DS} value is roughly estimated by using

$$\gamma^{DS} \approx \gamma_\alpha + \gamma_\beta - 2\sqrt{\gamma_\alpha \gamma_\beta} \ , \qquad (2-20)$$

where γ_α and γ_β are the surface tensions of component α and β. τ_{el} for an isolated circler domain with a radius R is expressed as[54]

$$\tau_{el} = \frac{u^2}{4\pi\varepsilon_0\varepsilon} \ln\left(\frac{e^2\Delta}{4R}\right) \ , \qquad (2-21)$$

where u is a difference of dipole densities perpendicular to the interface between two coexisting phase, ε_0 is permittivity in vacuum, ε is a relative permittivity of medium in which the dipole exists, and Δ is a cut-off distance between dipoles. Then, the equilibrium domain radius R_{eq} is given by[48,54];

$$R_{\mathrm{eq}} \approx 5\Delta \exp\left(\frac{4\pi\varepsilon_0\varepsilon\tau_0}{u^2}\right) . \qquad (2-22)$$

If τ_0 is more dominant than τ_{el}, the formation of large domains is preferable, and if τ_{el} is superior to τ_0, the domains with complicated shapes such as stripe and dendritic domains or many tiny domains are favorable.

2-3. *Results and Discussion on Pure systems*

State of Adsorbed Films

Figure 2-4 shows the γ vs. $m_{\mathrm{PC}}^{\mathrm{w}}$ and γ vs. $m_{\mathrm{Ch}}^{\mathrm{o}}$ curves of pure C14PC and Chol systems. As indicated by an arrow, the curve 1 has a kink point at $m_{\mathrm{PC}}^{\mathrm{w}} \approx 0.0017\ \mathrm{mmol\ kg^{-1}}$ corresponding to a phase transition of adsorbed film. The γ value decreases steeply with increasing $m_{\mathrm{PC}}^{\mathrm{w}}$, and becomes almost constant above another kink point at $m_{\mathrm{PC}}^{\mathrm{w}} \approx 0.11\ \mathrm{mmol\ kg^{-1}}$, which corresponds to critical micelle concentration (CMC)[2,6,55]. In the previous study on the structure of adsorbed CnPC film at the tetradecane/water (C14/W) and air/water (A/W) interfaces[2,6], the γ vs. $m_{\mathrm{PC}}^{\mathrm{w}}$ curve has an inflection point at $m_{\mathrm{PC}}^{\mathrm{w}} \approx 0.08\ \mathrm{mmol\ kg^{-1}}$ below CMC. From the electron density profile obtained by XR, it was suggested that CnPC molecules form bilayer in which charge-separated phosphocholine groups take upside-down arrangement to interact attractively between their neighbors. At the C6/W interface, the γ vs. $m_{\mathrm{PC}}^{\mathrm{w}}$ curve shows no inflection point even at concentration just below CMC, indicating that bilayer formation does not take place at the interface. The curve of pure Chol system has two distinct kink points at $m_{\mathrm{Ch}}^{\mathrm{o}} = 0.55$ and $0.95\ \mathrm{mmol\ kg^{-1}}$, indicating that the adsorbed Chol film takes three kinds of film sates depending on $m_{\mathrm{Ch}}^{\mathrm{o}}$.

To assign state of adsorbed films, the interfacial density Γ^{H} values were calculated by eqs. $(2-3)$ and $(2-4)$, and then the interfacial pressure π vs. mean area per molecule A curves were constructed by using eqs. $(2-5)$ and $(2-6)$. The results are shown in Figures 2-5 and 2-6, respectively. In the pure C14PC system (curve 1), the Γ^{H} value increases with $m_{\mathrm{PC}}^{\mathrm{w}}$ and changes discontinuously at the phase transition point. Above this point, the value converges into about $3.0\ \mu\mathrm{mol\ m^{-2}}$. It is seen from the π vs. A curves that the A value decreases steeply with increasing π below and changes

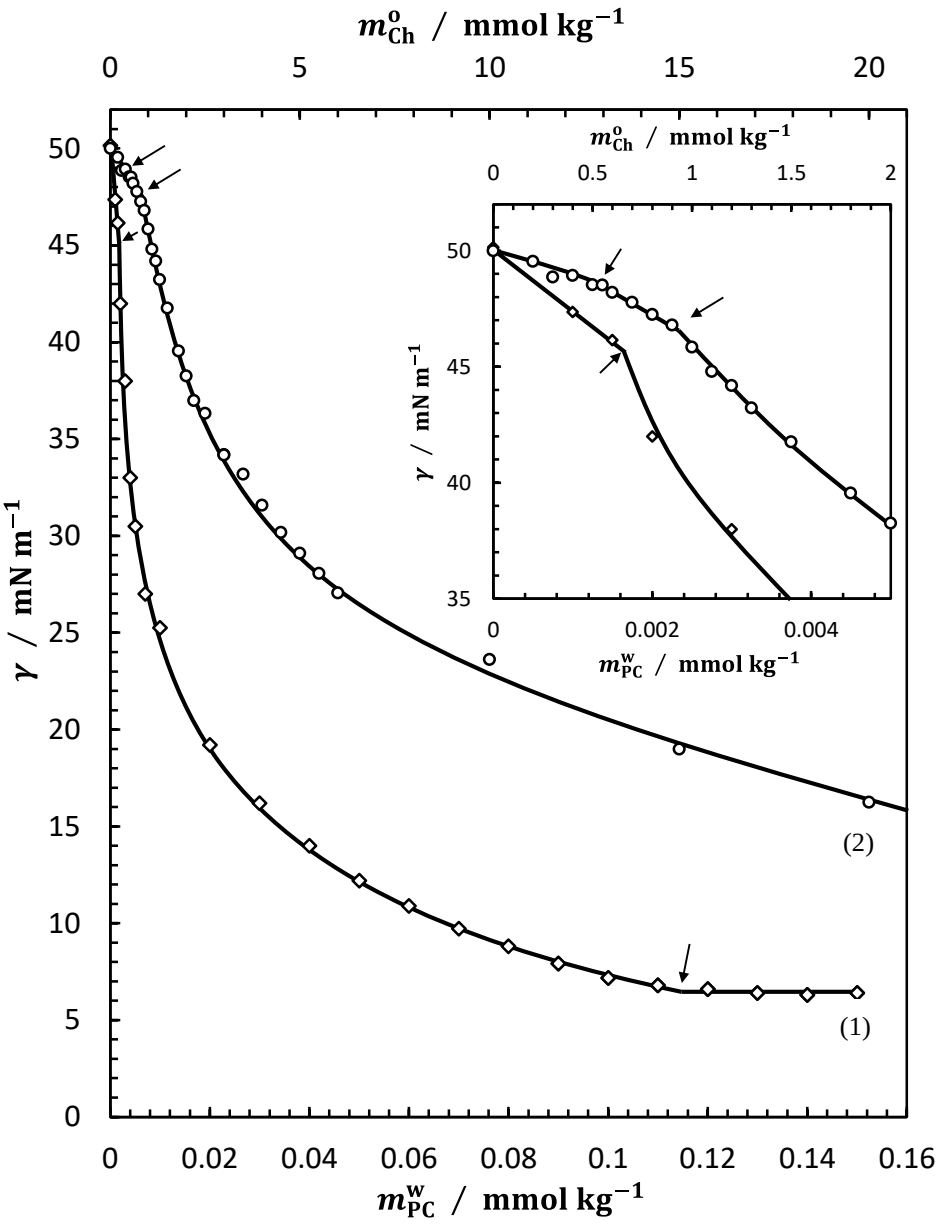

Figure 2-4. (1) The γ vs. m^{w}_{PC} curve in the pure C14PC, and (2) the γ vs. m^{o}_{Ch} curve in the pure Chol systems. Arrows indicate the kink points corresponding to the phase transition points and CMC. The inset expands the phase transition points on both curves.

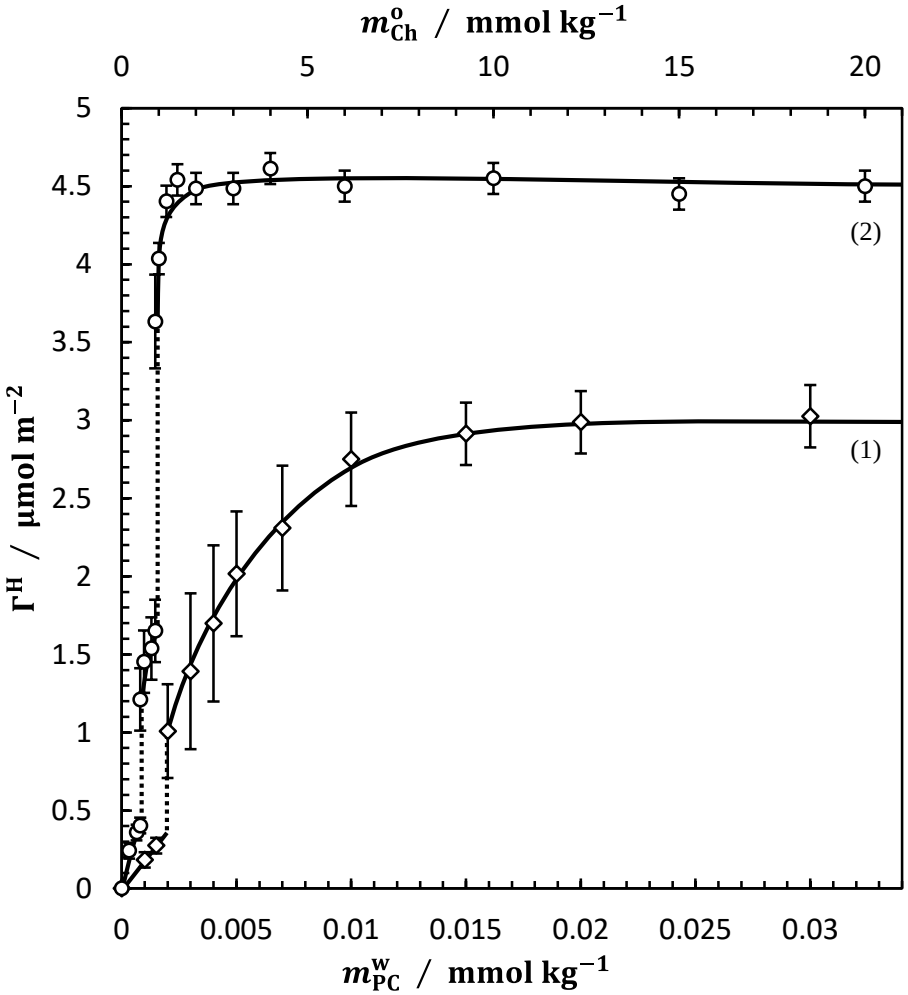

Figure 2-5. (1) The Γ^{H} vs. m^{w}_{PC} curve in the pure C14PC, and (2) Γ^{H} vs. m^{o}_{Ch} one in the pure Chol systems.

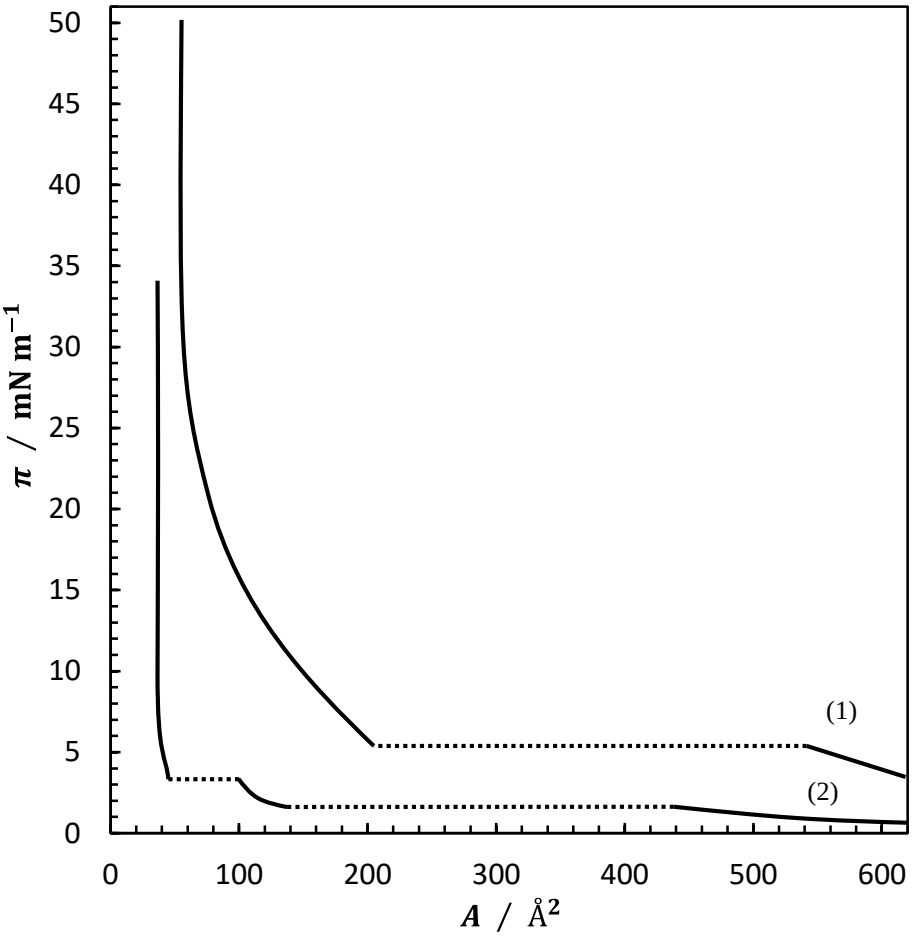

Figure 2-6. The π vs. A curves (1) in the pure C14PC and (2) in the pure Chol systems.

discontinuously at the phase transition point ($\pi^{\mathrm{eq}} \approx 5$ mN m^{-1}). Above this point, the π value increases gradually with decrease in A. The limited A value (≈ 55 Å^2) is larger than the cross-sectional area of C14PC molecule (≈ 35 Å^2). Thus, it is assumed that the adsorbed C14PC film shows the phase transition from gaseous (G) to expanded (E) states.

In the pure Chol system (curve 2), the Γ^{H} value changes discontinuously at the phase transition points, and converges into around 4.5 μmol m^{-2}. The π vs. A curve consists of three parts connected by two discontinuous changes. Above the second transition at $\pi^{\mathrm{eq}} \approx 3.5$ mN m^{-1}, the curve becomes almost vertical with an A value of about 37 Å^2, which is very close to that observed for the condensed (C) state of Langmuir Chol film ($A = 38$ Å^2)[56]. Thus, it is suggested that the adsorbed Chol film exhibits the G – E transition at low and E – C phase transitions at high π, respectively.

Structure of Adsorbed Films

The microscopic structure of the adsorbed film at the C6/W interface was investigated by XR. In Figure 2-7 are shown the R/R_F vs. Q_z plots measured at $m_{\mathrm{PC}}^{\mathrm{w}} = 0.005$ and 0.03 mmol kg^{-1}. Both plots were fitted well by one-slab model, in which the adsorbed film is assumed to consists of one slab with uniform electron density and thickness[37,39]. In this model, the thickness of the slab 1 L_1, the electron density normalized by that of pure water ρ_1/ρ_{w}, the interfacial roughness between the slab 1 and lower water phase σ_1, and that between the slab 1 and upper hexane phase σ_2 were employed as fitting parameters. The electron density profiles obtained are shown in Figure 2-8, and the fitted parameters are listed in Table 2-1, together with ρ_1/ρ_{w} and σ_i values estimated by interfacial tension data. It is reasonably assumed that the contrast of electron density between liquid hexane and hydrocarbon chain of C14PC molecule is very

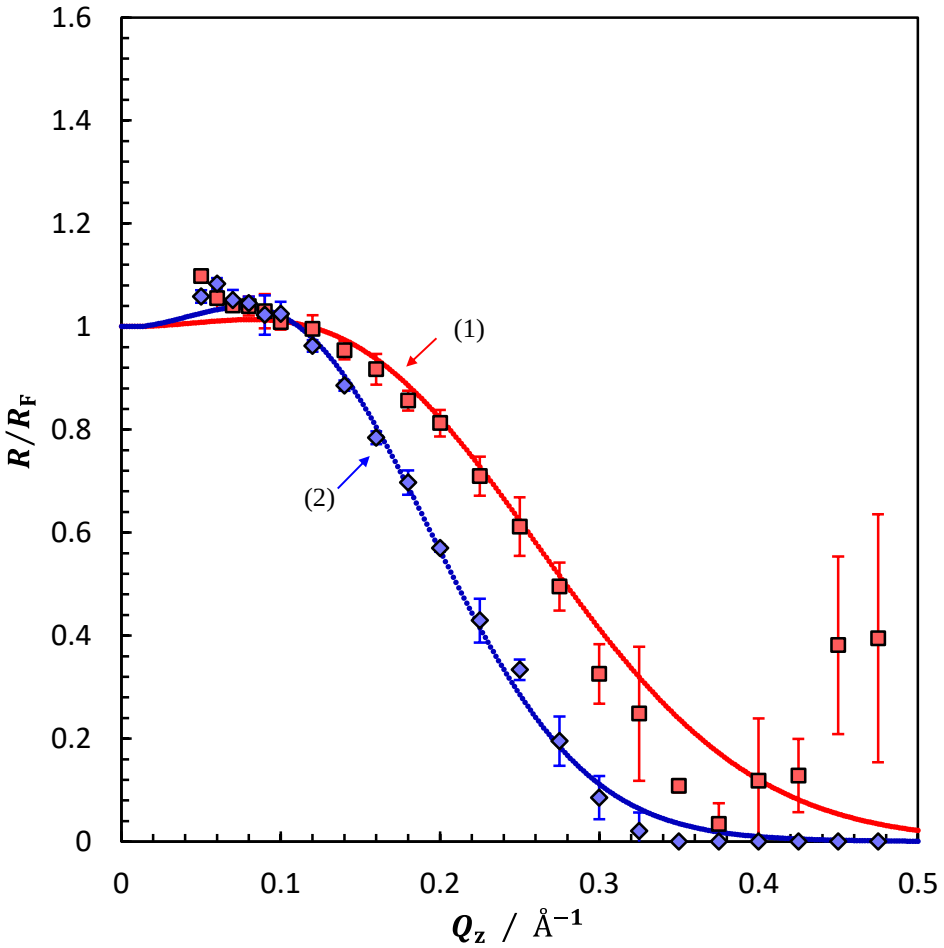

Figure 2-7. The R/R_F vs. Q_z plots in the pure C14PC system (1) at $m_{\mathrm{PC}}^{\mathrm{w}} = 0.005$ and (2) at 0.03 mmol kg^{-1}. The dotted lines represent the fitting curves.

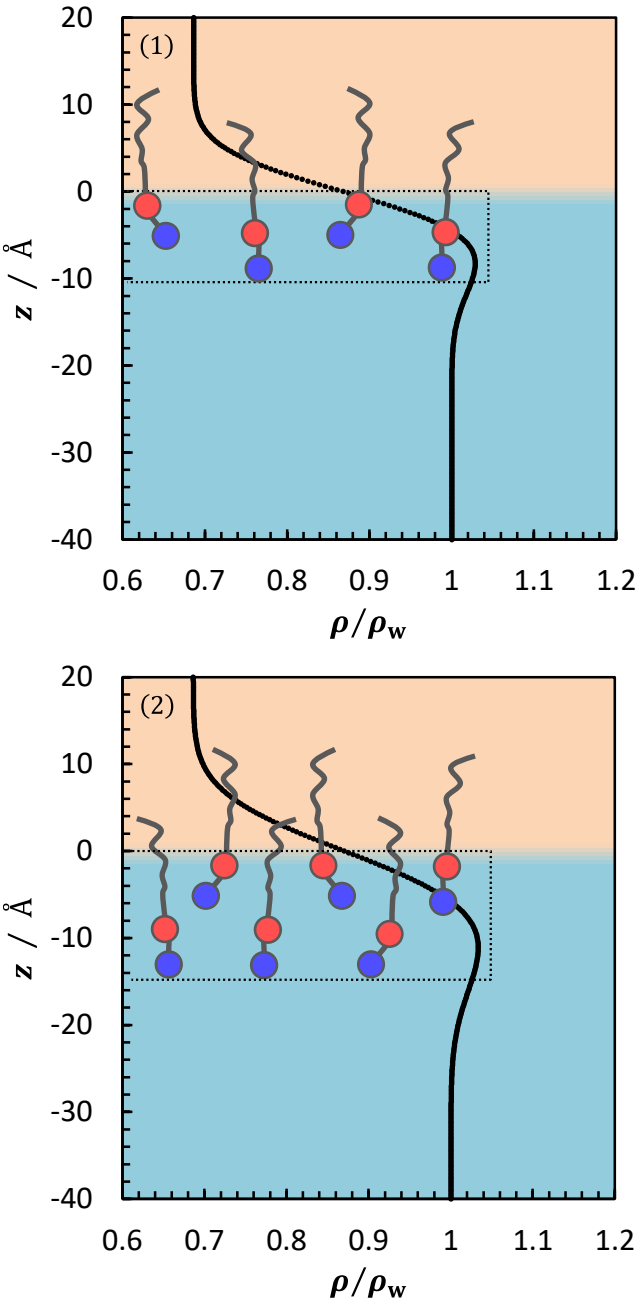

Figure 2-8. The electron density profiles normal to the interface in the pure C14PC system (1) at $m_{\mathrm{PC}}^{\mathrm{w}} = 0.005$ and (2) at $0.03\ \mathrm{mmol\ kg^{-1}}$.

Table 2-1. The fitting parameters for the slab model. The ρ/ρ_{w} and σ (σ_{cap}) value was calculated using $\Gamma^{\mathrm{H}}$and γ, and was put into parentheses.

System	$\frac{m_{\mathrm{PC}}^{\mathrm{w}},\ m_{\mathrm{Ch}}^{\mathrm{o}}}{\mathrm{mmol\ kg^{-1}}}$	Film State	Slab 1			Slab 2		
			$\frac{L_1}{\text{Å}}$	ρ_1/ρ_{w}	$\frac{\sigma_1,\sigma_2}{\text{Å}^{-1}}$	$\frac{L_2}{\text{Å}}$	ρ_2/ρ_{w}	$\frac{\sigma_2,\sigma_3}{\text{Å}^{-1}}$
Pure C14PC	0.005	E	10.5	1.05 (1.10 ± 0.05)	4.0 (4.5 ± 0.2)			
	0.03	E	14.7	1.05 (1.10 ± 0.05)	5.4 (6.2 ± 0.2)			
Pure Chol	0.4	G	12.3	0.78 (0.73)	4.0 (3.5 ± 0.1)			
	0.85	E	8.5	0.85 (0.84 ± 0.01)	3.2 (3.6 ± 0.1)	4.5	0.71 (0.73 ± 0.01)	3.2 (3.6 ± 0.1)
	1.0	C	8.5	1.01 (1.09 ± 0.03)	3.4 (3.6 ± 0.1)	6.5	0.81 (0.83 ± 0.02)	3.4 (3.6 ± 0.1)
	2.0	C	8.9	1.08 (1.09 ± 0.03)	3.5 (3.9 ± 0.1)	5.0	0.82 (0.82 ± 0.01)	3.5 (3.9 ± 0.1)

small in the expanded state and thus the slab 1 corresponds to phosphocholine (PC) group of adsorbed C14PC molecules. The L_1 values at both $m_{\mathrm{PC}}^{\mathrm{w}}$ are much larger than the length of PC group ($\sim$7 Å)[57], indicating that C14PC molecules take staggered arrangement to reduce the electrostatic repulsion between charges-separated head groups, as schematically demonstrated in Figure 2-8. The ρ_1/ρ_{w} values agree well with the calculated ones by interfacial density (see Table 2-1). Furthermore, it is noted that the L_1 value is smaller at $m_{\mathrm{PC}}^{\mathrm{w}} = 0.005$ than at 0.03 mmol kg^{-1}, suggesting that staggered arrangement become more remarkable with reducing intermolecular distance at high Γ^{H}.

In the case of pure Chol system, the R/R_F values measured in the G, E, and C states are plotted against Q_z in Figure 2-9. The solid lines are the fitted curve and the corresponding electron density profiles are shown in Figure 2-10. The fitted parameters are listed in Table 2-1. In the G state at $m_{\mathrm{Ch}}^{\mathrm{o}} = 0.4$ mmol kg^{-1}, the $R/R_F\,(Q_z)$ plots was fitted well by one-slab model. Because the electron density of hydroxyl (OH) group is almost same as that of bulk water phase, it is likely that the slab 1 represents the hydrophobic parts of Chol molecule. The L_1 value (12.3 Å) is smaller than the total lengths of sterol ($\sim$9 Å) and tail ($\sim$6 Å) parts of molecule[56,58]. The ρ_1/ρ_{w} value estimated using Γ^{H} is 0.73 consistent with the fitting value (0.78). Thus, Chol molecules are expected to take very loose packing and tilt from interface normal.

For both E and C states, the two-slab model, in which the film is assumed to have a structure consisting of two slabs with uniform thicknesses and electron densities[37,39], gives good fitting to the $R/R_F\,(Q_z)$ plots. The L_1 and L_2 values are respectively very close to the lengths of sterol and tail parts, suggesting that the Chol molecules are arranged in almost vertical to the interface. The ρ_1/ρ_{w} and ρ_2/ρ_{w} values in the E state at $m_{\mathrm{Ch}}^{\mathrm{o}} = 0.85$ mmol kg^{-1} agree well with those estimated for liquid mixture of Chol

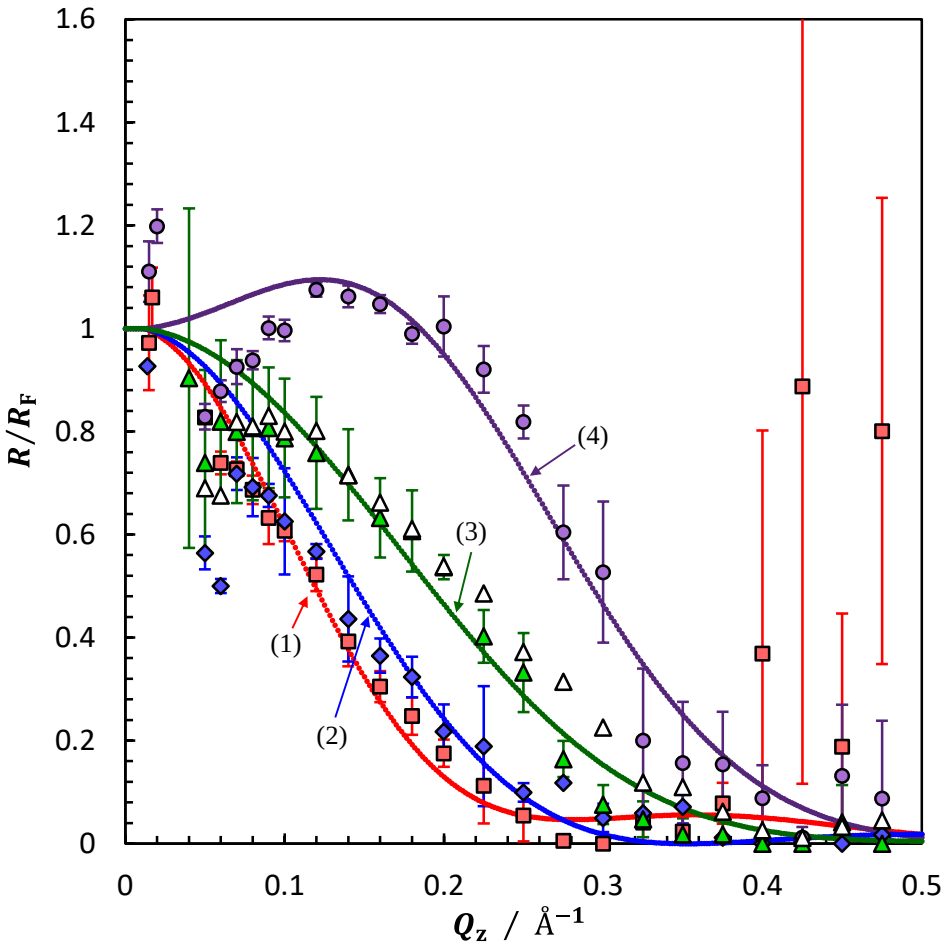

Figure 2-9. The $R/R_F\,(Q_z)$ plots in the pure Chol system (1) at $m_{\mathrm{Ch}}^{\mathrm{o}} = 0.4$, (2) 0.85, (3) 1.0, and (4) at 2.0 mmol kg^{-1}. The dotted lines represent the best fitting curves. The white triangles demonstrate the $R_{\mathrm{Coh}}(Q_z)$ plots at $C_{\mathrm{XR}} = 0.5$.

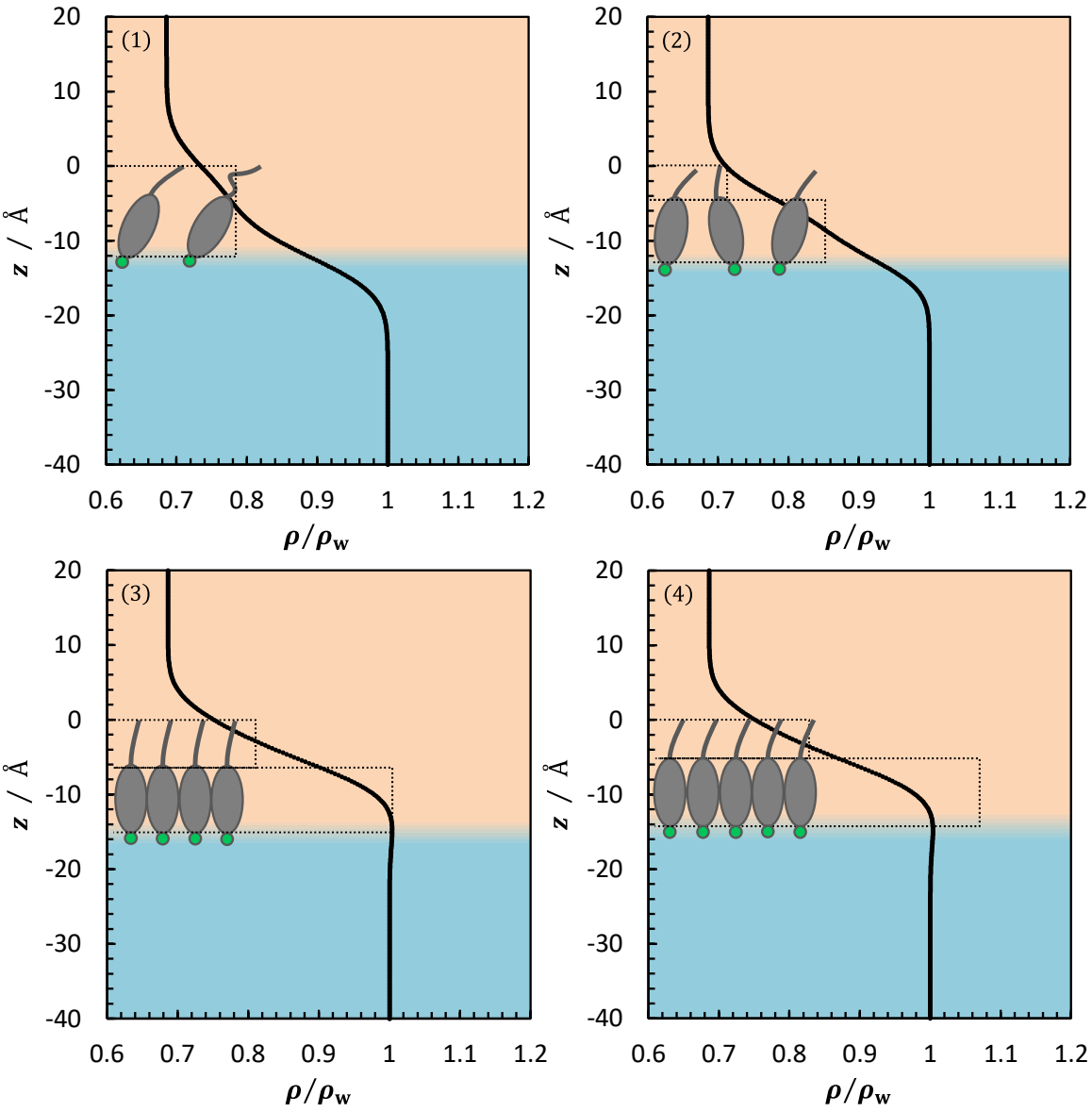

Figure 2-10. The electron density profiles normal to the interface for the pure Chol system (1) at $m_{\mathrm{Ch}}^{\mathrm{o}} = 0.4$, and (2) 0.85, (3) 1.0, and (4) at 2.0 mmol kg^{-1}.

and hexane. The values in the C state ($m_{\mathrm{Ch}}^{\mathrm{o}} = 1.0$ and $2.0\ \mathrm{mmol\ kg^{-1}}$), on the other hand, are very close to those calculated for the solid Chol state. Thus, it is reasonable that in the C film, hydrophobic part of the molecule are densely packed with each other.

The $R/R_F\,(Q_z)$ values measured at $m_{\mathrm{Ch}}^{\mathrm{o}} = 0.85$ and $1.0\ \mathrm{mmol\ kg^{-1}}$ just below and above the E – C phase transition point take intermediate value between those at 0.4 and $2.0\ \mathrm{mmol\ kg^{-1}}$. Thus, we tried to fit them by domain models with coherent and incoherent interferences, expressed by eqs. $(2-17)$ and $(2-18)$, respectively. In these procedures, only the coverage of the C domain C_{XR} was employed as a fitting parameter, and the reflectivity measured at well below and above the transition point were used as references R_1 (or r_1) and R_2 (or r_2). The $R/R_F\,(Q_z)$ plots at $m_{\mathrm{Ch}}^{\mathrm{o}} = 1.0\ \mathrm{mmol\ kg^{-1}}$ was successfully fitted by coherent model using the amplitudes r_i $(i = 1, 2)$ at $m_{\mathrm{Ch}}^{\mathrm{o}} = 2.0$ and $0.85\ \mathrm{mmol\ kg^{-1}}$. The results are shown by the white triangles in Figure 2-9, and $C_{\mathrm{XR}} = 0.5$ was obtained.

The interfacial density can be calculated by

$$\Gamma_{\mathrm{XR}}^{\mathrm{H}} = C_{\mathrm{XR}}\Gamma^{\mathrm{H},1} + (1 - C_{\mathrm{XR}})\Gamma^{\mathrm{H},2}\ , \qquad (2-23)$$

where $\Gamma^{\mathrm{H},1}$ and $\Gamma^{\mathrm{H},2}$ are respectively the interfacial densities of Chol at $m_{\mathrm{Ch}}^{\mathrm{o}} = 2.0$ and $0.85\ \mathrm{mmol\ kg^{-1}}$, and $\Gamma_{\mathrm{XR}}^{\mathrm{H}} = 3.2 \pm 0.3\ \mu\mathrm{mol\ m^{-2}}$ was obtained (see Table 2-2). This is a little smaller than that evaluated from the interfacial tension data Γ^{H} ($3.9 \pm 0.1\ \mu\mathrm{mol\ m^{-2}}$). Thus, it is highly expected that the condensed state just above the E – C phase transition point is heterogeneous film in which E domains are surrounded by the C region. The morphology of the film is observed by BAM in the latter part of this thesis.

Table 2-2. A list of Γ^{H}, $\Gamma^{\mathrm{H}}_{\mathrm{XR}}$, and $\Gamma^{\mathrm{H}}_{\mathrm{BAM}}$ at $m^{\mathrm{o}}_{\mathrm{Ch}} = 1.0$ mmol kg^{-1}.

$\boldsymbol{\Gamma^{\mathrm{H}}}$ / µmol m^{-2}	$\boldsymbol{\Gamma^{\mathrm{H}}_{\mathrm{XR}}}$ / µmol m^{-2}	$\boldsymbol{\Gamma^{\mathrm{H}}_{\mathrm{BAM}}}$ / µmol m^{-2}
3.9 ± 0.1	3.2 ± 0.3	4.1 ± 0.1

Domain Structure of Adsorbed Chol Film

The heterogeneous structure of the adsorbed Chol film was further examined by BAM. In Figure 2-11, typical images observed at $m_{\mathrm{Ch}}^{\mathrm{o}} = 0$, 0.8, 0.9 and $1.0\ \mathrm{mmol\ kg^{-1}}$ are shown. Interference patterns in all images indicate the existence of thick particles such as air bubble and artificial granule[59,60].

The images below $m_{\mathrm{Ch}}^{\mathrm{o}} = 0.9\ \mathrm{mmol\ kg^{-1}}$ are homogeneous within a spatial resolution limited by pixel size of CCD camera ($0.72\mu\mathrm{m}$). In contrast, the image at $m_{\mathrm{Ch}}^{\mathrm{o}} = 1.0\ \mathrm{mmol\ kg^{-1}}$ looks heterogeneous and dark circular domains with μm size are dispersed. Taking account of that the adsorbed film is in the C state just above the E – C phase transition, the dark domains should be low density E phase surrounded by high density condensed one. The fraction of area covered by bright region C_{BAM} was estimated by averaging over 10 images and about $0.9{\sim}0.95$. Furthermore, $\Gamma_{\mathrm{BAM}}^{\mathrm{H}}$ value calculated by $\Gamma_{\mathrm{BAM}}^{\mathrm{H}} = C_{\mathrm{BAM}}\Gamma^{\mathrm{H},1} + (1 - C_{\mathrm{BAM}})\Gamma^{\mathrm{H},2}$ was $4.2 \pm 0.1\ \mu\mathrm{mol\ m^{-2}}$, which is very close to that estimated by interfacial tension data, confirming that the condensed Chol film just above the E – C transition point is heterogeneous; the E domains are dispersed into the C region.

In the previous study on the adsorbed film of FC10OH at the C6/W interface, it was found that the E state is a heterogeneous film in which C domains of FC10OH are surrounded by low density G region. This is mainly driven by weak interaction between FC10OH and hexane molecules[37,38]. In contrast to this, in the present system, a low density E domains are surrounded by C region, *i.e.*, a kind of hole formation was found in the C state just above the E – C transition point. Thus, it is expected that the hole formation is induced by preferable interaction between Chol and hexane molecules at the interface.

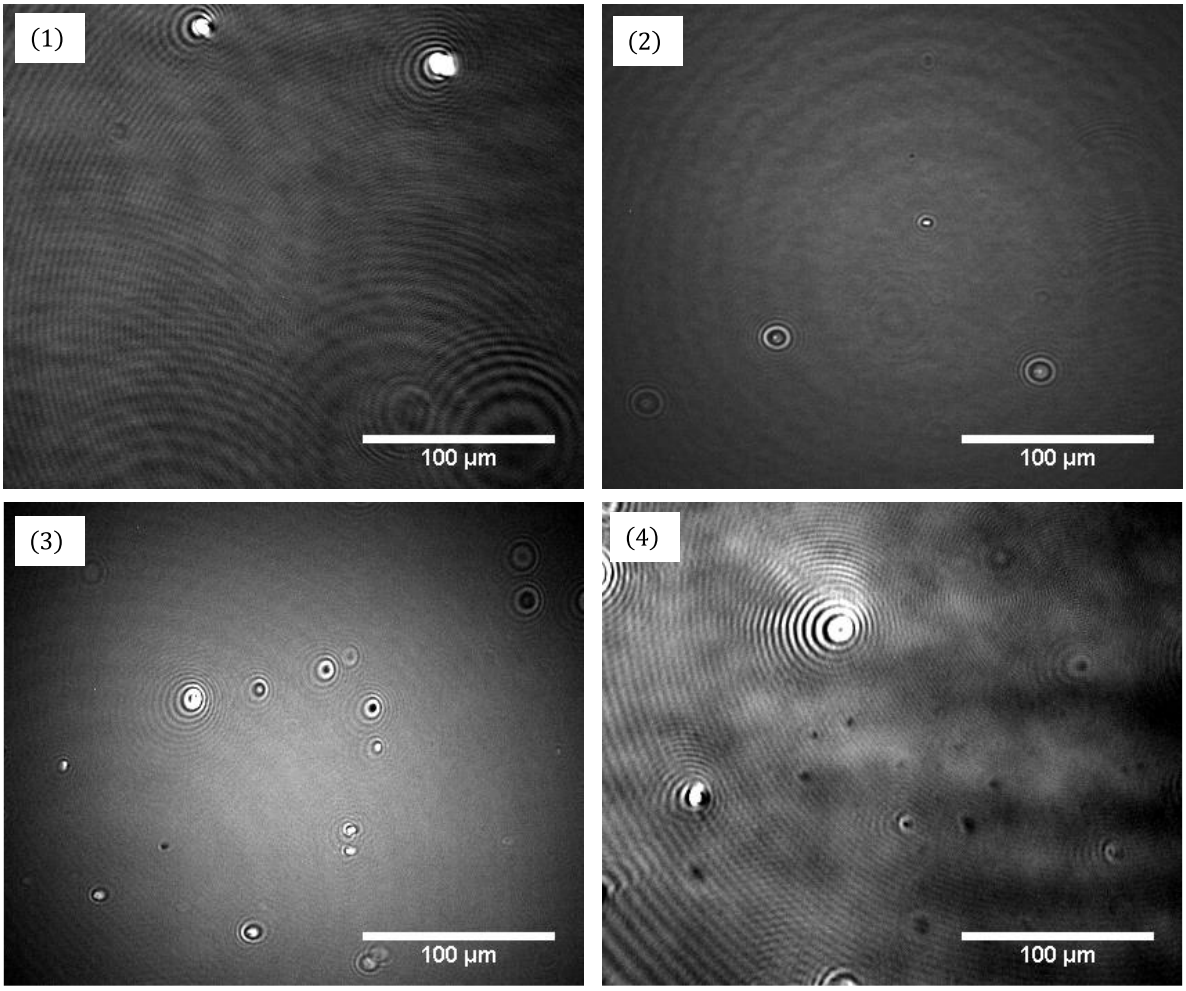

Figure 2-11. Typical images of adsorbed Chol film (1) at $m_{\mathrm{Ch}}^{\mathrm{o}} = 0$ (pure C6/W interface), (2) 0.8, (3) 0.9, and (4) at 1.0 mmol kg^{-1}.

Finally, let us briefly mention the line tension of the Chol system. First, a median of domain radius of over 100 domains (7.2 ± 0.5 μm) was calculated based on a domain size distribution in Figure 2-12 and was assigned to equilibrium one R_{eq}. Using a dipole moment of OH group normal to the interface u_{OH} (1.4 D), that of terminal-methyl group $u_{\mathrm{CH_3}}$ (0.4 D), relative permittivity of water ε_{w} (80) and hexane ε_{o} (1.9), and the cut – off distance between dipole Δ (7 Å) into eq. $(2-21)$[3], the dipole – dipole repulsions in water $\tau_{\mathrm{el}}^{\mathrm{w}}$ and in hexane $\tau_{\mathrm{el}}^{\mathrm{o}}$ were separately estimated to be -0.05 and -0.53 pN. Then, a τ_0 value of 0.51 pN was obtained by substituting R_{eq} and $\tau_{\mathrm{el}}(=\tau_{\mathrm{el}}^{\mathrm{w}}+\tau_{\mathrm{el}}^{\mathrm{o}})$ values into eq. $(2-22)$. The τ_0 value was also roughly estimated to be 0.21~0.54 pN by eq. $(2-19)$, where a thickness mismatch between C and E domains ΔL of ~1Å and the interfacial tension between the C domain and the surrounding (hexane) γ^{DS} (2.1~5.4 mN m^{-1}). The absolute values of τ_0 and τ_{el} is close to each other, which may induce a little amount of small circular E domain formation at the interface.

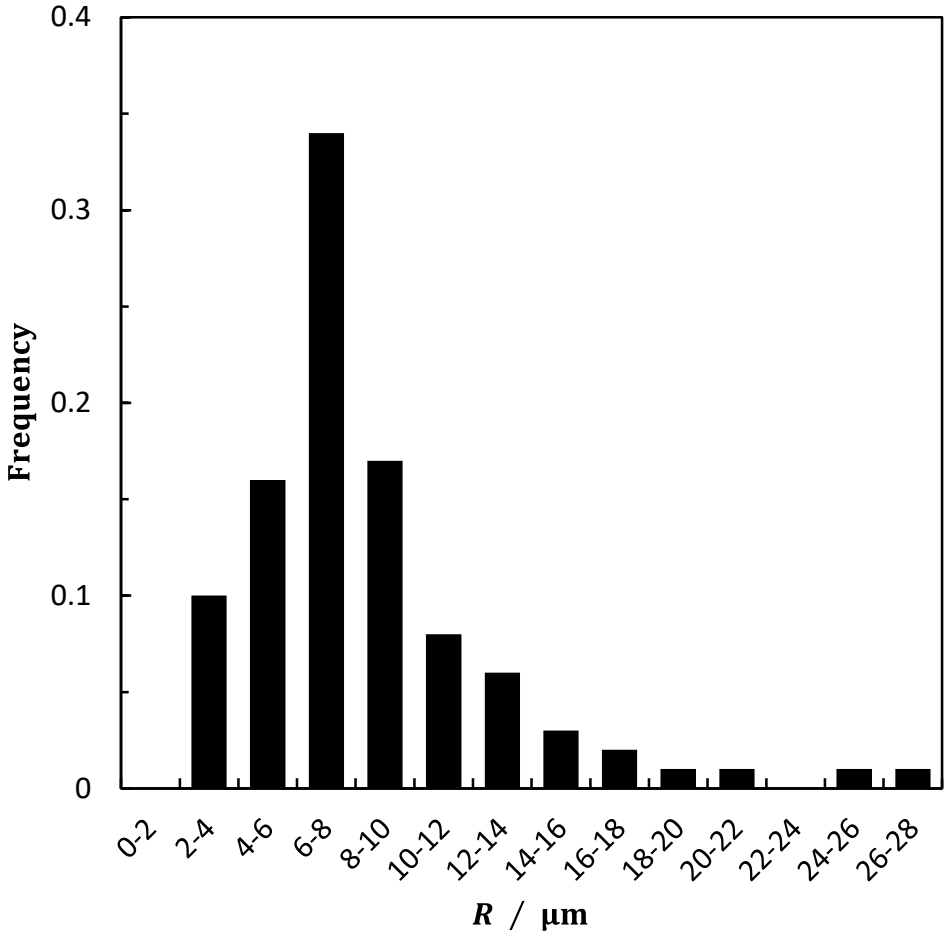

Figure 2-12. Domain radius R distribution at $m_{\mathrm{Ch}}^{\mathrm{o}} = 1.0\ \mathrm{mmol\,kg^{-1}}$ constructed by 100 domains data. This distribution gave us 7.2 ± 0.5 μm of median of domain radius.

2-4. *Results and Discussion on C14PC – Chol mixed system*

Film State and Molecular Miscibility

Figure 2-13 shows the γ vs. $m_{\mathrm{Ch}}^{\mathrm{o}}$ curves at given $m_{\mathrm{PC}}^{\mathrm{w}}$ and 298.15 K under atmospheric pressure. With increasing $m_{\mathrm{Ch}}^{\mathrm{o}}$, the γ value decreases slightly at low and largely at high $m_{\mathrm{Ch}}^{\mathrm{o}}$. Each curve has one or two kink points due to the phase transitions in the adsorbed film as connected by dotted lines. It is realized that four kinds of film states denoted by G, E, Im, and C appear depending on $m_{\mathrm{Ch}}^{\mathrm{o}}$ and $m_{\mathrm{PC}}^{\mathrm{w}}$. Four interfacial states will be assigned later. The γ value read from the γ vs. $m_{\mathrm{Ch}}^{\mathrm{o}}$ curves at given $m_{\mathrm{Ch}}^{\mathrm{o}}$ are plotted against $m_{\mathrm{PC}}^{\mathrm{w}}$ in Figures 2-14-1 and 2-14-2. The γ value decreases very steeply at low and gradually at high $m_{\mathrm{PC}}^{\mathrm{w}}$ with increasing $m_{\mathrm{PC}}^{\mathrm{w}}$. The curve at $m_{\mathrm{Ch}}^{\mathrm{o}} = 0.8\ \mathrm{mmol\ kg^{-1}}$ in Figure 2-14-2 has a distinct break point of the E – C phase transition at low $m_{\mathrm{PC}}^{\mathrm{w}}$ ($= 0.002\ \mathrm{mmol\ kg^{-1}}$), although the kink corresponding to the C – Im transition at high $m_{\mathrm{PC}}^{\mathrm{w}}$, which is appeared on the γ vs. $m_{\mathrm{Ch}}^{\mathrm{o}}$ curves, is obscure.

In Figure 2-15 are shown the $\Gamma_{\mathrm{Ch}}^{\mathrm{H}}$ vs. $m_{\mathrm{Ch}}^{\mathrm{o}}$ curves at constant $m_{\mathrm{PC}}^{\mathrm{w}}$. The $\Gamma_{\mathrm{Ch}}^{\mathrm{H}}$ value increases gradually with increasing $m_{\mathrm{Ch}}^{\mathrm{o}}$ and changes discontinuously at the phase transition points. Furthermore, the $\Gamma_{\mathrm{Ch}}^{\mathrm{H}}$ value at given $m_{\mathrm{Ch}}^{\mathrm{o}}$ reduces with increasing $m_{\mathrm{PC}}^{\mathrm{w}}$. The dependence of $\Gamma_{\mathrm{PC}}^{\mathrm{H}}$ on $m_{\mathrm{PC}}^{\mathrm{w}}$ are clearly shown in Figure 2-16. The $\Gamma_{\mathrm{PC}}^{\mathrm{H}}$ value increases steeply at low and converges into around 3.2 $\mu\mathrm{mol\ m^{-2}}$ at high $m_{\mathrm{PC}}^{\mathrm{w}}$; the values at $m_{\mathrm{PC}}^{\mathrm{w}}$ = 0.4 and 0.6 $\mathrm{mmol\ kg^{-1}}$ correspond to E, those at 0.8 and 1.0 $\mathrm{mmol\ kg^{-1}}$ to Im, and those above 1.2 $\mathrm{mmol\ kg^{-1}}$ to C state. It should be noted that the $\Gamma_{\mathrm{PC}}^{\mathrm{H}}$ value increases continuously even at the C – Im transition (curves 5 and 6), although it changes discontinuously at the G – E (curves 1 ~ 3) and E – C phase transition points (curve 5).

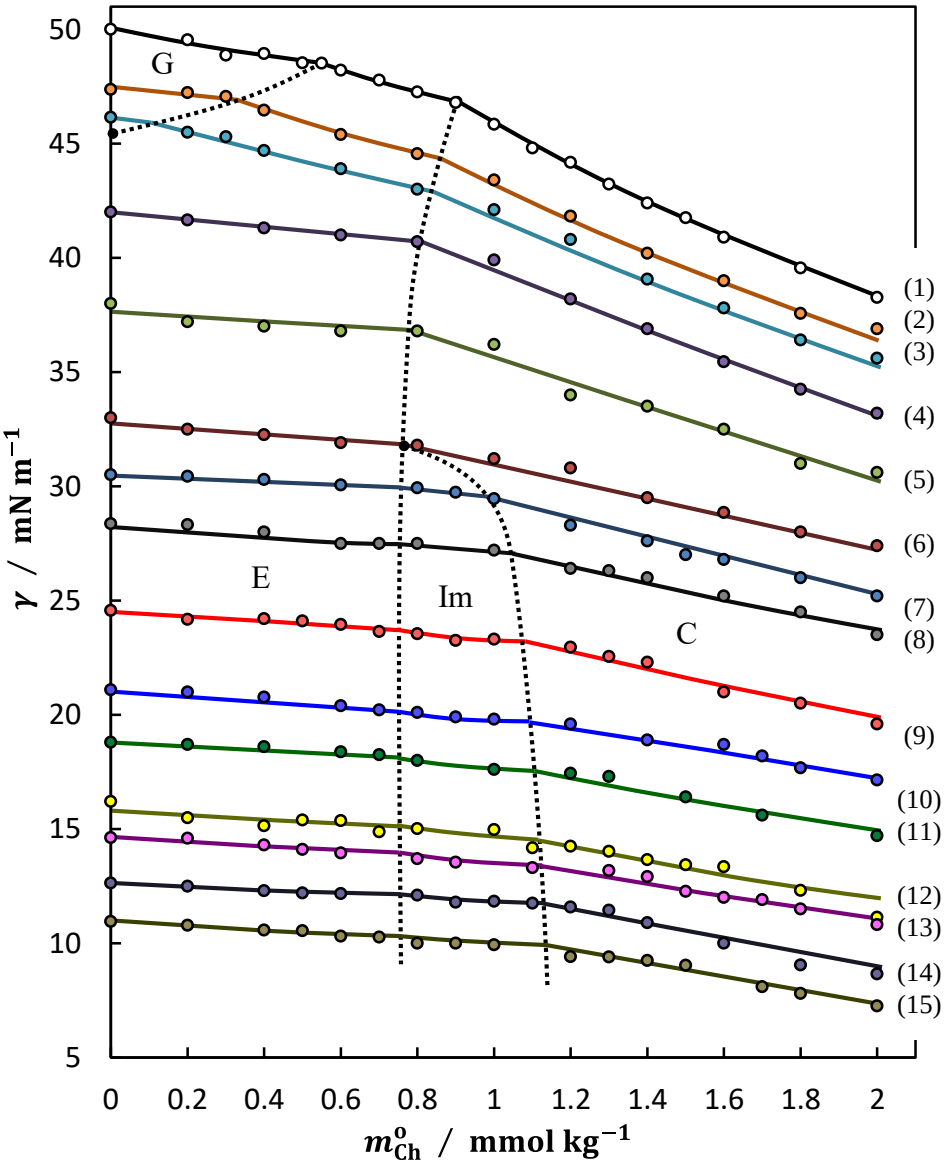

Figure 2-13. The γ vs. m^{o}_{Ch} curves at given (1) $m^{w}_{PC} = 0$ (pure Chol system), (2) 0.001, (3) 0.0015, (4) 0.002, (5) 0.003, (6) 0.004, (7) 0.005, (8) 0.007, (9) 0.01, (10) 0.015, (11) 0.02, (12) 0.03, (13) 0.04, (14) 0.05, and (15) at 0.06 mmol kg^{-1}. The dotted lines connect the phase transition points of the film.

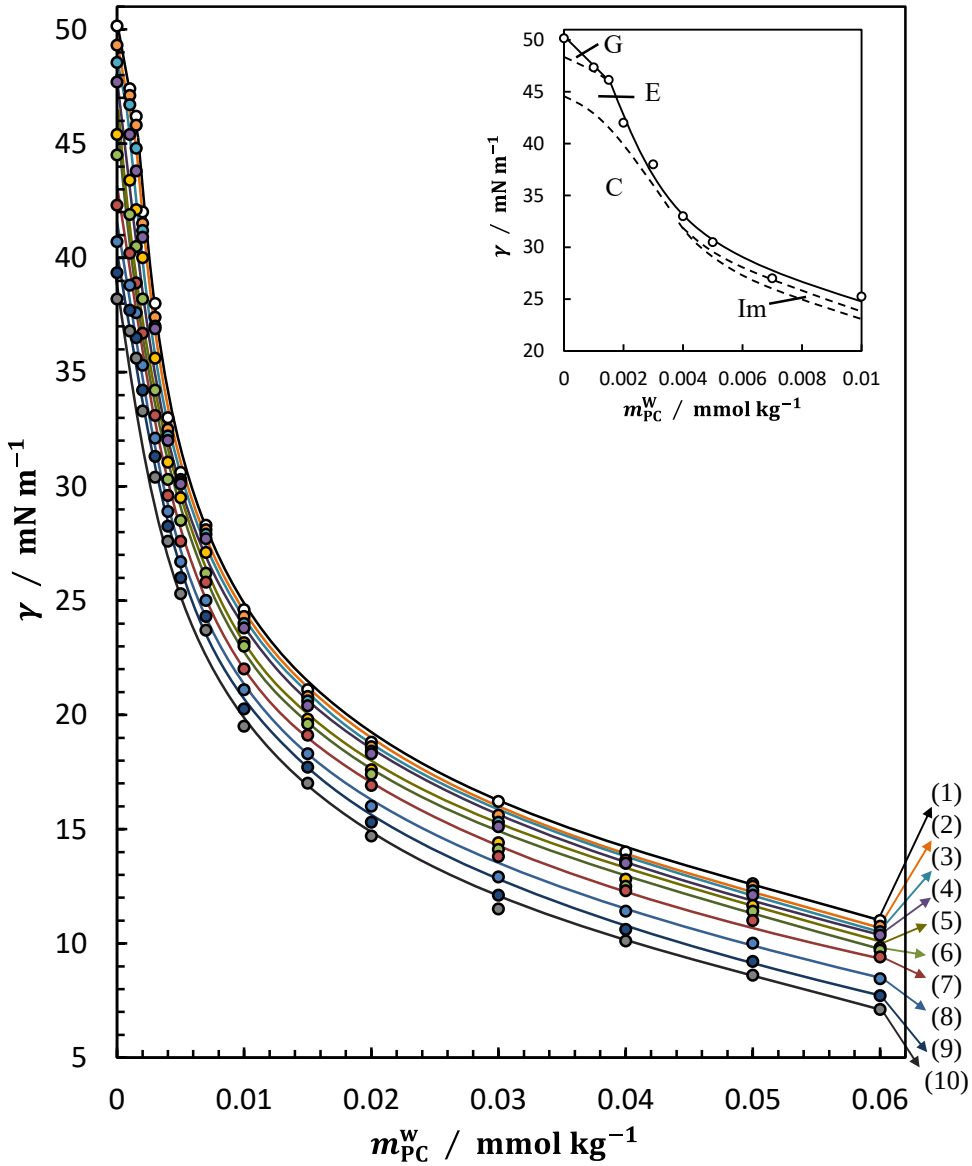

Figure 2-14-1. The γ vs. $m_{\mathrm{PC}}^{\mathrm{w}}$ curves at given (1) $m_{\mathrm{Ch}}^{\mathrm{o}} = 0$ (pure C14PC system), (2) 0.2, (3) 0.4, (4) 0.6, (5) 1.0, (6) 1.2, (7) 1.4, (8) 1.6, (9) 1.8, and (10) at 2.0 mmol kg^{-1}. The dotted lines in the inset, dividing the γ vs. $m_{\mathrm{PC}}^{\mathrm{w}}$ graph into four kinds of film state regions, are drawn by tracing the corresponding lines in Figure 2-13.

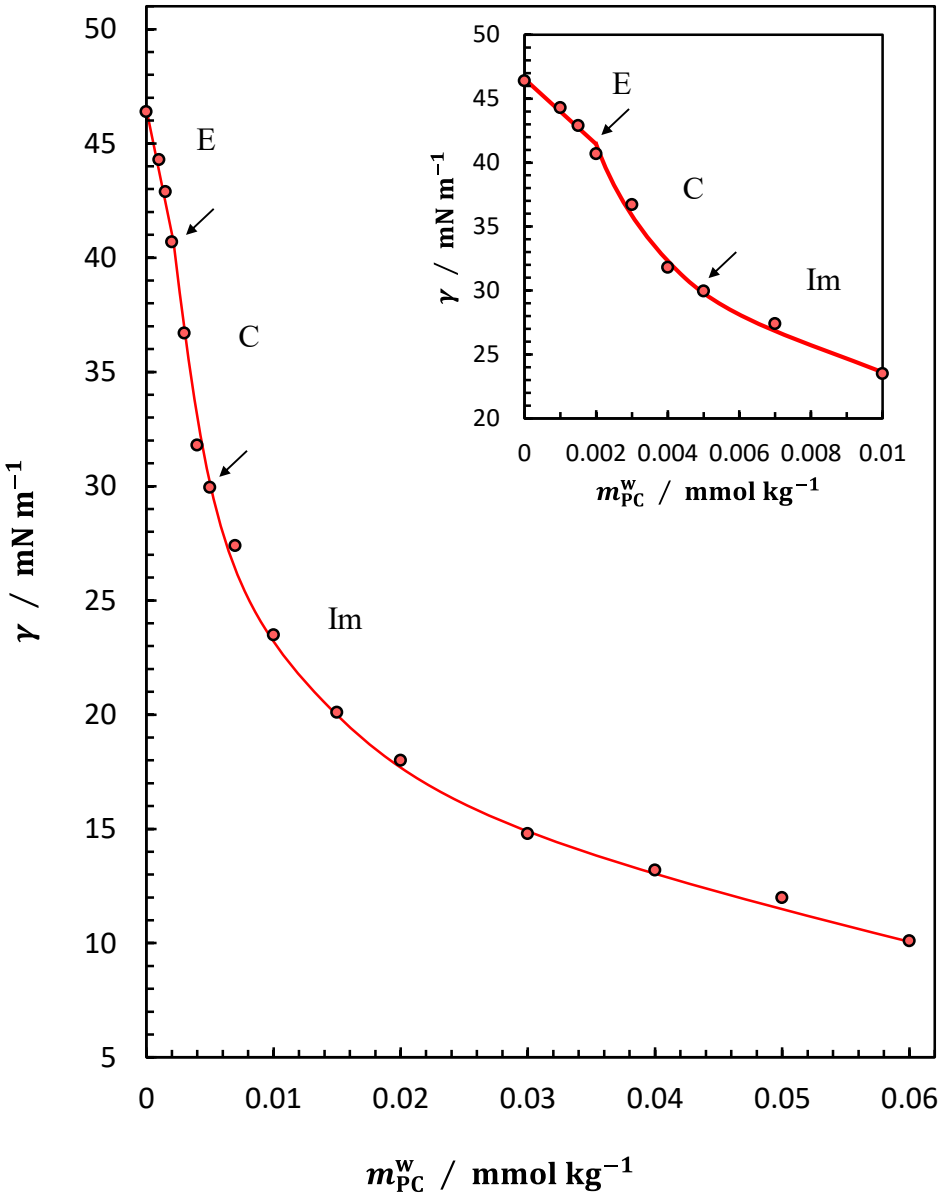

Figure 2-14-2. The γ vs. m_{PC}^{w} curves at given $m_{Ch}^{o} = 0.8\,\text{mmol kg}^{-1}$. The curve at low m_{PC}^{w} is expanded in the inset.

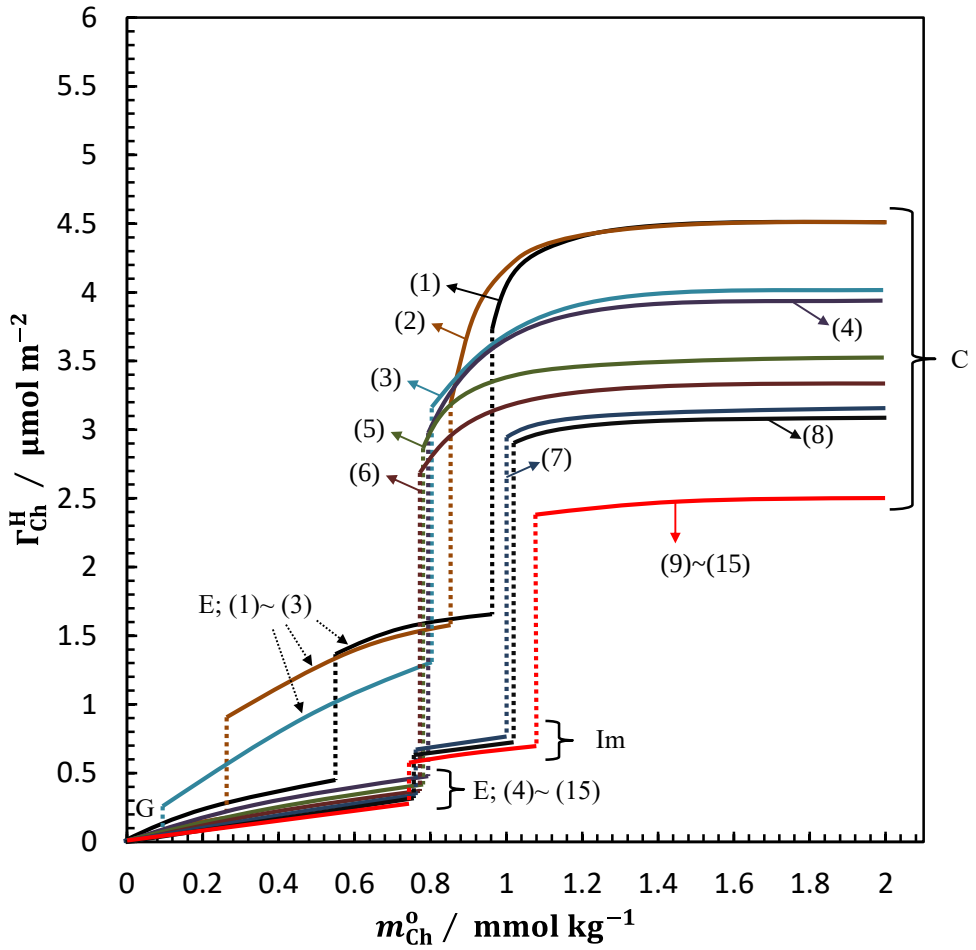

Figure 2-15. The Γ^{H}_{Ch} vs. m^{o}_{Ch} curves at given (1) $m^{w}_{PC} = 0$ (pure Chol system), (2) 0.001, (3) 0.0015, (4) 0.002, (5) 0.003, (6) 0.004, (7) 0.005, (8) 0.007, (9) 0.01, (10) 0.015, (11) 0.02, (12) 0.03, (13) 0.04, (14) 0.05, and (15) at 0.06 mmol kg^{-1}.

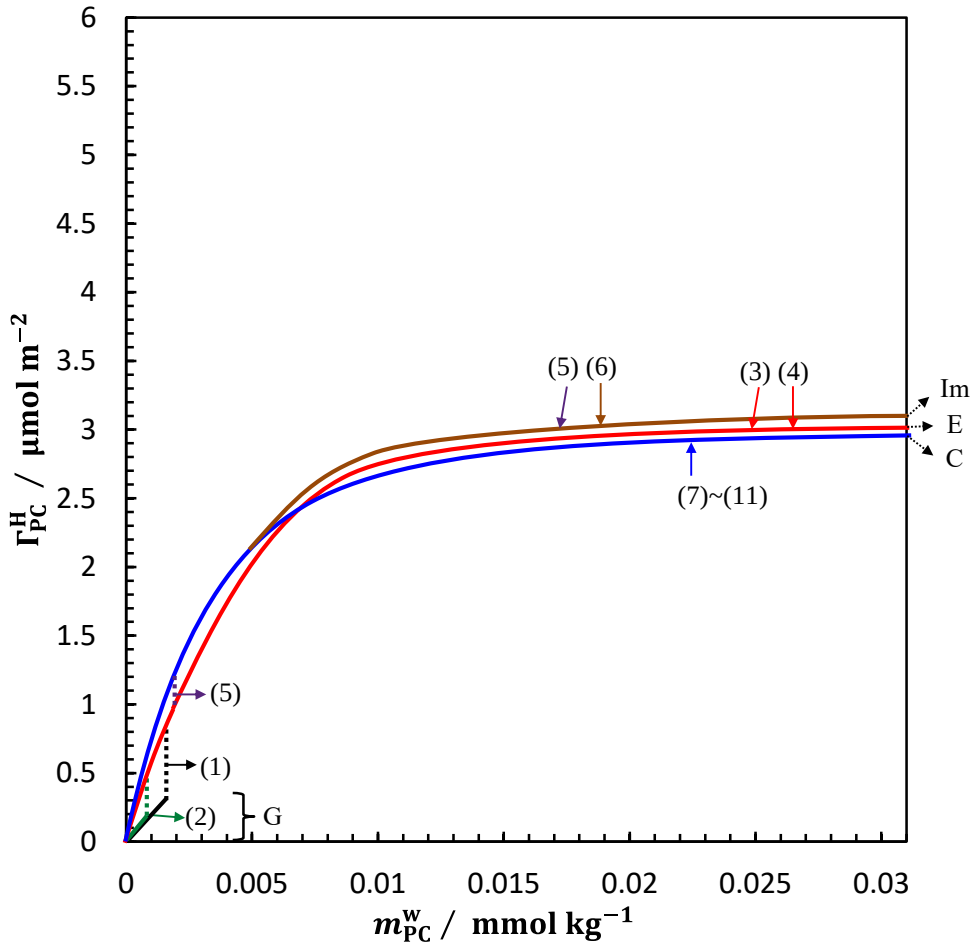

Figure 2-16. The Γ^{H}_{PC} vs. m^{w}_{PC} curves at given (1) $m^{o}_{Ch} = 0$, (2) 0.2, (3) 0.4, (4) 0.6, (5) 0.8, (6) 1.0, (7) 1.2, (8) 1.4, (9) 1.6, (10) 1.8, and (11) at 2.0 mmol kg^{-1}.

The total interfacial density Γ^{H} was calculated by $\Gamma^{\mathrm{H}} = \Gamma^{\mathrm{H}}_{\mathrm{PC}} + \Gamma^{\mathrm{H}}_{\mathrm{Ch}}$, and plotted against $m^{\mathrm{o}}_{\mathrm{Ch}}$ at given $m^{\mathrm{w}}_{\mathrm{PC}}$ in Figure 2-17. The value increases with increasing $m^{\mathrm{o}}_{\mathrm{Ch}}$ and converges into $4.5 \sim 5.5\ \mathrm{mmol\ m^{-2}}$ at high $m^{\mathrm{o}}_{\mathrm{Ch}}$ in the C state depending on $m^{\mathrm{w}}_{\mathrm{PC}}$, suggesting the mixing of C14PC molecules with Chol ones.

In order to assign the film state (G, E, Im, and C), the π vs. A curves at constant $m^{\mathrm{w}}_{\mathrm{PC}}$ are constructed by using eqs. $(2-5)$ and $(2-6)$, as drawn in Figure 2-18. The curves are classified by three types depending on $m^{\mathrm{w}}_{\mathrm{PC}}$; (a) the curve below $m^{\mathrm{w}}_{\mathrm{PC}} = 0.0015$, (b) those at $m^{\mathrm{w}}_{\mathrm{PC}} = 0.002 \sim 0.004$, (c) those above $m^{\mathrm{w}}_{\mathrm{PC}} = 0.005\ \mathrm{mmol\ kg^{-1}}$. In type (a), the curves consist of three parts, connected by two discontinuous changes corresponding to the G – E transition at low and the E – C one at high π^{eq}. Two film states in type (b) are assigned to the E and C state as depicted in Figure 2-13. In type (c), it is noted that a new film state was appeared in between the E and C states and assigned as the "intermediate (Im)" state. The curves in the C state are almost vertical, indicating that the compressibility of the film is very low. Taking account of our finding that the adsorbed film of pure Chol system takes the gaseous, expanded, and condensed states, three states G, E, and C in the mixed C14PC – Chol system corresponds to the gaseous, expanded, and condensed states, respectively. It is found that the A value decreases very slightly from $\sim 40\ \mathrm{Å^2}$ up to $\sim 30\ \mathrm{Å^2}$ with increasing $m^{\mathrm{w}}_{\mathrm{PC}}$. The minimum A value is smaller than the cross-sectional area of C14PC molecules ($\sim 38\ \mathrm{Å^2}$) and that of condensed Chol film ($\sim 35\ \mathrm{Å^2}$), suggesting that in the mixed C film, the C14PC and Chol molecules are more densely packed with each other compared to the C film of the pure Chol system. The A value in the Im state slightly decrease with increasing π, indicating that the Im film has a small compressibility. Above $m^{\mathrm{w}}_{\mathrm{PC}} = 0.01\ \mathrm{mmol\ kg^{-1}}$, the A value reduces to $\sim 42\ \mathrm{Å^2}$, which is close to but still larger than that in the C state ($30 \sim 38\ \mathrm{Å^2}$).

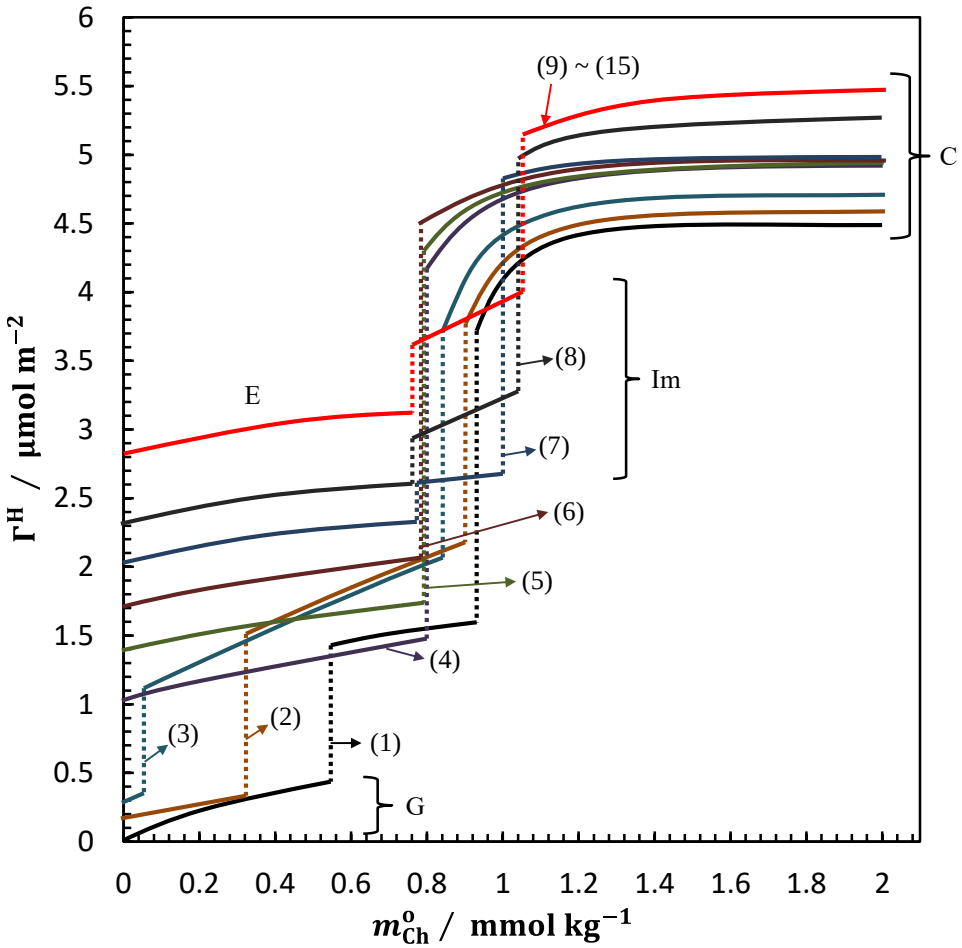

Figure 2-17. The Γ^{H} vs. m^{o}_{Ch} curves at given (1) $m^{w}_{PC} = 0$ (pure Chol system), (2) 0.001, (3) 0.0015, (4) 0.002, (5) 0.003, (6) 0.004, (7) 0.005, (8) 0.007, (9) 0.01, (10) 0.015, (11) 0.02, (12) 0.03, (13) 0.04, (14) 0.05, and (15) at 0.06 mmol kg^{-1}.

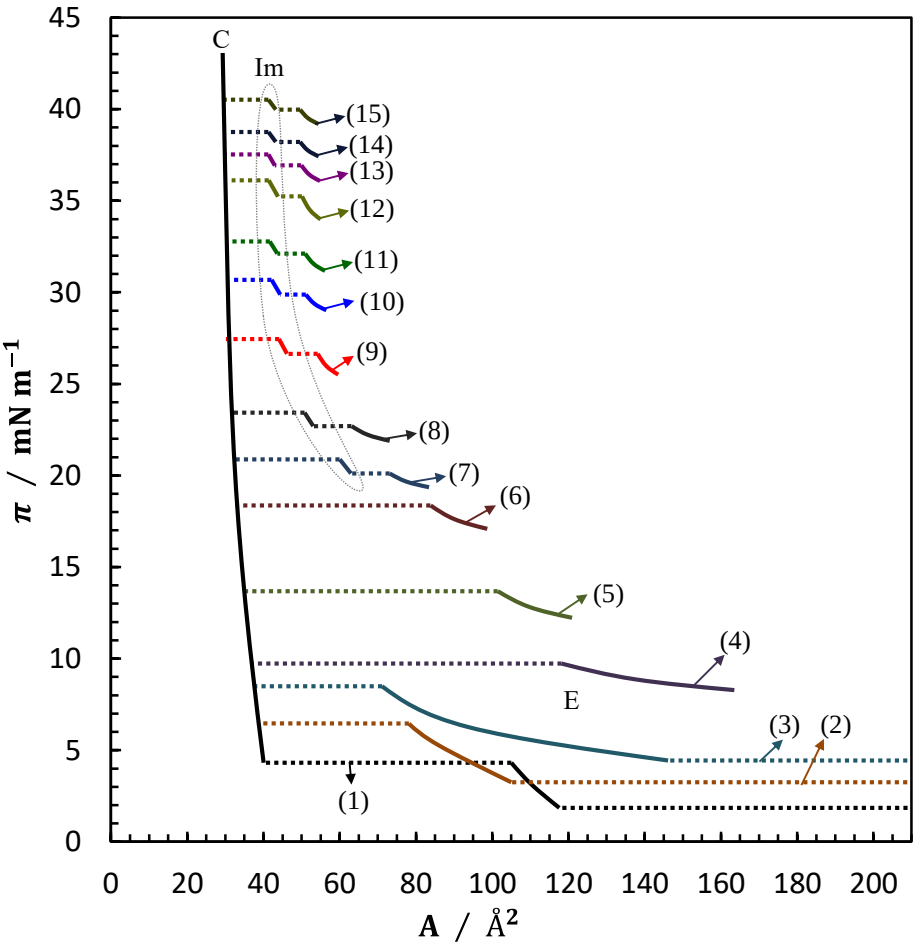

Figure 2-18. The π vs. A curves at given (1) $m_{\mathrm{PC}}^{\mathrm{w}} = 0$ (pure Chol system), (2) 0.001, (3) 0.0015, (4) 0.002, (5) 0.003, (6) 0.004, (7) 0.005, (8) 0.007, (9) 0.01, (10) 0.015, (11) 0.02, (12) 0.03, (13) 0.04, (14) 0.05, and (15) at 0.06 mmol kg^{-1}. The part of curve corresponding to the G state at $m_{\mathrm{PC}}^{\mathrm{w}} = 0{\sim}0.015$ mmol kg^{-1} located at $A > 450$ $\mathrm{Å}^2$ are not shown.

These properties are similar to those observed for Liquid condensed (LC) state of Langmuir monolayer[9,61], in which molecules are aligned regularly to each other but their hydrophobic chains have gauche defects. In addition, Langmuir film of pure Chol exhibits G and C phases, and that of mixed phospholipid (PL) – Chol systems takes liquid expanded (corresponding to the E state in this study) and LC phases[61–63]. Thus it is likely that the Im state appeared in the mixed C14PC – Chol adsorbed film corresponds to the LC ones.

Now let us discuss the miscibility of C14PC and Chol molecules in the adsorbed film. For doing this, the phase diagram of adsorption (PDA), which gives the quantitative relation between the compositions in the bulk solution and adsorbed film at a given interfacial tension, was constructed by using eqs. $(2-7)\sim(2-10)$. In Figure 2-19, the PDA at $\gamma = 40,\ 35,\ 27$, and $15\ \mathrm{mN\ m^{-1}}$ are shown. The blue and red lines represent respectively the m vs. X_{Ch} and m vs. $X_{\mathrm{Ch}}^{\mathrm{H}}$ curves. The total molality at the phase transition point m^{eq} vs. X_{Ch} curves of four kinds of phase transitions was drawn in Figure 2-20. The $X_{\mathrm{Ch}}^{\mathrm{H}}$ value increases with increasing X_{Ch} and changes discontinuously at the phase transition points. It is realized that C14PC and Chol molecules are miscible with each other in all film states from a macroscopic viewpoint and that Chol molecules are richer in the order of C, Im, and E states. In particular, the $X_{\mathrm{Ch}}^{\mathrm{H}}$ value in the C state is ~ 0.45 at $\gamma = 15\ \mathrm{mN\ m^{-1}}$, suggesting that C14PC and Chol molecules are mixed with almost equimolar ratio.

The mixing of molecules in the adsorbed film was further examined by estimating the activity coefficient of each component in the adsorbed film of α state, $f_i^{\mathrm{H},\alpha}$ ($i = \mathrm{PC}$, Ch and $\alpha = \mathrm{E},\ \mathrm{C}$) by using eq. $(2-8)$. The results are summarized in Figure 2-21.

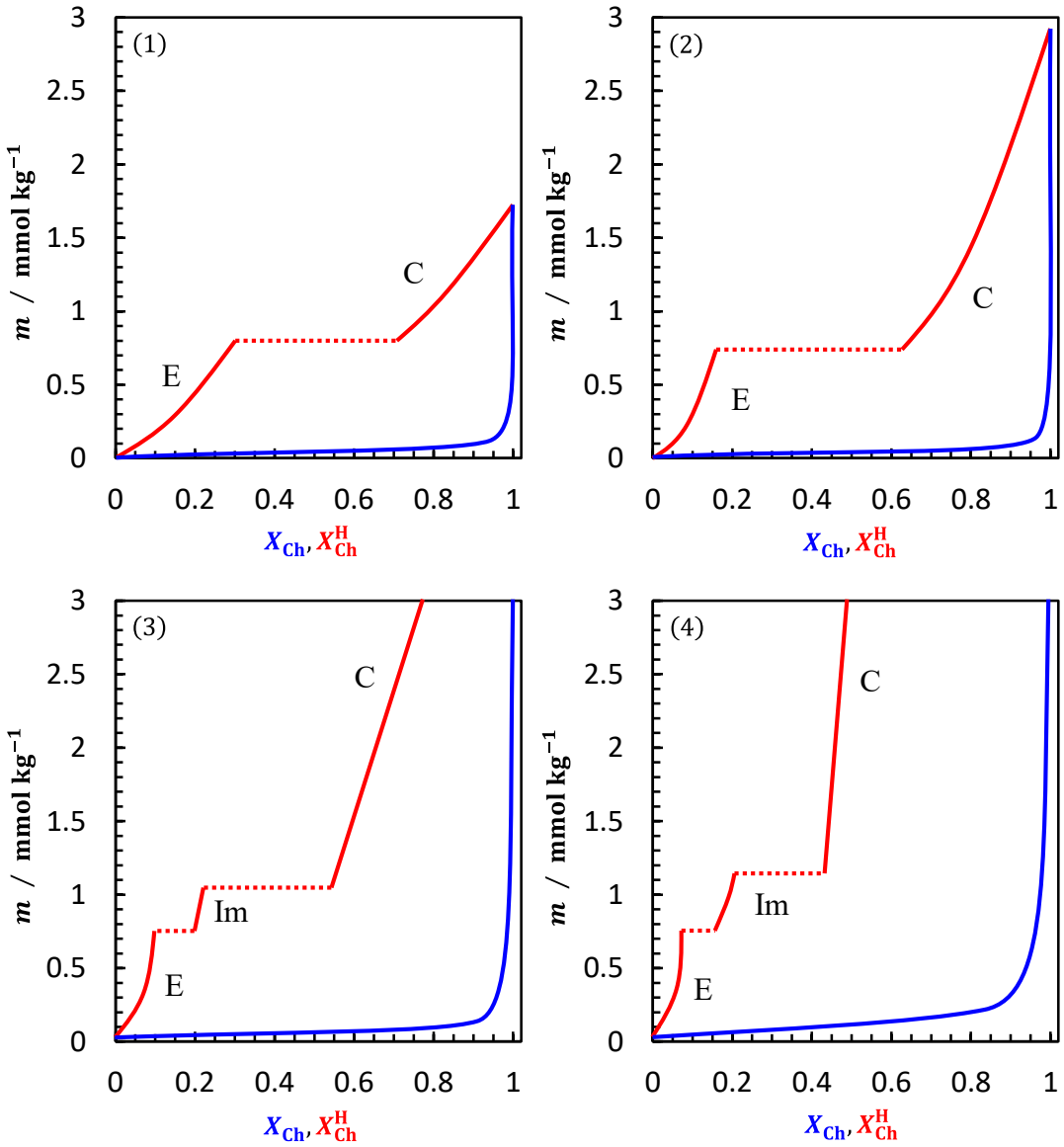

Figure 2-19. The phase diagrams of adsorption at given (1) $\gamma = 40$, (2) 35, (3) 27, (4) 15 mN m^{-1}. The m vs. $X_{\mathrm{Ch}}^{\mathrm{H}}$ and m vs. X_{Ch} curves intersect at $(m, X_{\mathrm{Ch}}) = (6.5, 1)$ in Figure (3) and at $(m, X_{\mathrm{Ch}}) = (22.6, 1)$ in Figure (4).

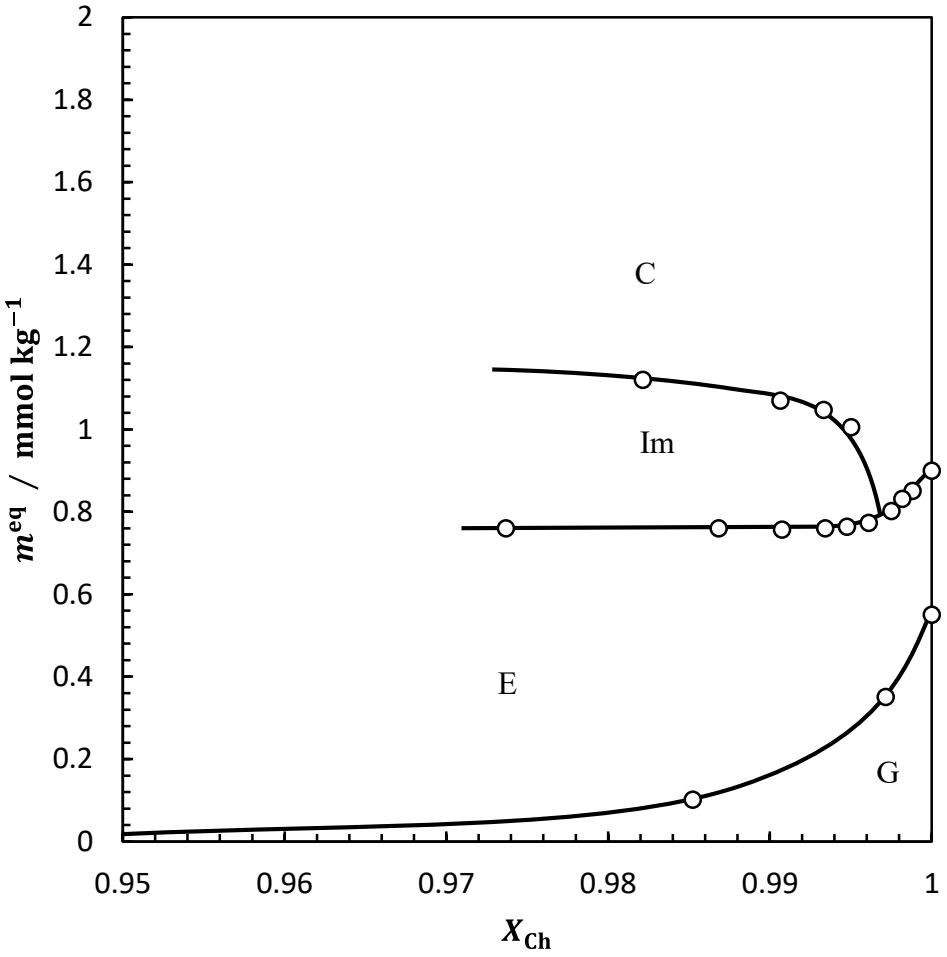

Figure 2-20. The m^{eq} vs. X_{Ch} curve.

In the E state, the $f_{\mathrm{PC}}^{\mathrm{H,E}}$ value is slightly larger or very close to unity, indicating that an intermolecular interaction between different molecules is very similar to those between the same ones. In the C state, on the other hand, the $f_{\mathrm{Ch}}^{\mathrm{H,C}}$ value is much smaller than unity. Taking account of that the interaction between C14PC molecules is repulsive because of charged PC group, this is due to the strong interaction between C14PC and Chol molecules, such as hydrogen bonding between the head groups as claimed by Takajo *et al.* and Pan *et al.*[64,65].

Here, let us examine the phase transition found in the mixed C14PC – Chol system thermodynamically. When two states α and β coexist in the adsorbed film at the phase transition point, the following equations hold simultaneously at constant T and p[66],

$$d\gamma^{\mathrm{eq}} = -\Gamma_{\mathrm{PC}}^{\mathrm{H},\alpha}\left(\frac{RT}{m_{\mathrm{PC}}^{\mathrm{w,eq}}}\right)dm_{\mathrm{PC}}^{\mathrm{w,eq}} - \Gamma_{\mathrm{Ch}}^{\mathrm{H},\alpha}\left(\frac{RT}{m_{\mathrm{Ch}}^{\mathrm{o,eq}}}\right)dm_{\mathrm{Ch}}^{\mathrm{o,eq}} \qquad (2-24)$$

and

$$d\gamma^{\mathrm{eq}} = -\Gamma_{\mathrm{PC}}^{\mathrm{H},\beta}\left(\frac{RT}{m_{\mathrm{PC}}^{\mathrm{w,eq}}}\right)dm_{\mathrm{PC}}^{\mathrm{w,eq}} - \Gamma_{\mathrm{Ch}}^{\mathrm{H},\beta}\left(\frac{RT}{m_{\mathrm{Ch}}^{\mathrm{o,eq}}}\right)dm_{\mathrm{Ch}}^{\mathrm{o,eq}} \qquad (2-25)$$

Eliminating $d\gamma^{\mathrm{eq}}$ from eqs. $(2-24)$ into $(2-25)$ gives following equation

$$\left(\frac{\partial m_{\mathrm{Ch}}^{\mathrm{o,eq}}}{\partial m_{\mathrm{PC}}^{\mathrm{w,eq}}}\right)_{T,p} = -\frac{m_{\mathrm{Ch}}^{\mathrm{o,eq}}}{m_{\mathrm{PC}}^{\mathrm{w,eq}}}\left(\frac{\Gamma_{\mathrm{PC}}^{\mathrm{H},\beta} - \Gamma_{\mathrm{PC}}^{\mathrm{H},\alpha}}{\Gamma_{\mathrm{Ch}}^{\mathrm{H},\beta} - \Gamma_{\mathrm{Ch}}^{\mathrm{H},\alpha}}\right) \qquad (2-26)$$

This equation tells us that the slope of $m_{\mathrm{Ch}}^{\mathrm{o,eq}}$ vs. $m_{\mathrm{PC}}^{\mathrm{w,eq}}$ curves in Figure 2-22 is related to the changes in the interfacial densities of individual components associated with the phase transition (see Figures 2-15 and 2-16, respectively). Three possibilities are extracted as fallows;

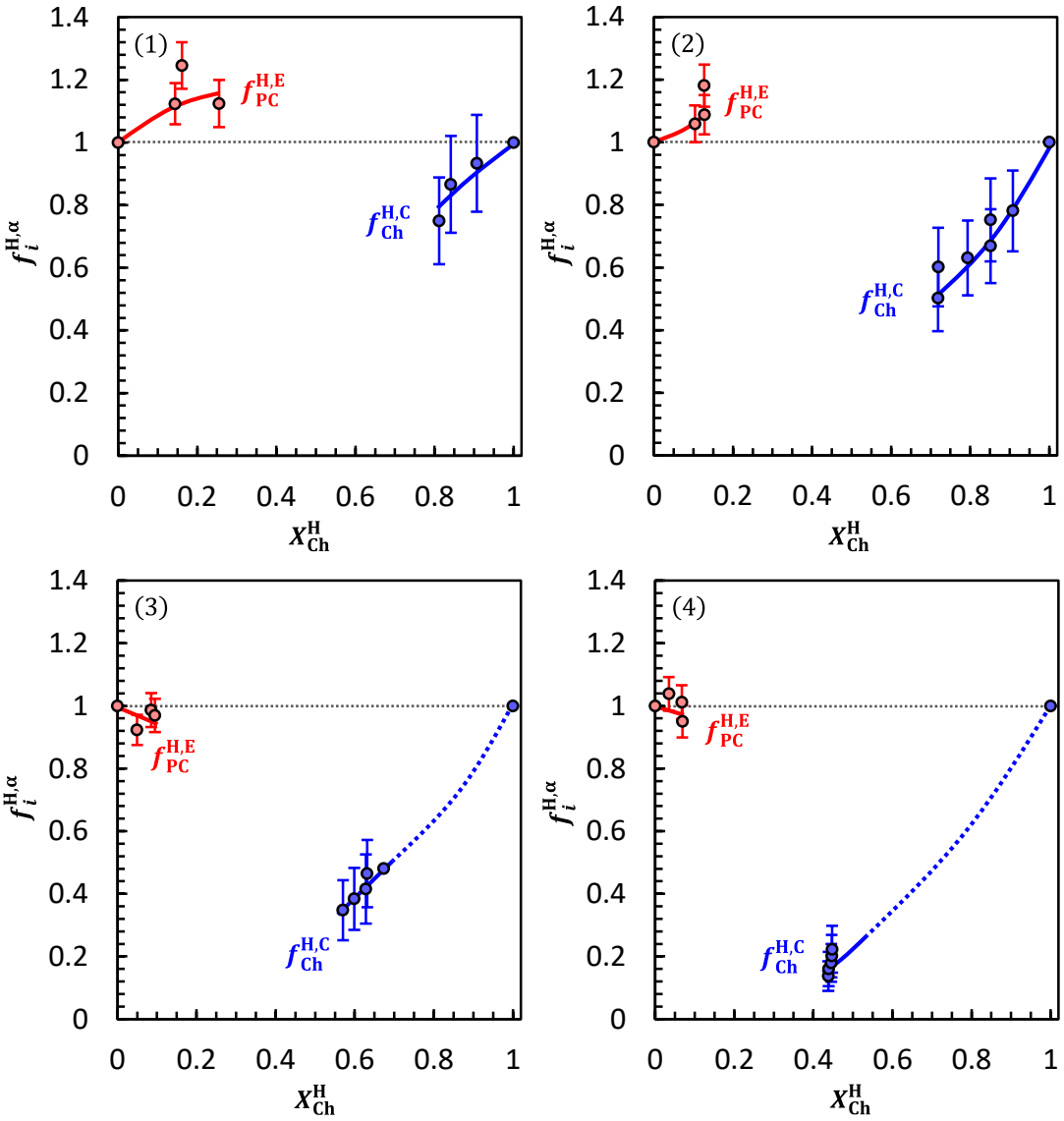

Figure 2-21. An activity coefficient of component i (i = PC or Ch) in the α (E or C) state at given (1) γ = 40, (2) 35, (3) 27, and (4) 15 mN m^{-1}.

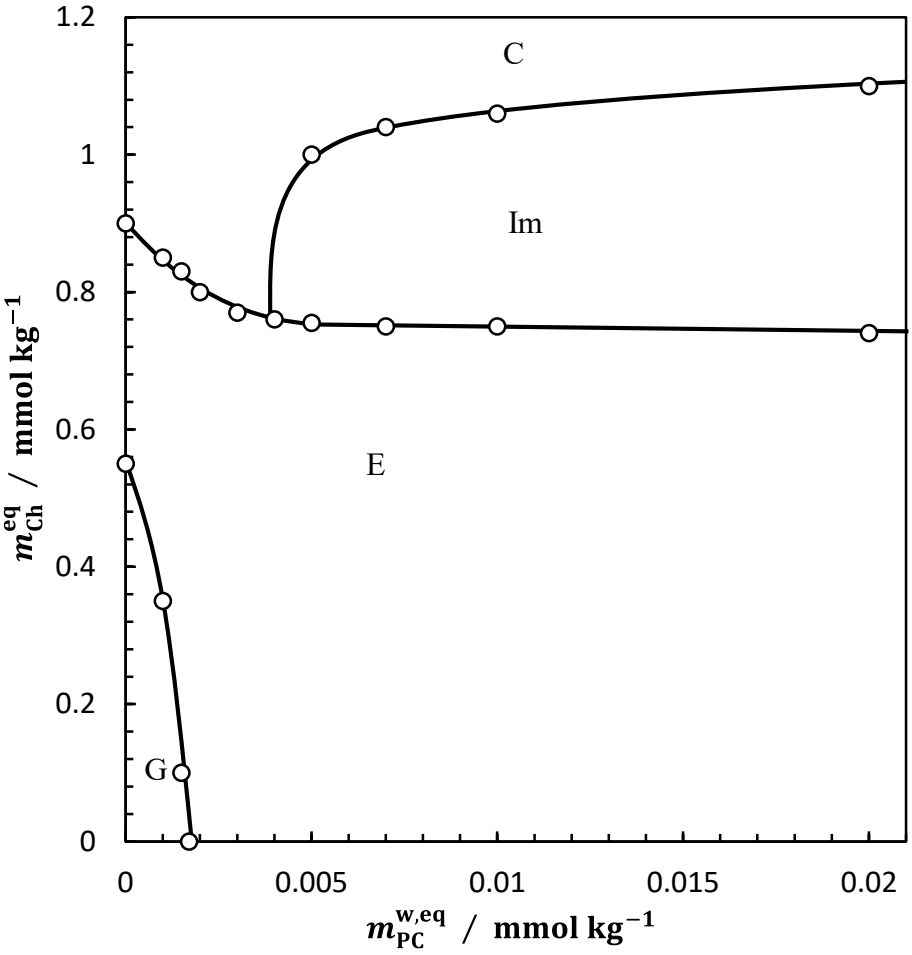

Figure 2-22. The $m_{\mathrm{Ch}}^{\mathrm{o,eq}}$ vs. $m_{\mathrm{PC}}^{\mathrm{w,eq}}$ curves.

$$\left(\frac{\partial m_{\mathrm{Ch}}^{\mathrm{o,eq}}}{\partial m_{\mathrm{PC}}^{\mathrm{w,eq}}}\right)_{T,p} > 0 \quad \Rightarrow (\mathrm{a}) \begin{cases} \Gamma_{\mathrm{PC}}^{\mathrm{H},\beta} - \Gamma_{\mathrm{PC}}^{\mathrm{H},\alpha} < 0 \\ \Gamma_{\mathrm{Ch}}^{\mathrm{H},\beta} - \Gamma_{\mathrm{Ch}}^{\mathrm{H},\alpha} > 0 \end{cases} \quad \text{or} \quad (\mathrm{b}) \begin{cases} \Gamma_{\mathrm{PC}}^{\mathrm{H},\beta} - \Gamma_{\mathrm{PC}}^{\mathrm{H},\alpha} > 0 \\ \Gamma_{\mathrm{Ch}}^{\mathrm{H},\beta} - \Gamma_{\mathrm{Ch}}^{\mathrm{H},\alpha} < 0 \end{cases} \qquad \text{(A)}$$

$$\left(\frac{\partial m_{\mathrm{Ch}}^{\mathrm{o,eq}}}{\partial m_{\mathrm{PC}}^{\mathrm{w,eq}}}\right)_{T,p} < 0 \quad \Rightarrow (\mathrm{a}) \begin{cases} \Gamma_{\mathrm{PC}}^{\mathrm{H},\beta} - \Gamma_{\mathrm{PC}}^{\mathrm{H},\alpha} > 0 \\ \Gamma_{\mathrm{Ch}}^{\mathrm{H},\beta} - \Gamma_{\mathrm{Ch}}^{\mathrm{H},\alpha} > 0 \end{cases} \quad \text{or} \quad (\mathrm{b}) \begin{cases} \Gamma_{\mathrm{PC}}^{\mathrm{H},\beta} - \Gamma_{\mathrm{PC}}^{\mathrm{H},\alpha} < 0 \\ \Gamma_{\mathrm{Ch}}^{\mathrm{H},\beta} - \Gamma_{\mathrm{Ch}}^{\mathrm{H},\alpha} < 0 \end{cases} \qquad \text{(B)}$$

$$\left(\frac{\partial m_{\mathrm{Ch}}^{\mathrm{o,eq}}}{\partial m_{\mathrm{PC}}^{\mathrm{w,eq}}}\right)_{T,p} \approx 0 \quad \Rightarrow \quad \Gamma_{\mathrm{PC}}^{\mathrm{H},\beta} - \Gamma_{\mathrm{PC}}^{\mathrm{H},\alpha} \approx 0 \qquad \text{(C)}$$

In the case A, the interfacial density of one component increases and that of the other decreases at the transition point. In case B, the interfacial densities of both components increase or decrease at the transition point. The case C indicates that the interfacial density of Chol changes discontinuously and that of C14PC does continuously accompanied by the phase transition. When α and β represent respectively E and C states, according to the results of $\Gamma_{\mathrm{PC}}^{\mathrm{H}}$ and $\Gamma_{\mathrm{Ch}}^{\mathrm{H}}$ a right hand side (rhs) of eq. $(2-26)$ is expected to be -30 ± 2.5 at $m_{\mathrm{PC}}^{\mathrm{w,eq}} = 0.002$ mmol kg^{-1} and thus the E – C transition corresponds to the case B-a. This value is good agreement with a left hand side (lhs) of the eq. $(2-26)$ of -29.0 ± 3.5. On the other hand, Im – C transition ($\alpha =$ Im, $\beta =$ C) requires the case A-a because $\Gamma_{\mathrm{Ch}}^{\mathrm{H,C}} - \Gamma_{\mathrm{Ch}}^{\mathrm{H,Im}} > 0$ holds. Our experimental data shows that a lhs is 18.0 ± 8.0 at $m_{\mathrm{PC}}^{\mathrm{w,eq}} = 0.005$ mmol kg^{-1}. Since $\Gamma_{\mathrm{Ch}}^{\mathrm{H,C}} - \Gamma_{\mathrm{Ch}}^{\mathrm{H,Im}} \approx 2.3$ μmol m^{-2} at the transition, the $\Gamma_{\mathrm{PC}}^{\mathrm{H,C}} - \Gamma_{\mathrm{PC}}^{\mathrm{H,Im}}$ value should be 0.1~0.3 μmol m^{-2}. This small difference in $\Gamma_{\mathrm{PC}}^{\mathrm{H}}$ cannot be detected as a break point on the γ vs. $m_{\mathrm{PC}}^{\mathrm{w}}$ curve within an experimental error in γ value (± 0.05 mN m^{-1}). The E – Im and Im – C transitions at high $m_{\mathrm{PC}}^{\mathrm{w,eq}}$ corresponds to the case C, indicating that the change in $\Gamma_{\mathrm{PC}}^{\mathrm{H}}$ is negligibly small even when $\Gamma_{\mathrm{Ch}}^{\mathrm{H}}$ increases discontinuously at the transition point. Our experimental results satisfy this requirement.

Structure of Mixed Adsorbed Film

X-ray reflectivity measurement was applied to examine microscopic structure of the mixed film. Figures 2-23 ~ 2-28 show the $R/R_F\,(Q_z)$ plots at various $m_{\mathrm{Ch}}^{\mathrm{o}}$ under fixed $m_{\mathrm{PC}}^{\mathrm{w}} = 0.002, 0.005,$ and $0.03\ \mathrm{mmol\,kg^{-1}}$ and the corresponding electron density profiles. The parameters fitted by slab models are summarized in Table 2-3. The R/R_F vs. Q_z plots in the E state were fitted well by two-slab, and those in the Im and C states was by three-slab models.

In the E state, the L_1 and ρ_1/ρ_{w} values of slab 1 are almost identical with those of the pure C14PC film and therefore the head groups take a staggered arrangement at the interface. The ρ_2/ρ_{w} value (0.71) is a little larger than the electron density of bulk hexane phase ($\rho_{\mathrm{h}}/\rho_{\mathrm{w}} = 0.68$) and close to that estimated for the mixture sterol ring and liquid tetradecane (0.74 ± 0.01). The L_2 value is nearly equal to the length of sterol ring. These indicates that in the E state, Chol molecules mix with C14PC ones taking staggered arrangement as shown in Figures 2-26 ~ 2-28.

The film structure of C is very different from that of E state. Noticeable differences are as follows. (i) L_1 value (5.7 Å) is much smaller in the C state than in the E one and almost equal to the height of PC groups (~5.6 Å). (ii) The ρ_2/ρ_{w} value is much larger in the C state than in the E one and close to the estimated value for the 1:1 mixture of sterol ring and liquid-ordered tetradecane with all-trans conformation[37]. (iii) Slab 3 is needed to fit $R/R_F\,(Q_z)$ plots and ρ_3/ρ_{w} value is similar to that of liquid-ordered alkane. Thus, it is plausible C14PC and Chol molecules are densely packed and orient almost normal to the interface to form solid-like film. This molecular arrangement is primarily due to the hydrogen bonding of PC with OH groups and the van der Waals interaction induced by effective packing of sterol and hydrocarbon chains of C14PC.

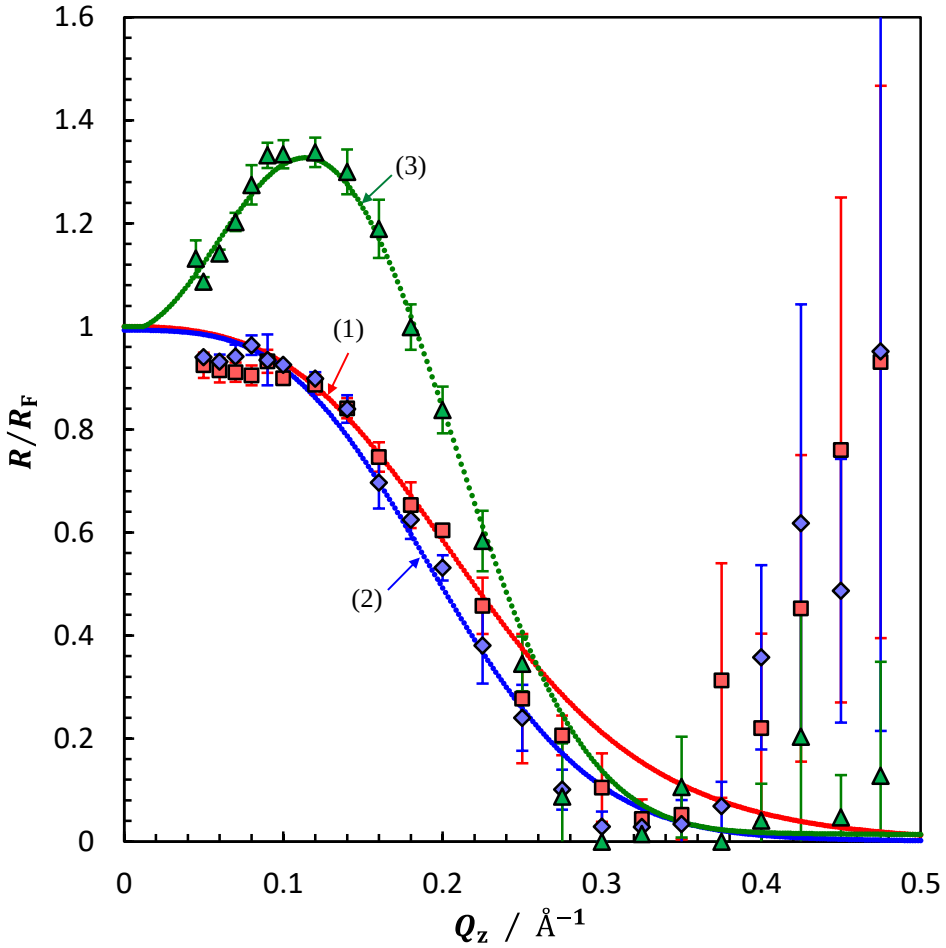

Figure 2-23. The $R/R_F\,(Q_z)$ plots $m_{PC}^{w} = 0.002$ at (1) $m_{Ch}^{o} = 0.8$, (2) 1.0, and (3) at 2.0 mmol kg^{-1}. The dotted lines represent the best fitting curves.

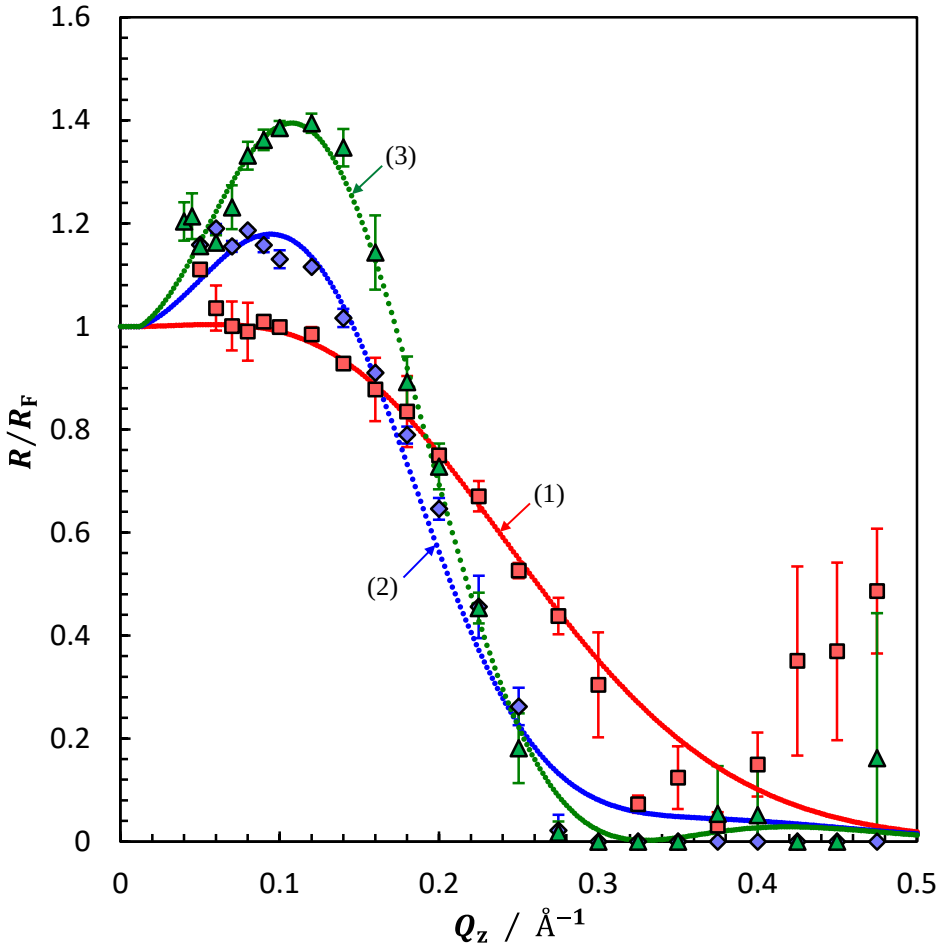

Figure 2-24. The $R/R_F\,(Q_z)$ plots $m_{\mathrm{PC}}^{\mathrm{w}} = 0.005$ at (1) $m_{\mathrm{Ch}}^{\mathrm{o}} = 0.2$, (2) 1.0, and (3) at 2.0 mmol kg^{-1}. The dotted lines represent the best fitting curves.

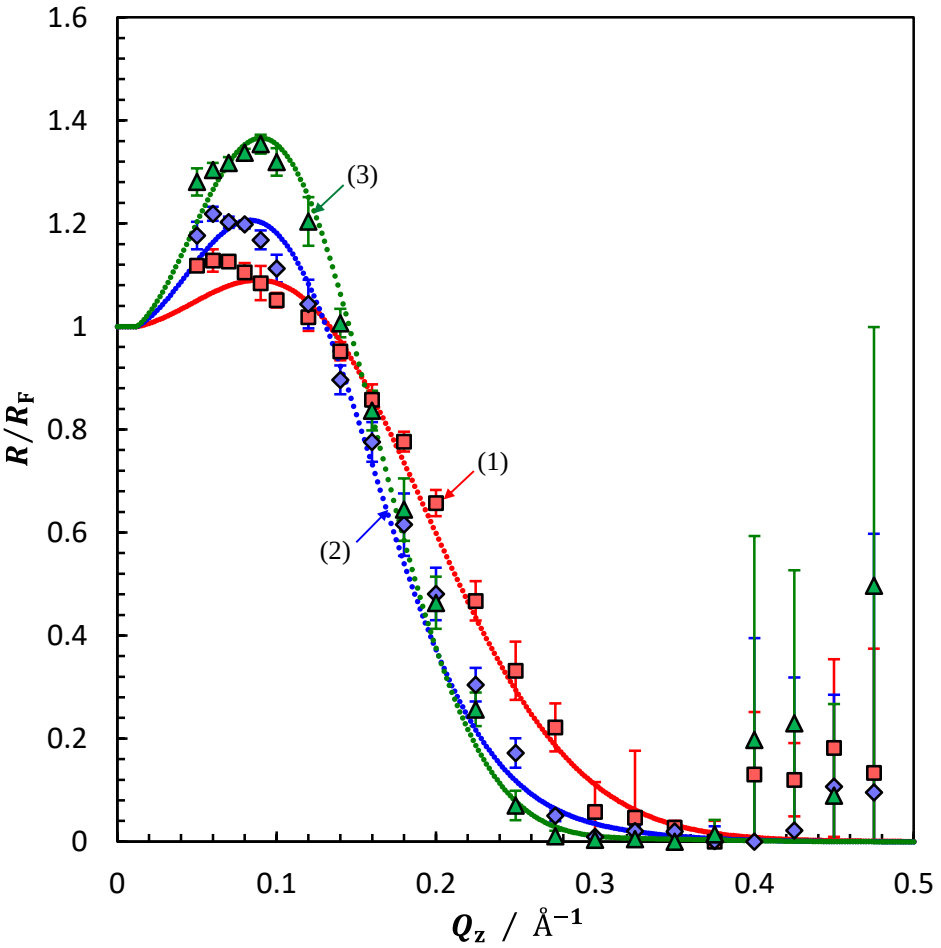

Figure 2-25. The $R/R_F\,(Q_z)$ plots $m_{PC}^{w} = 0.03$ at (1) $m_{Ch}^{o} = 0.2$, (2) 1.0, and (3) at 2.0 mmol kg^{-1}. The dotted lines represent the best fitting curves.

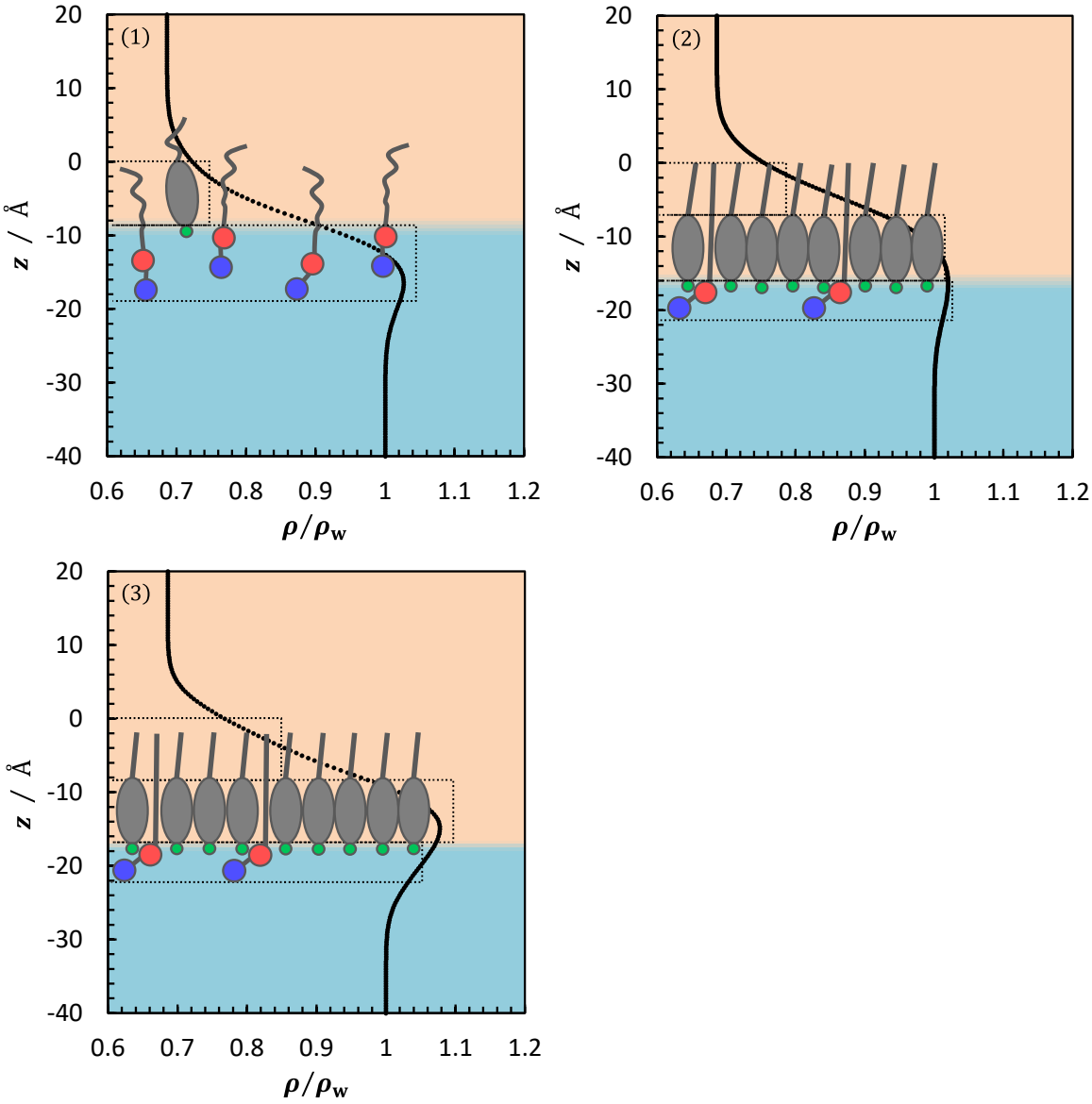

Figure 2-26. The electron density profiles normal to the interface under $m_{\mathrm{PC}}^{\mathrm{w}} = 0.002$ at (1) $m_{\mathrm{Ch}}^{\mathrm{o}} = 0.8$, (2) 1.0, and (3) at 2.0 mmol kg^{-1}.

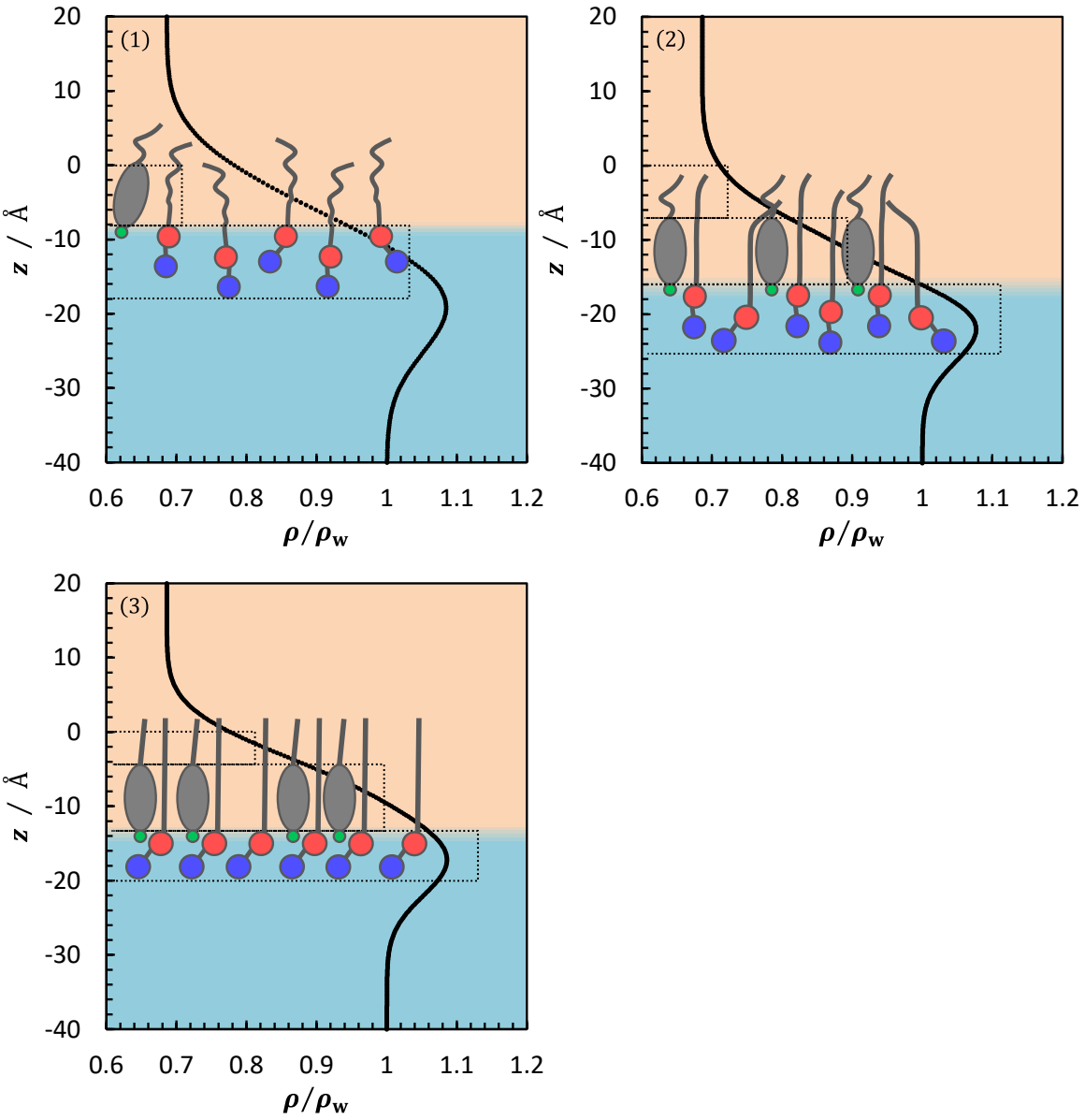

Figure 2-27. The electron density profiles normal to the interface under given $m_{\mathrm{PC}}^{\mathrm{w}} = 0.005$ at (1) $m_{\mathrm{Ch}}^{\mathrm{o}} = 0.2$, (2) 1.0, and (3) at 2.0 mmol kg^{-1}.

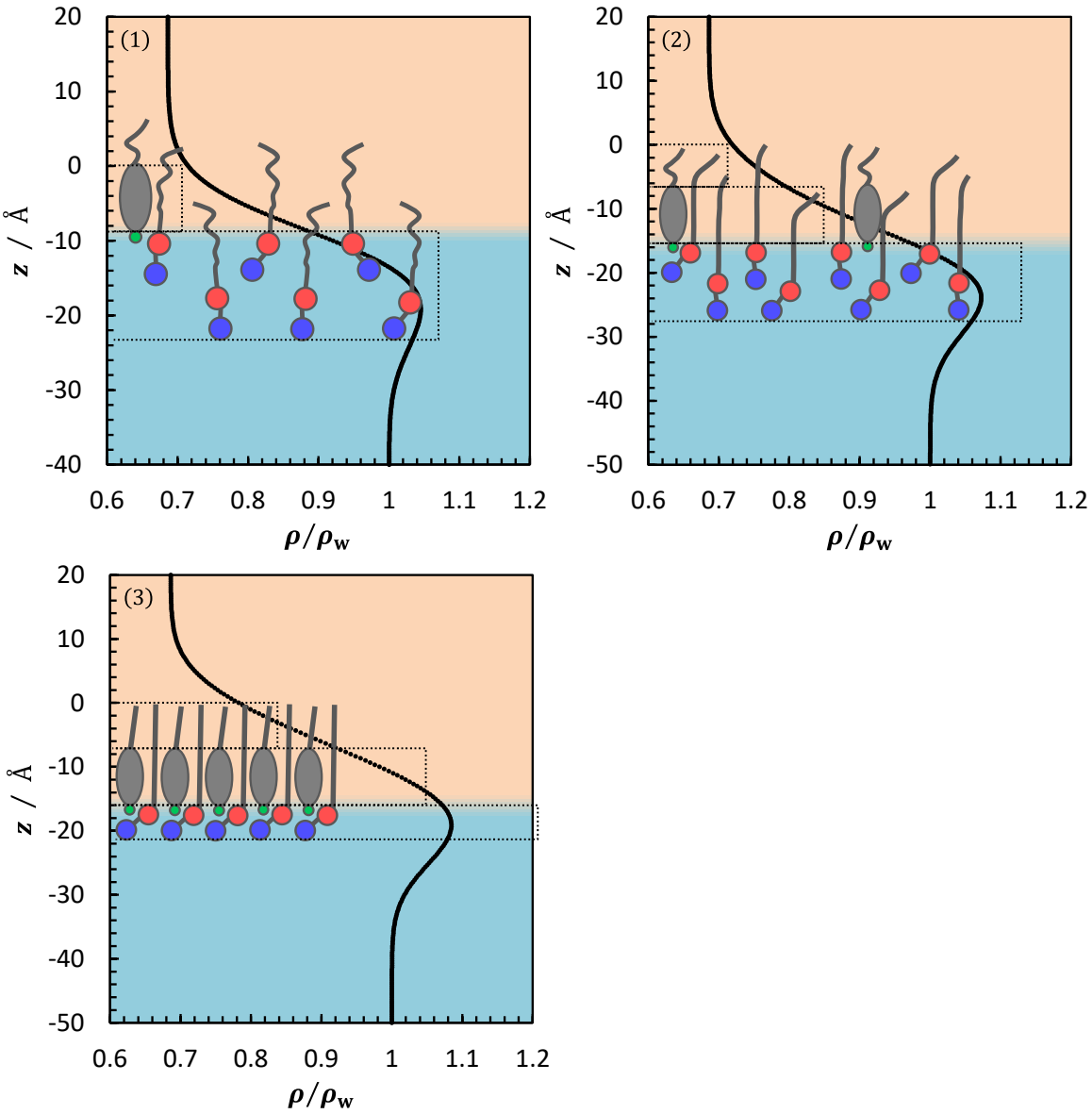

Figure 2-28. The electron density profiles normal to the interface at given $m_{\mathrm{PC}}^{\mathrm{w}} = 0.03$ at (1) $m_{\mathrm{Ch}}^{\mathrm{o}} = 0.2$, (2) 1.0, and (3) at 2.0 mmol kg^{-1}.

Table 2-3 The fitting parameters for the slab model. The ρ/ρ_{w} and σ (σ_{cap}) value was calculated using Γ^{H},$X_{\mathrm{Ch}}^{\mathrm{H}}$, and γ, and was put into parentheses.

$m_{\mathrm{PC}}^{\mathrm{w}}$ / mmol kg^{-1}	$m_{\mathrm{Ch}}^{\mathrm{o}}$ / mmol kg^{-1}	Film state	$X_{\mathrm{Ch}}^{\mathrm{H}}$	Slab 1 = PC group + water			Slab 2 = Sterol + chain (+hexane)			Slab 3 = Tail + chain (+hexane)		
				L_1 / Å	ρ_1/ρ_{w}	σ_1,σ_2 / Å^{-1}	L_2 / Å	ρ_2/ρ_{w}	σ_2,σ_3 / Å^{-1}	L_3 / Å	ρ_3/ρ_{w}	σ_3,σ_4 / Å^{-1}
0.002	0.8	E	0.3	10.4	1.05 (1.05 ± 0.03)	4.0 (3.9 ± 0.1)	8.4	0.75 (0.72 ± 0.01)	4.0 (3.9 ± 0.1)			
	1.0	C	0.8	5.6	1.03 (1.11)	4.1 (3.9 ± 0.1)	9.0	1.02 (1.07 ± 0.03)	4.1 (3.9 ± 0.1)	6.0	0.79 (0.83 ± 0.02)	4.1 (3.9 ± 0.1)
	2.0	C	0.9	5.8	1.06 (1.1)	3.7 (4.2 ± 0.1)	8.3	1.10 (1.07 ± 0.03)	3.7 (4.2 ± 0.1)	8.2	0.84 (0.83 ± 0.02)	3.7 (4.2 ± 0.1)
0.005	0.2	E	0.07	10.1	1.06 (1.10)	4.0 (4.5 ± 0.2)	8.1	0.71 (0.75 ± 0.01)	4.0 (4.5 ± 0.2)			
	1.0	Im	0.3	9.6	1.11 (1.10)	4.0 (4.6 ± 0.2)	8.9	0.90 (0.84 ± 0.01)	4.0 (4.6 ± 0.2)	7.2	0.72 (0.73 ± 0.01)	4.0 (4.6 ± 0.2)
	2.0	C	0.65	6.9	1.15 (1.13)	4.4 (4.6 ± 0.2)	9.0	1.00 (1.01 ± 0.02)	4.4 (4.6 ± 0.2)	4.7	0.81 (0.82 ± 0.02)	4.4 (4.6 ± 0.2)
0.03	0.2	E	0.04	14.2	1.07 (1.09 ± 0.02)	5.4 (6.2 ± 0.2)	8.8	0.71 (0.74 ± 0.01)	5.4 (6.2 ± 0.2)			
	1.0	Im	0.2	12.0	1.13 (1.17)	5.8 (6.6 ± 0.3)	9.1	0.85 (0.85 ± 0.01)	5.8 (6.6 ± 0.3)	6.6	0.72 (0.71 ± 0.01)	5.8 (6.6 ± 0.3)
	2.0	C	0.44	5.7	1.21 (1.25)	6.0 (7.1 ± 0.4)	8.6	1.05 (0.97 ± 0.02)	6.0 (7.1 ± 0.4)	7.7	0.84 (0.82 ± 0.01)	6.0 (7.1 ± 0.4)

Concerning the Im state, L_1 and ρ_2/ρ_w values are intermediate in between those of E and C states, even though L_2 is very close to each other. Furthermore, the ρ_3/ρ_w ($=0.72$) value of Im state is smaller than that of C state and almost equal to the calculated value for the liquid mixture of sterol ring, tetradecane, and hexane molecules. These suggest that the packing of molecules in Im state is looser compared to that in C state, and hexane molecules are intercalated between adsorbed C14PC and Chol molecules in the upper part of the adsorbed film as schematically illustrated in Figures 2-27 and 2-28.

Domain Formation in Mixed Adsorbed Film

The heterogeneous structure of the mixed film was observed at various concentrations around E – C phase transition points by BAM. In Figure 2-29, the points at which dark domain was observed were denoted by yellow stars and those of homogeneous images by red stars. Some typical images at $m_{PC}^{w} = 0.001\sim0.004$ under fixed $m_{Ch}^{o} = 1.2$ mmol kg^{-1} are shown in Figure 2-30. Circular dark domains less than 20 μm are surrounded by bright region, which looks very similar to those observed in the pure Chol system.

A median of domain radius was estimated from the size distribution over at least 100 domains and assigned to R_{eq}, as plotted against m_{PC}^{w} in Figure 2-31. R_{eq} values are smaller in the mixed system than in the pure Chol one. Then the coverages of the dark domain C_{BAM} was estimated to be $0.05\sim0.1$.

Here, let us estimate the composition of coexisting E and C domains. By assuming that the interfacial density of E domain is equal to that of E state at the E – C transition point and that the structure of C domain is as same as that in the C state at high m_{Ch}^{o} (ex. 2.0 mmol kg^{-1}) at which the interfacial density converges into a saturated value,

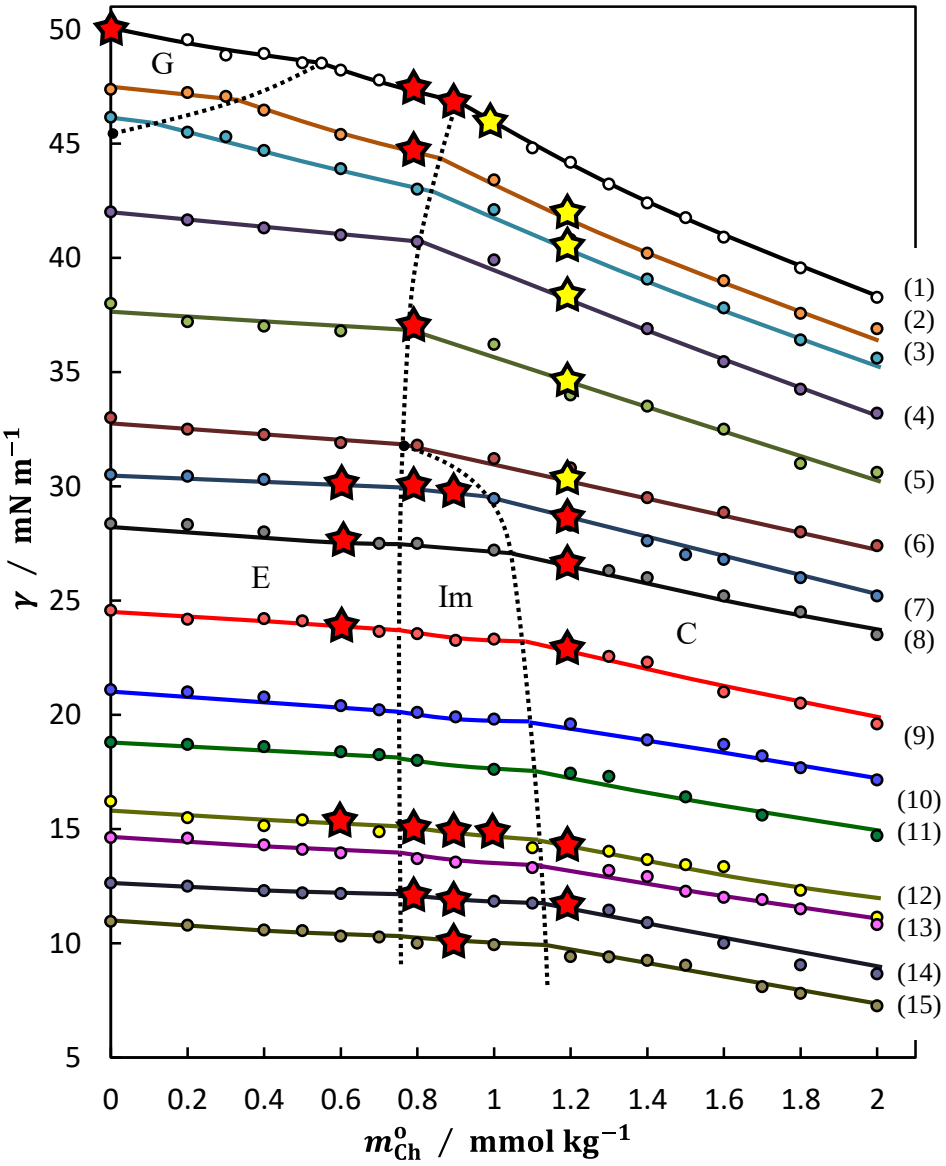

Figure 2-29. The concentration map based on Figure 2-13. The yellow and red stars indicate the concentrations at which domains are observed and are not by BAM, respectively.

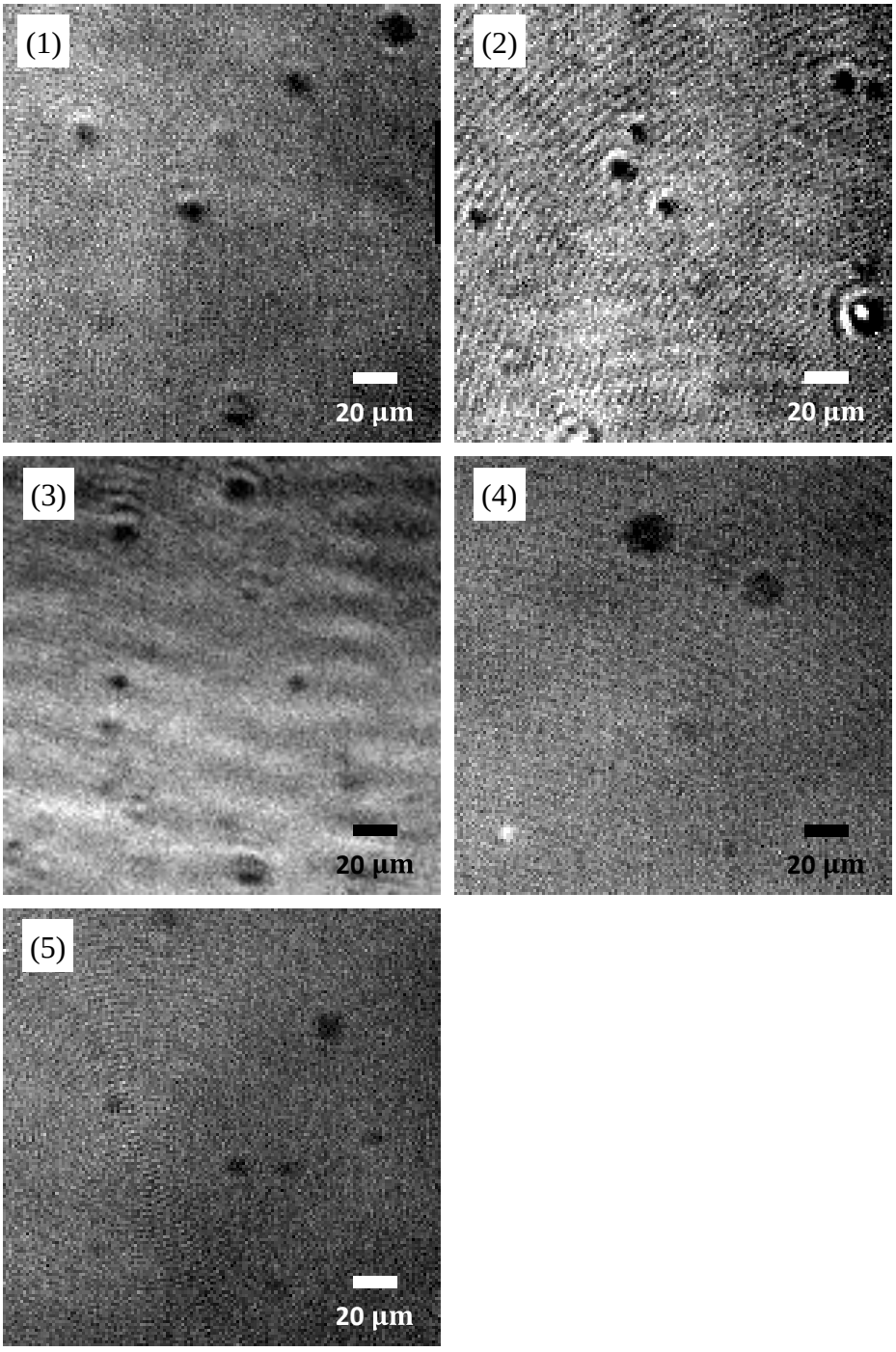

Figure 2-30. Typical images of the mixed film under fixed $m_{\mathrm{Ch}}^{\mathrm{o}} = 1.2$ at (1) $m_{\mathrm{PC}}^{\mathrm{w}} =$ 0.001, (2) 0.0015, (3) 0.002, (4) 0.003, and (5) at 0.004 mmol kg^{-1}.

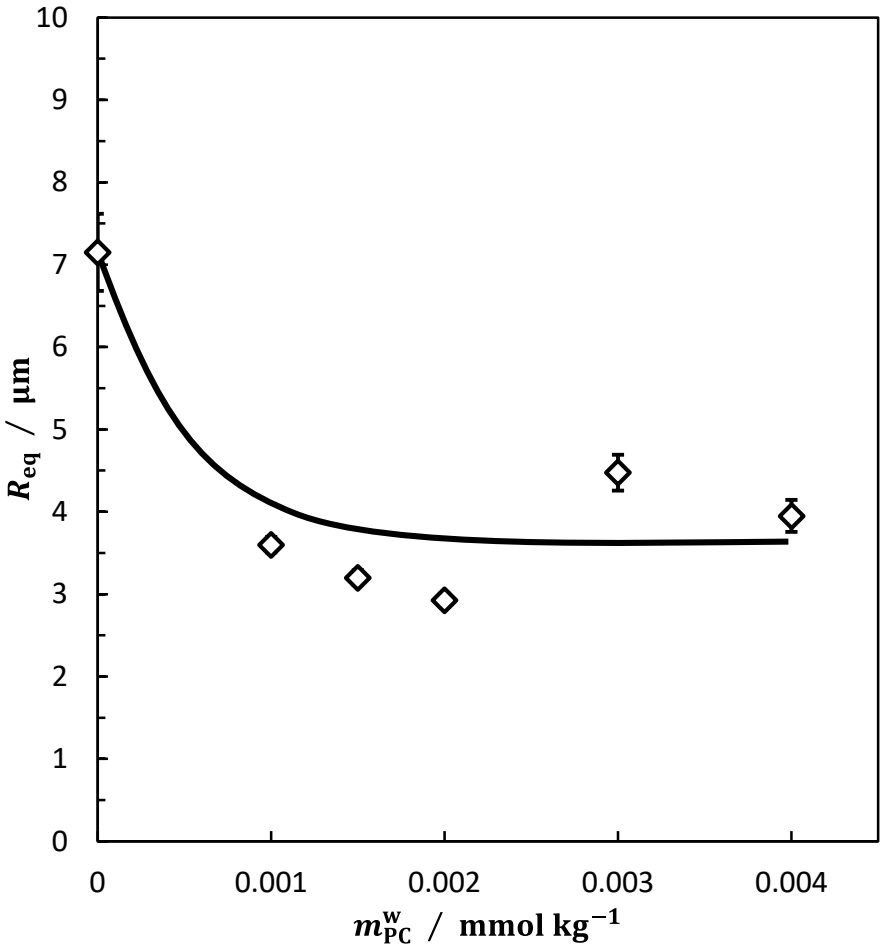

Figure 2-31. Equilibrium domain radius R_{eq} vs. $m_{\mathrm{PC}}^{\mathrm{w}}$ curve at given $m_{\mathrm{Ch}}^{\mathrm{o}} = 1.2$ except the value at $m_{\mathrm{PC}}^{\mathrm{w}} = 0$ and at $m_{\mathrm{Ch}}^{\mathrm{o}} = 1.0$ mmol kg^{-1}.

the interfacial densities of component i in the E and C domains are related to the coverage of them by

$$\Gamma_{i,\mathrm{BAM}}^{\mathrm{H}} = C_{\mathrm{BAM}}\Gamma_{i,\mathrm{BAM}}^{\mathrm{H,E}} + (1 - C_{\mathrm{BAM}})\Gamma_{i,\mathrm{BAM}}^{\mathrm{H,C}} \ . \qquad (2-27)$$

Since interfacial density of component i Γ_i^{H} was already evaluated from the interfacial tension data, if $\Gamma_{i,\mathrm{BAM}}^{\mathrm{H}}$ coinsides with Γ_i^{H}, the estimation of C_{BAM} and thus the calculation of $\Gamma_{i,\mathrm{BAM}}^{\mathrm{H,E}}$ and $\Gamma_{i,\mathrm{BAM}}^{\mathrm{H,C}}$ are reliable. The results are listed in Table 2-4 at given $m_{\mathrm{PC}}^{\mathrm{w}}$ where dark domains were observed by BAM. It is clearly seen that the agreement of both $\Gamma_{i,\mathrm{BAM}}^{\mathrm{H}}$ and Γ_i^{H} is good enough to estimate the compositions of coexisting domains.

In Figure 2-32 are plotted the composition of Chol in the E domain $X_{\mathrm{Ch}}^{\mathrm{H,E}}$ and that in C domain $X_{\mathrm{Ch}}^{\mathrm{H,C}}$ against $m_{\mathrm{PC}}^{\mathrm{w}}$. The C domain is richer in Chol than E domain, and the composition gap between them becomes larger with increasing $m_{\mathrm{PC}}^{\mathrm{w}}$, indicating that Chol molecules are more miscible with C14PC ones in the C domain mainly due to strong hydrogen bonding between OH and PC groups and effective vdW interaction of hydrophobic chains.

In the estimation of line tension in the mixed system, however, an attention should be payed to calculate τ_{el} because the value of dipole moments and their direction. In a mixed system in which the components a and b respectively have the dipole moments u_a and u_b, dipole density difference between coexisting domains u is calculated by

$$\begin{aligned} u^2 &= \left\{\left(\Gamma_a^{\mathrm{H},1}u_a + \Gamma_b^{\mathrm{H},1}u_b\right) - \left(\Gamma_a^{\mathrm{H},2}u_a + \Gamma_b^{\mathrm{H},2}u_b\right)\right\}^2 \\ &= \left(\Gamma_a^{\mathrm{H},1} - \Gamma_a^{\mathrm{H},2}\right)^2 u_a^2 + \left(\Gamma_b^{\mathrm{H},1} - \Gamma_b^{\mathrm{H},2}\right)^2 u_b^2 \\ &\quad + 2\left(\Gamma_a^{\mathrm{H},1} - \Gamma_a^{\mathrm{H},2}\right)\left(\Gamma_b^{\mathrm{H},1} - \Gamma_b^{\mathrm{H},2}\right)u_a u_b \ , \end{aligned} \qquad (2-28)$$

where the first and second terms relate respectively to the dipole – dipole repulsions

Table 2-4. The list of $\Gamma_{i,\mathrm{BAM}}^{\mathrm{H}}$ and Γ_i^{H}. In the calculation of $\Gamma_{i,\mathrm{BAM}}^{\mathrm{H}}$ by eq. $(2-27)$, $0.05{\sim}0.1$ of C_{BAM} was used.

$\boldsymbol{m_{\mathrm{PC}}^{\mathrm{w}}}$ / mmol kg^{-1}	$\boldsymbol{\Gamma_i^{\mathrm{H}}}$ / μmol m^{-2}	$\boldsymbol{\Gamma_{i,\mathrm{BAM}}^{\mathrm{H}}}$ / μmol m^{-2}
0.001	$\Gamma_{\mathrm{PC}}^{\mathrm{H}} = 0.45 \pm 0.1$ $\Gamma_{\mathrm{Ch}}^{\mathrm{H}} = 4.3 \pm 0.1$	$\Gamma_{\mathrm{PC}}^{\mathrm{H}} = 0.46 \pm 0.04$ $\Gamma_{\mathrm{Ch}}^{\mathrm{H}} = 4.2 \pm 0.1$
0.0015	$\Gamma_{\mathrm{PC}}^{\mathrm{H}} = 0.69 \pm 0.1$ $\Gamma_{\mathrm{Ch}}^{\mathrm{H}} = 3.9 \pm 0.1$	$\Gamma_{\mathrm{PC}}^{\mathrm{H}} = 0.70 \pm 0.04$ $\Gamma_{\mathrm{Ch}}^{\mathrm{H}} = 3.9 \pm 0.1$
0.002	$\Gamma_{\mathrm{PC}}^{\mathrm{H}} = 0.90 \pm 0.2$ $\Gamma_{\mathrm{Ch}}^{\mathrm{H}} = 3.9 \pm 0.1$	$\Gamma_{\mathrm{PC}}^{\mathrm{H}} = 1.02 \pm 0.05$ $\Gamma_{\mathrm{Ch}}^{\mathrm{H}} = 3.7 \pm 0.1$
0.003	$\Gamma_{\mathrm{PC}}^{\mathrm{H}} = 1.34 \pm 0.2$ $\Gamma_{\mathrm{Ch}}^{\mathrm{H}} = 3.4 \pm 0.1$	$\Gamma_{\mathrm{PC}}^{\mathrm{H}} = 1.36 \pm 0.05$ $\Gamma_{\mathrm{Ch}}^{\mathrm{H}} = 3.3 \pm 0.1$
0.004	$\Gamma_{\mathrm{PC}}^{\mathrm{H}} = 1.61 \pm 0.1$ $\Gamma_{\mathrm{Ch}}^{\mathrm{H}} = 3.2 \pm 0.1$	$\Gamma_{\mathrm{PC}}^{\mathrm{H}} = 1.63 \pm 0.04$ $\Gamma_{\mathrm{Ch}}^{\mathrm{H}} = 3.1 \pm 0.1$

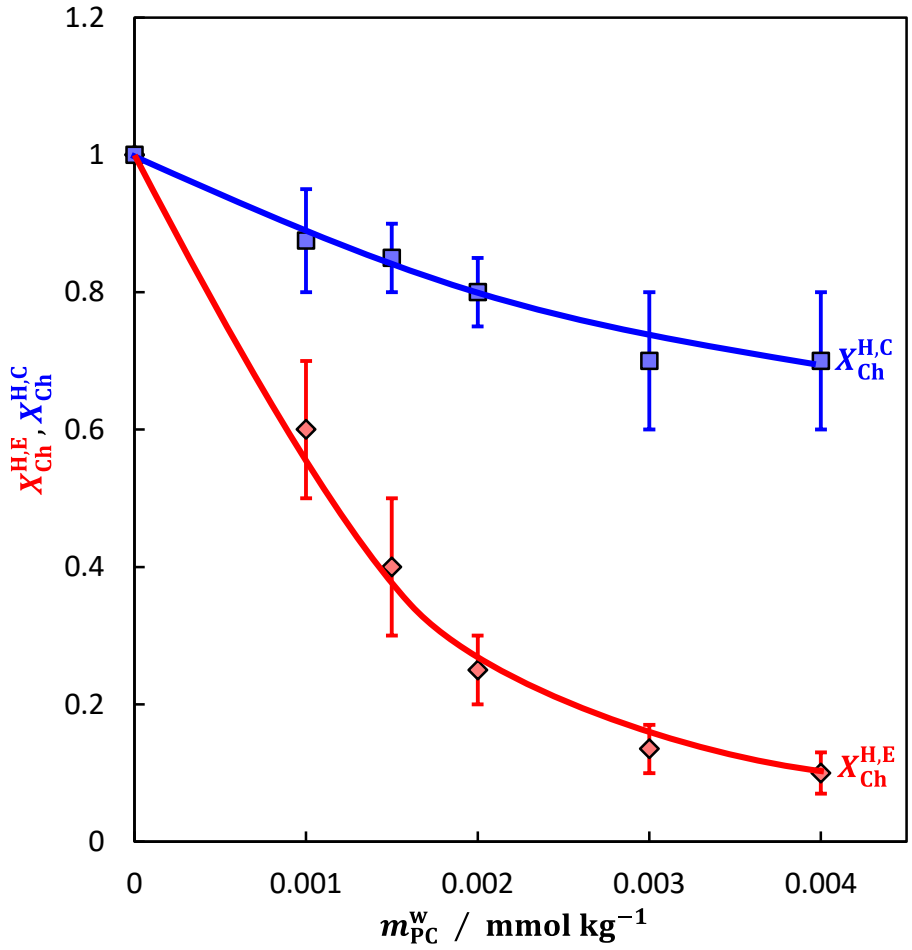

Figure 2-32. The domain compositions $X_{\mathrm{Ch}}^{\mathrm{H,\,E}}$ and $X_{\mathrm{Ch}}^{\mathrm{H,\,C}}$ calculated using the result of eq. $(2-27)$.

between the same components, and the cross term to that between components a and b. If the dipole moments u_a and u_b point to opposite directions, the cross term becomes negative, indicating the attractive interaction between a and b. Thus, the interactions between the same kinds as well as different ones should be taken into account in the mixed system and are weighted by factors of interfacial density differences to calculate u. However, so far, it is not established that the equation to count correct number and distance of pairs of dipole at a given compositions of domains and thus it is very hard to estimate accurate value of τ_{el}.

For solving or avoiding this problems, it is necessary to choose a mixed system in which the dipole moments of a mixture are similar to each other, or to establish an equation of τ_{el} which is appropriate for a mixed system. Then, in order to take an opportunity to discuss on the effect of line tension on the domain formation, in the next chapter, we employ the adsorbed film of methyl palmitate and Chol mixture at the C6/W interface, because their dipole moments are similar to each other.

2-5. *Conclusions*

In this study, the molecular miscibility and domain formation in the adsorbed film of C14PC and Chol mixture at the C6/W interface was examined by interfacial tensiometry, XR, and BAM. Noticeable points are summarized as follows;

(i) Depending on $m_{\mathrm{PC}}^{\mathrm{w}}$ and $m_{\mathrm{Ch}}^{\mathrm{o}}$, the adsorbed film takes the gaseous (G), expanded (E), condensed (C), and intermediate (Im) states. The last one corresponds to the Liquid condensed one in Langmuir monolayer.

(ii) In the E film, Chol molecules mix with C14PC ones taking staggered arrangement to reduce the repulsive interaction between charges-separated PC groups. In contrast, in the C film, they mixed and densely packed with C14PC ones being aligned in parallel with up to almost 1:1 ratio because of the hydrogen bonding and effective packing between C14PC and Chol molecules. The Im film whose $X_{\mathrm{Ch}}^{\mathrm{H}}$ is about 0.2 exhibits an intermediate packing and molecular arrangement properties between those in the E and C films.

(iii) Just above the E – C phase transition points, the hole domain with the E state are formed in the C region probably due to the preferable interaction between Chol and hexane solvent. The domain size decreases with mixing of C14PC with Chol molecules inside and outside of domain, suggesting the correlation between molecular miscibility and line tension.

(iv) Since the equation of line tension is not applicable to the adsorbed film of C14PC – Chol mixture whose dipoles are different magnitudes and signs with each other, the correlation is still unclear. To avoid this problem, the adsorbed film of methyl palmitate – Chol mixture will be adopted in the Chapter 3.

2-6. *References*

[1] D.F. Evance, The Colloidal Domain, 2nd ed., Wiley-VCH, Weinheim, **1999**.

[2] S. Hiraki, T. Goto, H. Tanida, K. Nitta, T. Ina, T. Uruga, H. Matsubara, M. Aratono, T. Takiue, *Colloids Surfaces A Physicochem. Eng. Asp.*, 482, **2015**, 454–463.

[3] J.N. Israelachvili, Intermolecular and Surface Forces, 3rd ed., Academic Press, **2011**.

[4] D. López-Díaz, I. García-Mateos, M.M. Velázquez, *J. Colloid Interface Sci.*, 299, **2006**, 858–866.

[5] D.A. Mannock, R.N.A.H. Lewis, T.P.W. McMullen, R.N. McElhaney, *Chem. Phys. Lipids*, 163, **2010**, 403–448.

[6] A. Zarbakhsh, A. Querol, J. Bowers, M. Yaseen, J.R. Lu, J.R.P. Webster, *Langmuir*, 21, **2005**, 11704–11709.

[7] M. Pasenkiewicz-Gierula, K. Baczynski, M. Markiewicz, K. Murzyn, *Biochim. Biophys. Acta - Biomembr.*, 1858, **2016**, 2305–2321.

[8] R. Pichot, R.L. Watson, I.T. Norton, *Int. J. Mol. Sci.*, 14, **2013**, 11767–11794.

[9] V. Kaganer, H. Möhwald, P. Dutta, *Rev. Mod. Phys.*, 71, **1999**, 779–819.

[10] C.M. Knobler, R.C. Desai, *Annu. Rev. Phys. Chem.*, 43, **1992**, 207–236.

[11] M.P. Krafft, *Biochimie*, 94 ,**2012**, 11–25.

[12] D. Langevin, *Chem. Phys. Chem.*, 9, **2008**, 510–522.

[13] B.P. Binks, MODERN ASPECTS OF EMULSION SCIENCE, Royal Society of Chemistry, Cambridge London, **1998**.

[14] B.M. Discher, Y. Won, S.D. Ege, J.C.-M. Lee, F.S. Bates, D.E. Disher, D.A. Hammer, *Science*, 80, 284, **1999**, 1143–1146.

[15] T. Okamoto, *J. Oleoscience*, 7, **2007**, 105–110.

[16] G.W. Feigenson, *Nat. Chem. Biol.*, 2, **2006**, 560–563.

[17] G. Van Meer, D.R. Voelker, G.W. Feigenson, *Nat. Rev. Mol. Cell Biol*., 9, **2008**, 112–124.

[18] K. Simons, E. Ikonen, *Nature*, 387, **1997**, 569–72.

[19] G.W. Feigenson, *Biochim. Biophys. Acta - Biomembr.*, 1788, **2009**, 47–52.

[20] T.A. Daly, M. Wang, S.L. Regen, *Langmuir*, 27, **2011**, 2159–2161.

[21] H.M. McConnell, *Annu. Rev. Biophys. Biomol. Struct.*, 32, **2003**, 469–492.

[22] F.A. Heberle, G.W. Feigenson, *Cold Spring Harb Perspect Biol*., **2011**, 1–14.

[23] S.L. Goh, J.J. Amazon, G.W. Feigenson, *Biophys. J.*, 104, **2013**, 853–862.

[24] F.M. Goñi, A. Alonso, L.A. Bagatolli, R.E. Brown, D. Marsh, M. Prieto, J.L. Thewalt, *Biochim. Biophys. Acta - Mol. Cell Biol. Lipids*, 1781, **2008**, 665–684.

[25] N. Tamai, T. Izumikawa, S. Fukui, M. Uemura, M. Goto, H. Matsuki, S. Kaneshina, *Biochim. Biophys. Acta - Biomembr.*, 1828, **2013**, 2513–2523.

[26] G. Pabst, N. Kučerka, M.P. Nieh, M.C. Rheinstädter, J. Katsaras, *Chem. Phys. Lipids*, 163, **2010**, 460–479.

[27] F.A. Heberle, R.S. Petruzielo, J. Pan, P. Drazba, N. Kuc, *J. Am. Chem. Soc.*, 135, **2013**, 6853–6859.

[28] A.C. Brown, S.P. Wrenn, *Langmuir*, 29, **2013**, 9832–9840.

[29] M. Flasiński, M. Broniatowski, P. Wydro, P. Dynarowicz-Łątka, *J. Phys. Chem. B*, 116, **2012**, 3155–3163.

[30] J.R. Silvius, *Biophys. J.*, 85, **2003**, 1034–1045.

[31] J.T. Buboltz, *Phys. Rev. E - Stat. Nonlinear, Soft Matter Phys.*, 76, **2007**, 1–7.

[32] A.C. Brown, K.B. Towles, S.P. Wrenn, *Langmuir*, 23, **2007**, 11188–11196.

[33] A.C. Brown, K.B. Towles, S.P. Wrenn, *Langmuir*, 23, **2007**, 11188–11196.

[34] F.A. Heberle, J. Wu, S.L. Goh, R.S. Petruzielo, G.W. Feigenson, *Biophys. J*., 99, **2010**, 3309–3318.

[35] D.J. Benvegnu, H.M. McConnell, *J. Phys. Chem.*, 97, **1993**, 6686–6691.

[36] P.I. Kuzmin, S.A. Akimov, Y.A. Chizmadzhev, J. Zimmerberg, F.S. Cohen, Biophys. J., 88, **2005,** 1120–1133.

[37] S. V. Pingali, T. Takiue, G. Luo, A.M. Tikhonov, N. Ikeda, M. Aratono, M.L. Schlossman, J. Phys. Chem. B, 109, **2005**, 1210–1225.

[38] M. Aratono, D. Murakami, H. Matsubara, T. Takiue, *J. Phys. Chem. B*, 113, **2009**, 6347–6352.

[39] R. Fukuhara, H. Tanida, K. Nitta, T. Ina, T. Uruga, H. Matsubara, M. Aratono, T. Takiue, *J. Phys. Chem. B*, 118, **2014**, 12451–12461.

[40] H. Sakamoto, A. Murao, Y. Hayami, *J. Inst. Image Inf. Telev. Eng.*, 56, **2002**, 1643–1650.

[41] M. Aratono, A. Ohta, H. Minamizawa, N. Ikeda, H. Iyota, T. Takiue, *J. Colloid Interface Sci.*, 217, **1999**, 128–136.

[42] K. Motomura, *J. Colloid Interface Sci*., 64, **1978**, 348–354.

[43] M. Aratono, M. Villeneuve, T. Takiue, N. Ikeda, H. Iyota, *J. Colloid Interface Sci*., 200, **1998**, 161–171.

[44] T. Takiue, T. Tottori, K. Tatsuta, H. Matsubara, H. Tanida, K. Nitta, T. Uruga, M. Aratono, *J. Phys. Chem. B*, 116, **2012**, 13739–13748.

[45] P.S. Pershan, *Faraday Discuss. Chem. Soc.*, 89, **1990**, 231–245.

[46] Z. Zhang, D.M. Mitrinovic, S.M. Williams, Z. Huang, M.L. Schlossman, *J. Chem. Phys.*, 110, **1999**, 7421–7432.

[47] J. Als-Nielsen, D. Jacquemain, K. Kjaer, F. Leveiller, M. Lahav, L. Leiserowitz,

Phys. Rep., 246, **1994**, 251–313.

[48] E.S. Wu, W.W. Webb, *Phys. Rev. A*, 8, **1973**, 2065–2076.

[49] F.P. Buff, R.A. Lovett, F.H. Stillinger, *Phys. Rev. Lett.*, 15, **1965**, 621–623.

[50] S. Hénon, J. Meunier, *Rev. Sci. Instrum.*, 62, **1991**, 936–939.

[51] S. Uredat, G.H. Findenegg, *Langmuir*, 15, **1999**, 1108–1114.

[52] C.A. Schneider, W.S. Rasband, K.W. Eliceiri, *Nat. Methods*, 9, **2012**, 671–675.

[53] H.M. McConnell, V.T. Moy, *J. Phys. Chem.*, 92, **1988**, 4520–4525.

[54] A.A. Bischof, A. Mangiarotti, N. Wilke, *Soft Matter*, 11, **2015**, 2147–2156.

[55] J. Lipfert, L. Columbus, V.B. Chu, S.A. Lesley, S. Doniach, *J. Phys. Chem. B*, 111, **2007**, 12427–12438.

[56] A. Ivankin, I. Kuzmenko, D. Gidalevitz, *Phys. Rev. Lett.*, 104, **2010**, 1–4.

[57] G. Kevc, D. Marsh, PHOSPHOLIPID BILAYERS: Physical Principles and Models, Wiley-VCH, **1987**.

[58] H. Rapaport, I. Kuzmenko, S. Lafont, K. Kjaer, P.B. Howes, J. Als-Nielsen, M. Lahav, L. Leiserowitz, *Biophys. J.*, 81, **2001**, 2729–2736.

[59] J. Campos-Terán, C. Garza, H.I. Beltrán, R. Castillo, *Thin Solid Films*, 520, **2012**, 2211–2219.

[60] J. Galvan-Miyoshi, S. Ramos, J. Ruiz-Garcia, R. Castillo, *J. Chem. Phys.*, 115, **2001**, 8178–8184.

[61] V. Knecht, M. Müller, M. Bonn, S.J. Marrink, A.E. Mark, *J. Chem. Phys.*, 122, **2005**.

[62] K. Hac-Wydro, K. Luty, *Colloids Surfaces B Biointerfaces*, 116, **2014**, 138–146.

[63] K. Kim, S.Q. Choi, Z.A. Zell, T.M. Squires, J.A. Zasadzinski, *Proc. Natl. Acad. Sci. U. S. A.*, 110, **2013**, E3054-60.

[64] Y. Takajo, H. Matsuki, S. Kaneshina, M. Aratono, M. Yamanaka, *Colloids Surfaces B Biointerfaces*, 59, **2007**, 52–58.

[65] J. Pan, X. Cheng, F.A. Heberle, B. Mostofian, N. Kučerka, P. Drazba, J. Katsaras, *J. Phys. Chem. B*, 116, **2012**, 14829–14838.

[66] D. Murakami, Thesis of Dr., Kyushu University, **2009**.

Chapter 3. Molecular Miscibility and Domain Formation in Adsorbed Film of MePa – Chol Mixture at C6/W Interface

3-1. *Introduction*

In the previous Chapter, the molecular mixing and domain formation in the adsorbed film of C14PC – Chol mixture at the C6/W interface was investigated by the interfacial tensiometry, XR, and BAM. The construction of PDA and evaluation of activity coefficient in adsorbed film indicated the mixing of C14PC and Chol deviates negatively from ideal mixing primarily due to the hydrogen bonding between head groups and effective packing of corn shaped C14PC and inverted corn shaped Chol molecules. Furthermore, it was found that the expanded (E) domains dispersed into the condensed (C) phase region in the C state just above the E – C phase transition point. Despite of these findings, the relation between molecular miscibility and domain structure was not clearly understood, because C14PC and Chol molecules have different dipole moments with different orientations which make it difficult to calculate τ_0 and τ_{el} from eqs. $(2-21)$ and $(2-22)$ in the mixed system. Although some researcher have evaluated the τ_0 and τ_{el} values for Langmuir monolayer of phospholipid (PL) – Chol mixed system[1–4], the equations derived by McConnell have not been improved to apply for the mixed system probably because the quantitative information on the molecular miscibility in the coexisting domains was not necessary to evaluate them. Thus, in order to examine the effect of molecular mixing on domain formation more quantitatively, as we proposed in Chapter 2, two components are needed to satisfy the following conditions; (i) the dipole moments of components are close to each other[5–7], and (ii) two components interact favorably with each other.

Methyl palmitate (MePa) has dipole pointing upward in methyl ester (Mee) group and that in terminal methyl one and their moments are calculated to be ~ 1.7 D and ~ 0.4 D[7,8], respectively. Furthermore, a strong mutual interaction is expected between head groups of MePa and Chol molecules because their hydrophilic parts work respectively as hydrogen bond acceptor and donor from the viewpoint of molecular structure[9–12]. Thus, it is highly appropriate to employ mixed MePa – Chol system and investigate the relation of molecular mixing and domain formation from the viewpoint of line tension.

The interfacial tension of the hexane solution of the mixture against water was measured as a function of total molality and composition of the mixture at 298.15 K under atmospheric pressure. The phase diagram of adsorption (PDA) was constructed and the activity coefficient of a component in the adsorbed film was estimated in order to examine the molecular miscibility at the interface. XR was applied to gain the microscopic information on adsorbed film and BAM to observe heterogeneity of the adsorbed film.

3-2. *Experimental*

Materials

Methyl palmitate (MePa) purchased from Aldrich Chemical Co. Ltd. (> 99 %) was purified by recrystallization twice from ethanol. Its purity was checked by gas-liquid chromatography and by the equilibrium interfacial tension value between hexane (C6) solution and water (W) phases. Cholesterol (Chol), hexane, and water were prepared in the same manner as described in Chapter 2-2.

Interfacial Tensiometry

The interfacial tension γ at the C6 solution/W interface was measured as functions of the total molality of MePa – Chol mixture m and the composition of Chol in the hexane solution X_{Ch} defined by defined respectively by

$$m = m_{\mathrm{Pa}} + m_{\mathrm{Ch}} \ , \qquad (3-1)$$

and

$$X_{\mathrm{Ch}} = \frac{m_{\mathrm{Ch}}}{m} \qquad (3-2)$$

at $298.15\ \mathrm{K}$ under atmospheric pressure by the pendant drop method[13] (see Figure 2-1). Here m_{Pa} and m_{Ch} are respectively the molality of MePa and Chol in the solution.

Thermodynamics of Adsorption

A total differential of interfacial tension γ is expressed as functions of temperature T, pressure p, m, and X_{Ch} by[14,15]

$$\mathrm{d}\gamma = -\Delta s \mathrm{d}T + \Delta v \mathrm{d}p - \Gamma^{\mathrm{H}}\left(\frac{RT}{m}\right)\mathrm{d}m - \Gamma^{\mathrm{H}}RT\left(\frac{X_{\mathrm{Ch}}^{\mathrm{H}} - X_{\mathrm{Ch}}}{X_{\mathrm{Pa}}X_{\mathrm{Ch}}}\right)\mathrm{d}X_{\mathrm{Ch}} \ , \qquad (3-3)$$

where Γ^{H} and $X_{\mathrm{Ch}}^{\mathrm{H}}$ are respectively the total interfacial density and the composition of

Chol in the film, defined by

$$\Gamma^{\mathrm{H}} = \Gamma^{\mathrm{H}}_{\mathrm{Pa}} + \Gamma^{\mathrm{H}}_{\mathrm{Ch}} \qquad (3-4)$$

and

$$X^{\mathrm{H}}_{\mathrm{Ch}} = \frac{\Gamma^{\mathrm{H}}_{\mathrm{Ch}}}{\Gamma^{\mathrm{H}}} \ . \qquad (3-5)$$

Here, Δy $(\Delta y = s, v)$ is thermodynamic quantity changes associated with an adsorption of MePa and Chol molecules from the hexane solution to the interface defined by

$$\Delta y = y^{\mathrm{H}} - \Gamma^{\mathrm{H}}_{\mathrm{PC}} y_{\mathrm{Pa}} - \Gamma^{\mathrm{H}}_{\mathrm{Ch}} y_{\mathrm{Ch}} \ , \qquad (3-6)$$

where y_i is the partial molar thermodynamic quantity of solute i in the hexane solution and y^{H} is the interfacial excess thermodynamic quantity defined with reference to the two dividing planes and water zero, simultaneously[15,16]. The Γ^{H} value is calculated by

$$\Gamma^{\mathrm{H}} = -\left(\frac{m}{RT}\right)\left(\frac{\partial \gamma}{\partial m}\right)_{T,p,X_{\mathrm{Ch}}} \ , \qquad (3-7)$$

and the $X^{\mathrm{H}}_{\mathrm{Ch}}$ one by

$$X^{\mathrm{H}}_{\mathrm{Ch}} = X_{\mathrm{Ch}} - \frac{X_{\mathrm{Pa}} X_{\mathrm{Ch}}}{m}\left(\frac{\partial m}{\partial X_{\mathrm{Ch}}}\right)_{T,p,m} \ . \qquad (3-8)$$

The interfacial pressure π, mean area per molecule A, and activity coefficient of component i in the adsorbed film f_i^{H} are respectively evaluated by eqs. $(2-5)$, $(2-6)$, and $(2-9)$.

X-ray Reflectometry

The experimental conditions and the equations for fitting the reflectivity data are followed in Chapter 2-2.

Brewster Angle Microscopy

The experimental procedure are followed in Chapter 2-2.

3-3. *Results and Discussion*

Film State and Molecular Miscibility

Figures 3-1-1 and 3-1-2 show the γ vs. m curves at given X_{Ch}. The curve of pure MePa system (curve 1) shows the monotonic decrease in γ with increasing m. The curves at $X_{\mathrm{Ch}} = 0.10,\ 0.21,\ 0.40,$ and 0.61 have a break point due to the phase transition of the adsorbed film as indicated by arrows. The curves above $X_{\mathrm{Ch}} = 0.79$, on the other hand, have two kinks, suggesting that three different film states appear at the interface.

The total molality m^{eq} and the interfacial tension γ^{eq} values at the phase transition point were plotted against X_{Ch} in Figure 3-2. The curves connecting the plots demonstrate the appearance of three kinds of film states denoted by G, E, and C, depending on m and X_{Ch}. The m^{eq} values at the G – E and G – C phase transitions increase and the corresponding γ^{eq} ones decrease with decreasing X_{Ch}. The m^{eq} vs. X_{Ch} curve of E – C transition has a shallow maximum and the γ^{eq} vs. X_{Ch} one minimum at about $X_{\mathrm{Ch}} \approx 0.9$. It is noted that three types of these curves intersects with each other at $X_{\mathrm{Ch}} \approx 0.7$, indicating the triple point of the adsorbed film at which the G, E, and C film states are appeared simultaneously.

To clarify the film state of the present system, first, the total interfacial density Γ^{H} was calculated by applying eq. $(3-7)$ to the γ vs. m curves. The Γ^{H} vs. m curves at constant X_{Ch} are shown in Figures 3-3-1 and 3-3-2. The Γ^{H} value of pure MePa system ($X_{\mathrm{Ch}} = 0$) increases monotonically and then converges into about $1.3\ \mu\mathrm{mol\ m^{-2}}$. The value above $X_{\mathrm{Ch}} = 0.10$ including pure Chol system ($X_{\mathrm{Ch}} = 1$) changes discontinuously at phase transition points, and converges into around $4.3\ \mu\mathrm{mol\ m^{-2}}$ which is very close to the Γ^{H} value of the condensed Chol film ($\sim 4.5\ \mu\mathrm{mol\ m^{-2}}$).

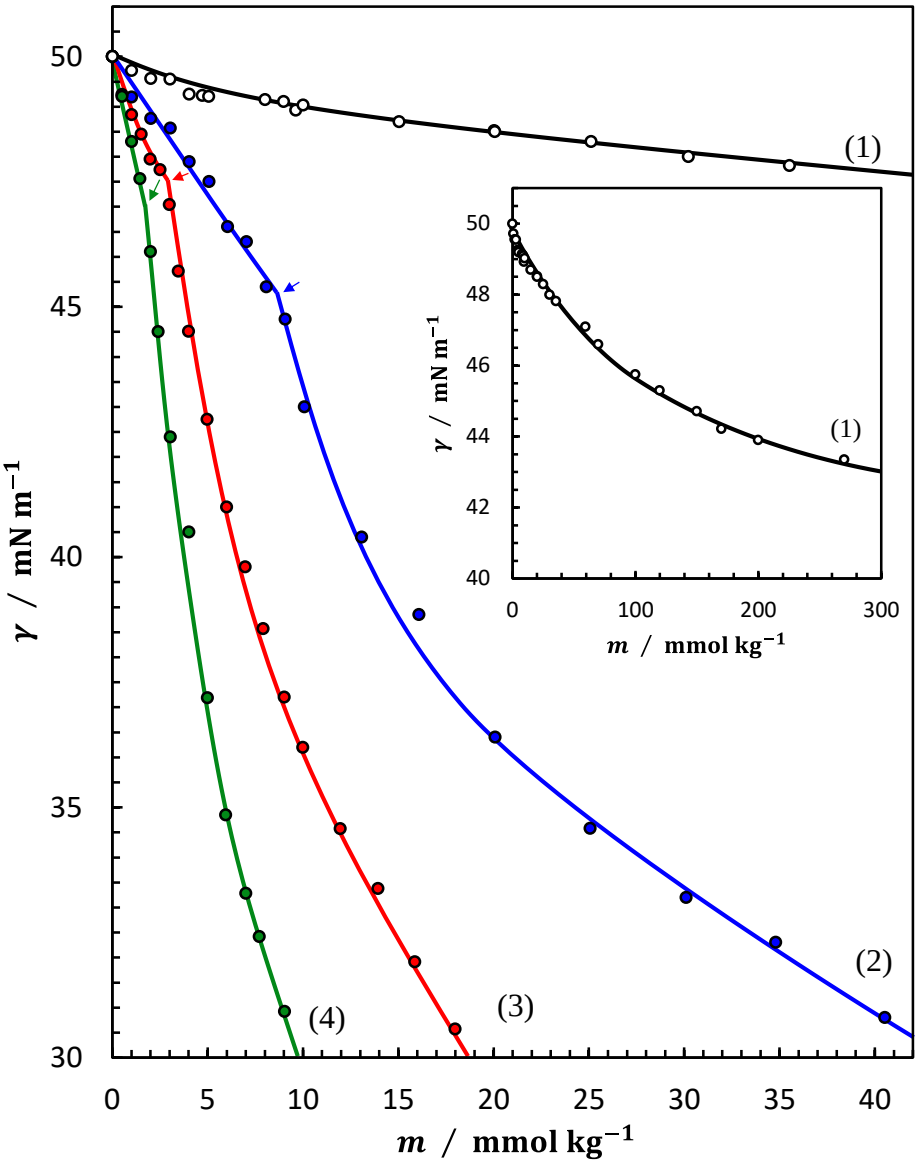

Figure 3-1-1. The γ vs. m curves at given (1) $X_{\mathrm{Ch}} = 0$ (pure MePa system), (2) 0.10, (3) 0.21, and (4) at 0.40. The arrows indicate the phase transition point. The inset shows reduced curve 1.

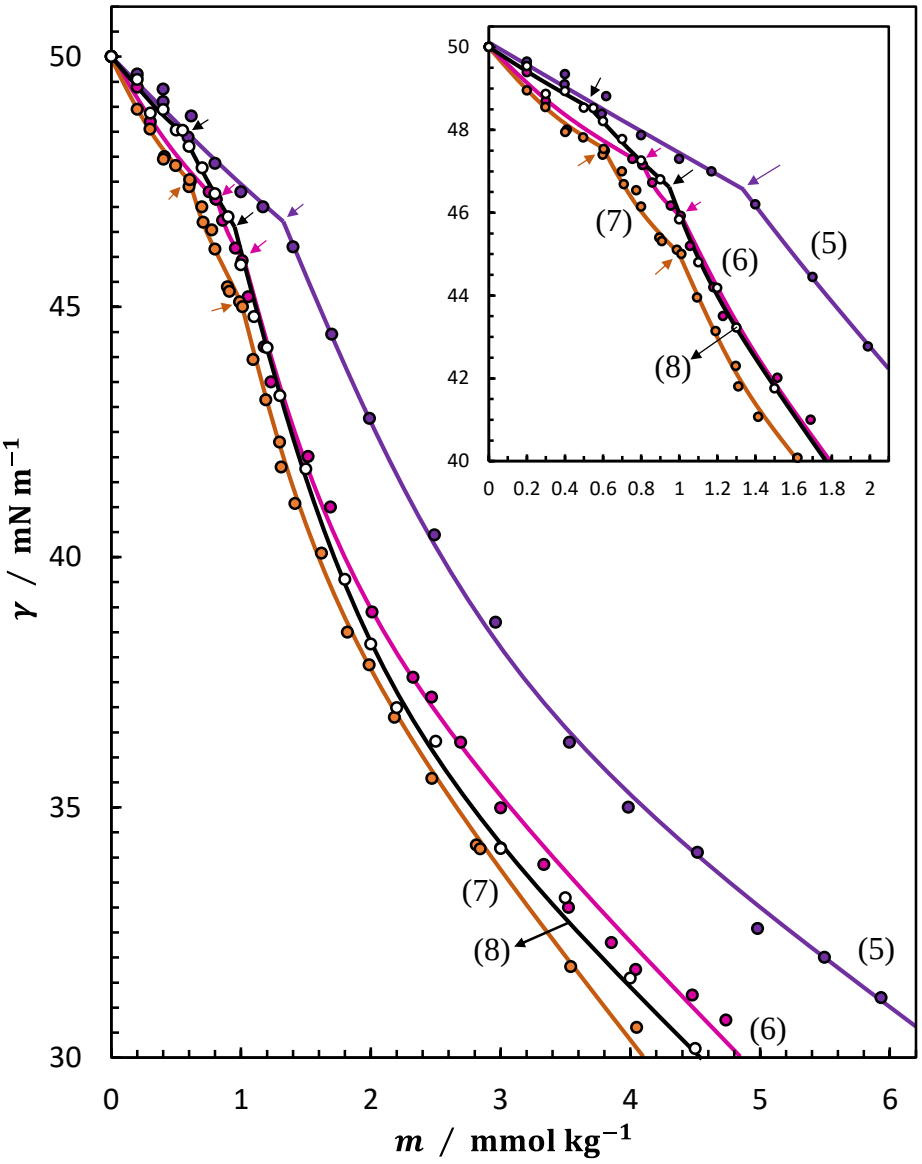

Figure 3-1-2. The γ vs. m curves at given (5) $X_{\mathrm{Ch}} = 0.61$, (6) 0.79, (7) 0.90, and (8) at 1 (pure Chol system). The arrows indicate the phase transition points. The curves at low m are manifested in the inset.

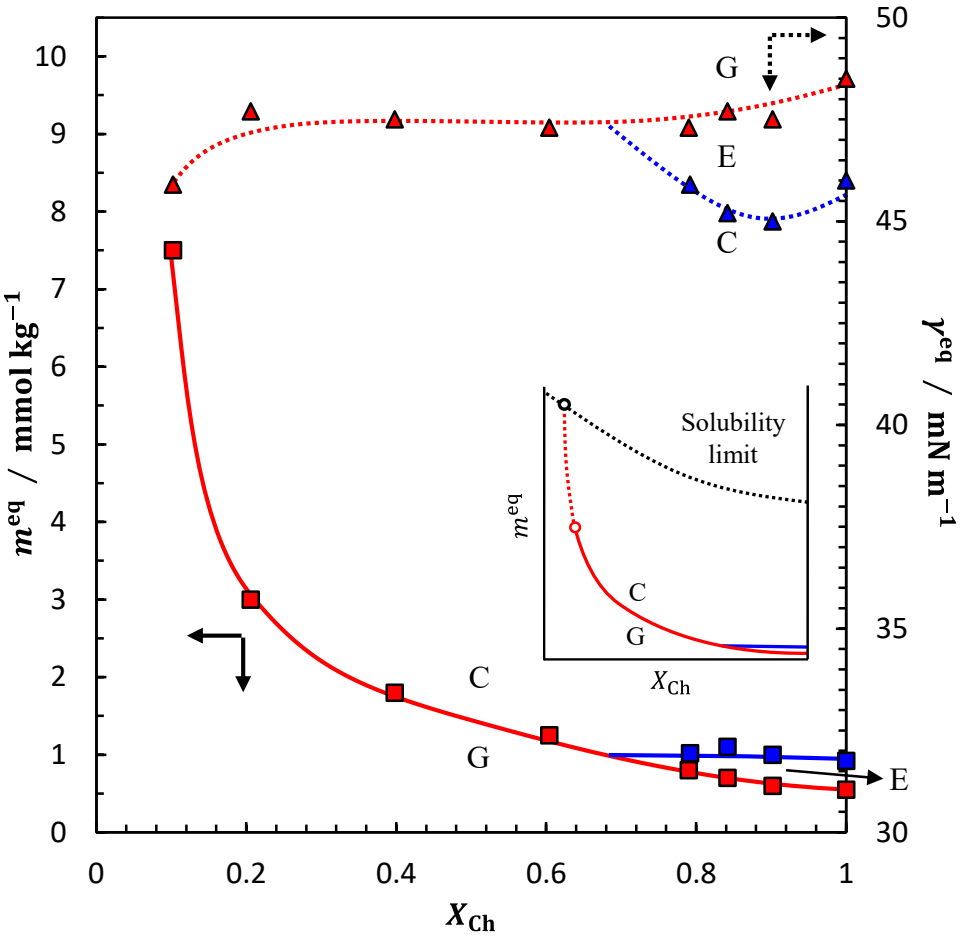

Figure 3-2. The m^{eq} vs. X_{Ch} and γ^{eq} vs. X_{Ch} curves at the phase transition points. The former drawn by a solid line associates with the y-axis on left side and the latter drawn by a dotted line on right side. The red line connects the G – E (or C) phase transition points, and the blue line does the E – C ones. They intersect at the triple point with each other at X_{Ch}~0.7. The m^{eq} value at low X_{Ch} is expected to reach to the solubility limit, as shown in the inset.

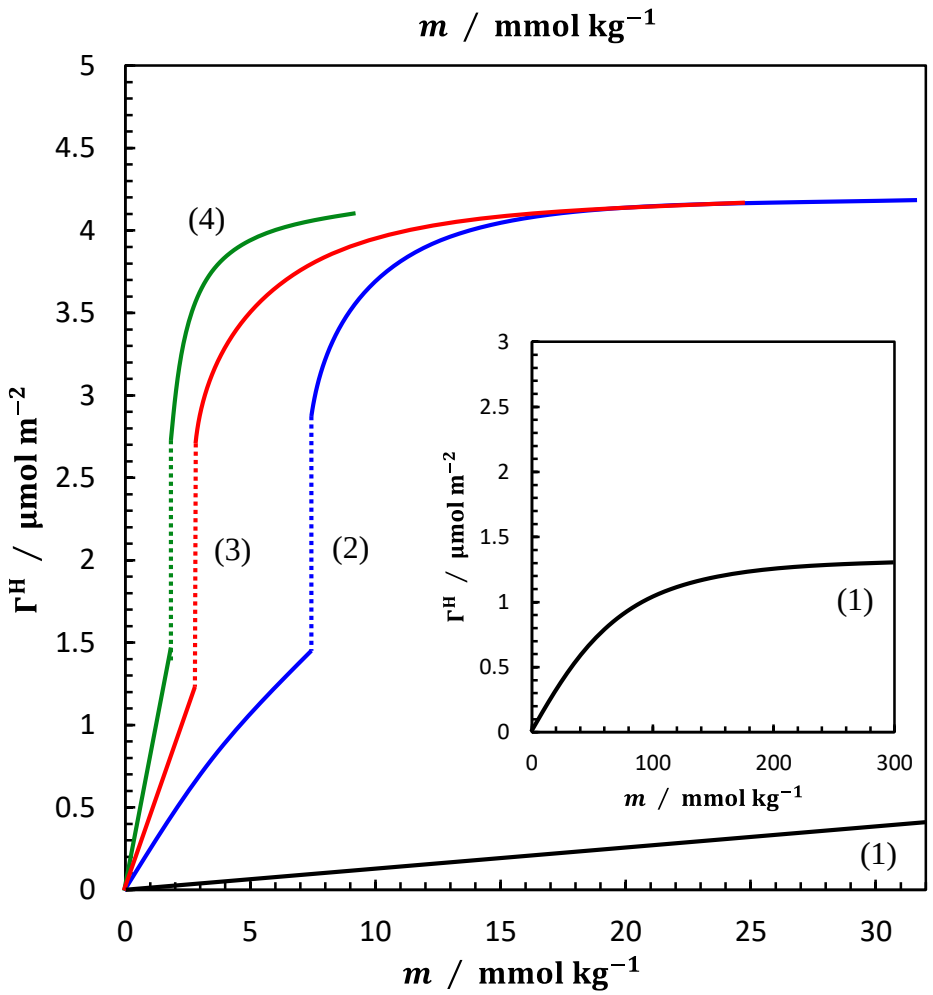

Figure 3-3-1. The Γ^{H} vs. m curves at given (1) $X_{\mathrm{Ch}} = 0$ (pure MePa system), (2) 0.10, (3) 0.21, and (4) at 0.40. The inset shows the reduced curve 1.

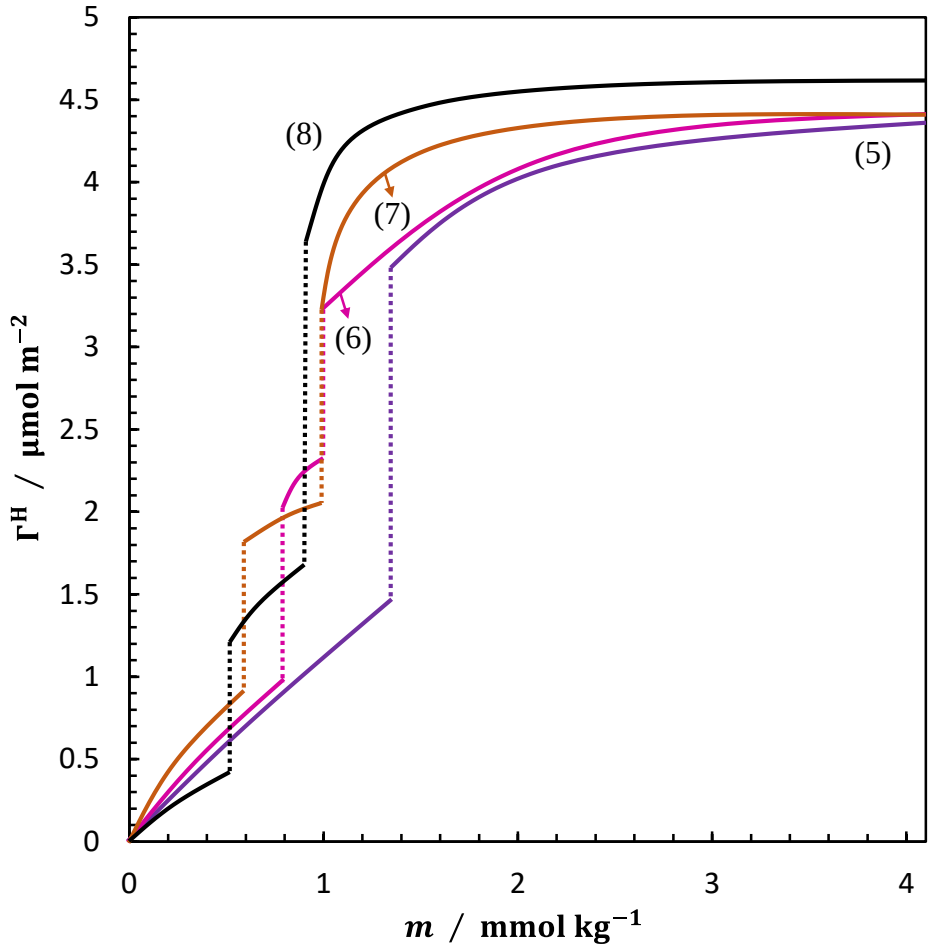

Figure 3-3-2. The Γ^{H} vs. m curves at given (5) $X_{Ch} = 0.61$, (6) 0.79, (7) 0.90, and (8) at 1 (pure Chol system).

Then the interfacial pressure π vs. mean area per adsorbed molecule A curves were constructed by eqs. $(2-5)$ and $(2-6)$ and shown in Figure 3-4. The curves are classified into three types depending on X_{Ch}; (a) the curve at $X_{\mathrm{Ch}}=0$, (b) those at $X_{\mathrm{Ch}}=0.10\sim0.61$, and (c) those above $X_{\mathrm{Ch}}=0.79$. In type (c), the curves consist of three parts connected by two discontinuous changes. Taking account of our finding that the adsorbed Chol film exhibits two kinds of phase transitions from gaseous to expanded and from expanded to condensed states, three interfacial states G, E, and C are assigned respectively to gaseous, expanded, and condensed states. In the C state, the π vs. A curves are almost vertical at $A=37\sim39$ Å^2, which is very close to that of the condensed Chol film (38 Å^2) and larger than the cross-sectional area of MePa molecules ($\sim$20 Å^2)[17]. In type (a), the A value decreases monotonically with increasing π. Because the value (>130 Å^2) is much larger than 20 Å^2, it is expected that adsorbing MePa molecules form G film within a the experimental concentration range employed in this study.

Here we briefly mention the variation of G – C phase transition point with X_{Ch}. It is seen from Figure 3-2 that m^{eq} and γ^{eq} may diverge to infinity with decreasing X_{Ch} or reach critical point above which the G and C states become indistinguishable. Since the critical behavior between gas and solid states rarely appear in three dimensional substances, one of the plausible explanations is that the G – C transition point terminates at the solubility limit of Chol – MePa mixture in the hexane solution as schematically shown in the inset of Figure 3-2.

Next, let us discuss on the miscibility of MePa and Chol molecules in the adsorbed film by constructing phase diagram of adsorption (PDA). The $X_{\mathrm{Ch}}^{\mathrm{H}}$ value was calculated by applying eq. $(3-8)$ to the m vs. X_{Ch} curve at given γ. In Figure 3-5 are shown the

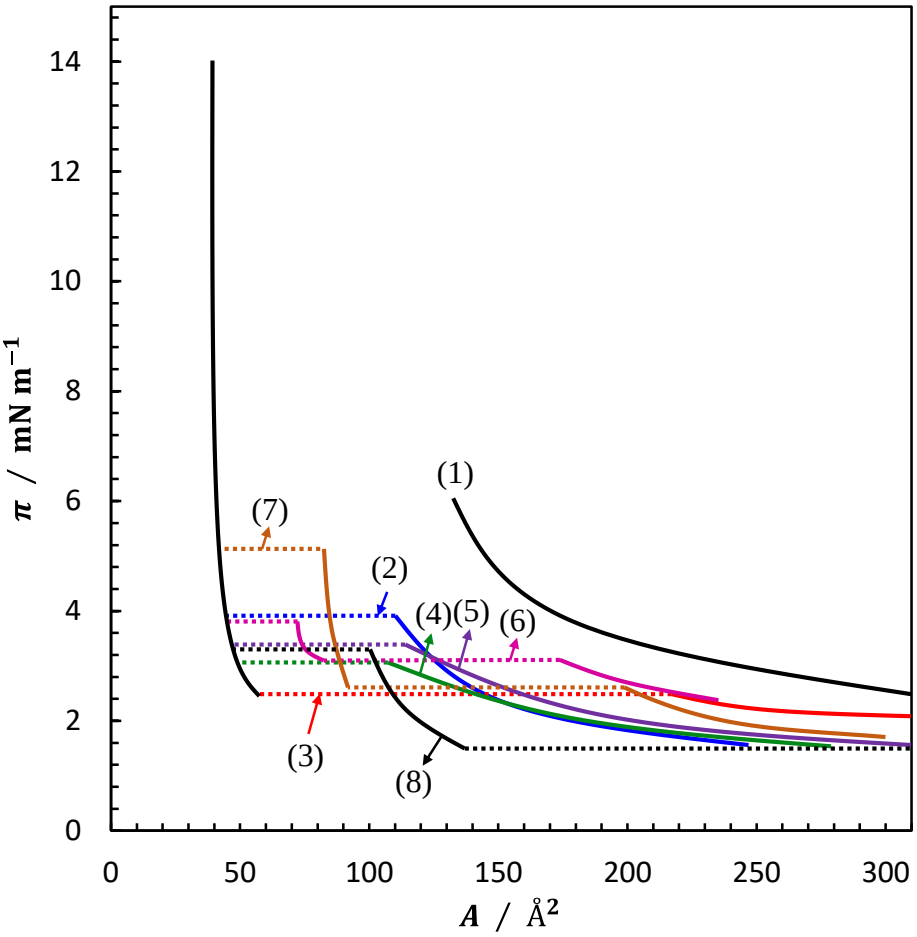

Figure 3-4. The π vs. A curves at given (1) $X_{\mathrm{Ch}} = 0$ (pure MePa system), (2) 0.10, (3) 0.21, (4) 0.40, (5) 0.61, (6) 0.79, (7) 0.90, and (8) 1 (pure Chol system). The curve 8 connects a rest part located at $A > 420$ Å^2 outside of this Figure.

m vs. $X_{\mathrm{Ch}}^{\mathrm{H}}$ and m vs. X_{Ch} curves at $\gamma = 48.0,\ 45.0,\ 43.0$, and $30.0\ \mathrm{mN\ m^{-1}}$. The PDA in the G state shows that the $X_{\mathrm{Ch}}^{\mathrm{H}}$ value takes 0.8 in minimum and thus MePa and Chol are less miscible with each other. In the C state at $\gamma = 45.0$, 43.0, and $30.0\ \mathrm{mN\ m^{-1}}$, the PDAs exhibit a negative azeotrope at $X_{\mathrm{Ch}} = X_{\mathrm{Ch}}^{\mathrm{H}} \approx 0.9$, suggesting that the mutual interaction between MePa and Chol molecules is stronger than those between same ones. The $X_{\mathrm{Ch}}^{\mathrm{H}}$ values changes from 0.9 at $X_{\mathrm{Ch}} = 0.90$ to 0.7 at $X_{\mathrm{Ch}} = 0.10$, indicating that the C state is richer in Chol compared to bulk hexane solution, and that MePa and Chol molecules are less miscible even in the C state. It is noted that the shape of PDA looks very similar both in the G and C states.

The molecular mixing in the C state was further examined by evaluating the activity coefficient of Chol in the adsorbed film $f_{\mathrm{Ch}}^{\mathrm{H,C}}$ by using eq. $(2-9)$. The results are summarized in Figure 3-6. At all γ, the $f_{\mathrm{Ch}}^{\mathrm{H,C}}$ vs. $X_{\mathrm{Ch}}^{\mathrm{H}}$ curves have a shallow minimum at around $X_{\mathrm{Ch}}^{\mathrm{H}} = 0.9$ at which $f_{\mathrm{Ch}}^{\mathrm{H,C}}$ is slightly less than unity. The $f_{\mathrm{Ch}}^{\mathrm{H,C}}$ value below $X_{\mathrm{Ch}}^{\mathrm{H}} = 0.90$ increases and exceed unity with decreasing $X_{\mathrm{Ch}}^{\mathrm{H}}$. This is attributable to a balance of the two factors; (i) the hydrogen bonding between carbonyl group of MePa and hydroxyl group of Chol molecule, which causes negative deviation from ideal mixing, and (ii) the loss of effective packing of cylindrical shape MePa molecule with cpp (critical packing parameter) ≈ 1 and inverted corn like Chol molecule with cpp ≥ 1, preventing molecules from mixing each other.

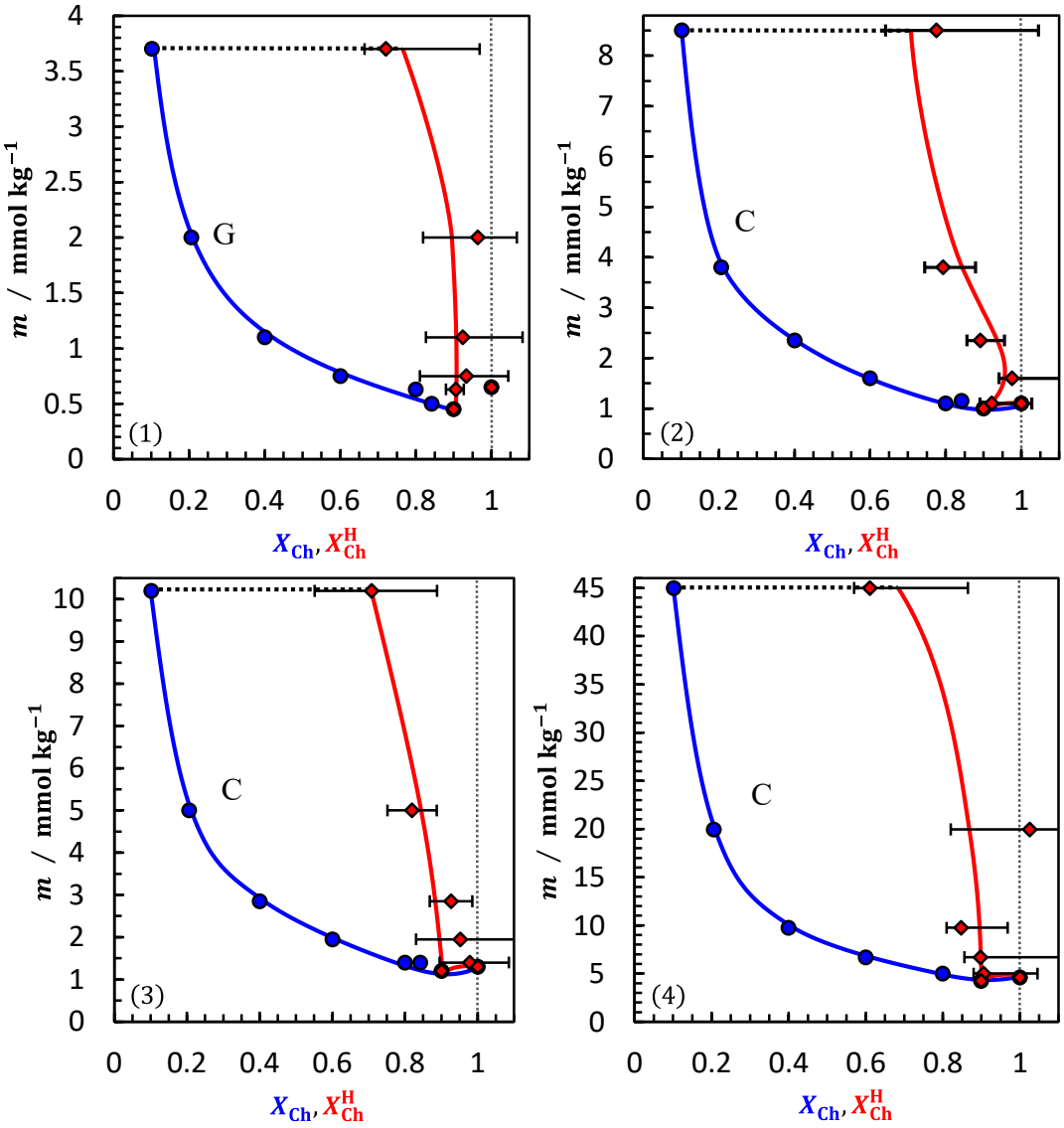

Figure 3-5. The PDA at given (1) $\gamma = 48.0$, (2) 45.0, (3) 43.0, and (4) at 30.0 mN m^{-1}. The curves intersect with each other at $(m, X_{\mathrm{Ch}}) = (30.2, 0)$ in Figure (1).

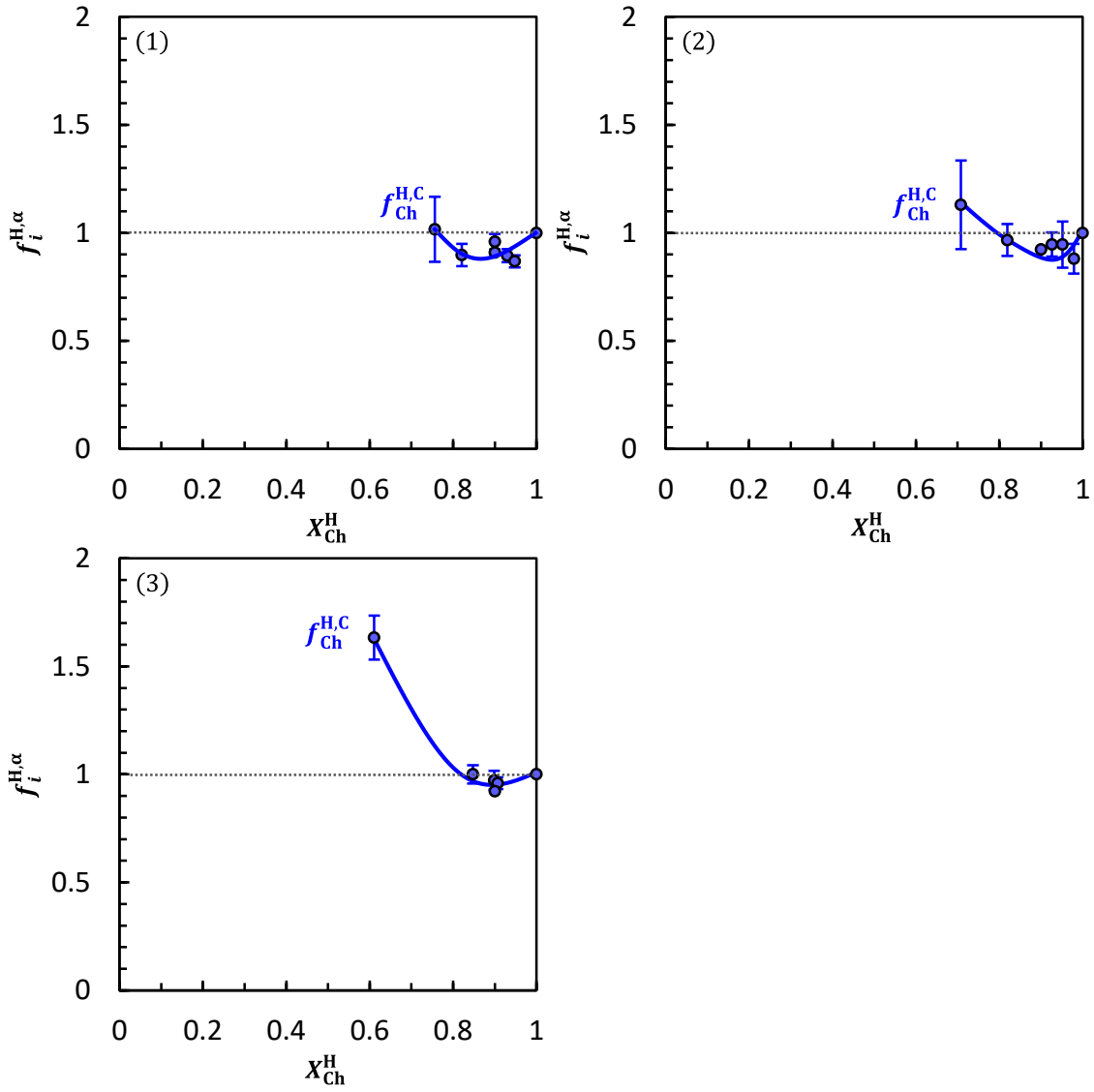

Figure 3-6. The $f_{\mathrm{Ch}}^{\mathrm{H,C}}$ vs. $X_{\mathrm{Ch}}^{\mathrm{H}}$ plots at (1) $\gamma = 45.0$, (2) 43.0, and (3) 30.0 mN m^{-1}.

Structure of Mixed Adsorbed Film

The microscopic structure of the adsorbed film was examined by XR analysis. Figures 3-7-1 and 3-7-2 show the R/R_{F} vs. Q_z plots at $m = 1.5$, 2.4, and 10.0 mmol kg^{-1} under fixed $X_{\mathrm{Ch}} = 0.40$ and those at $m = 0.4$, 0.8, 1.2 and 4.4 mmol kg^{-1} under fixed $X_{\mathrm{Ch}} = 0.90$, respectively. The electron density profiles determined by slab model fitting are respectively shown in Figures 3-7-3 and 3-7-4, and the corresponding fitted parameters for the slab models are listed in Table 3-1. The $R/R_{\mathrm{F}}\,(Q_z)$ plots in the G state (plots 1 in Figures 3-7-1 and 3-7-2) were fitted well by slab model, although the reflectivity is extremely low because of low interfacial density. The results are shown by red lines. L_1 ($= 12.5$ Å) at $X_{\mathrm{Ch}} = 0.40$ is regarded as the length of hydrophobic part and very close to that obtained for the G film of pure Chol system. The ρ_1/ρ_{w} value is larger than that of hexane phase and almost equal to the calculated value by using Γ^{H} and $X_{\mathrm{Ch}}^{\mathrm{H}}$. The L_1 value at $X_{\mathrm{Ch}} = 0.90$, on the other hand, is close to the size of Mee group (~3 Å)[6], and L_2 and ρ_2/ρ_{w} ones to those at $X_{\mathrm{Ch}} = 0.40$. The ρ_1/ρ_{w} value is almost equal to the estimated slab density composed of hydrated Mee group. These results suggest that the Chol molecules take tilt orientation from normal to the interface, as illustrated in Figures 3-7-3 and 3-7-4.

In the C state at $m = 10.0$ ($X_{\mathrm{Ch}} = 0.40$) and 4.4 mmol kg^{-1} ($X_{\mathrm{Ch}} = 0.90$), three-slab model gave good fitting as shown by green lines. Slab 1 corresponds to hydrophilic part and slabs 2 and 3 to hydrophobic part. The ρ_1/ρ_{w} value is as same as that of hydrated Mee group. Furthermore, the ρ_2/ρ_{w} value agrees well with the one calculated for sterol ring and liquid-ordered alkane mixture, and the ρ_3/ρ_{w} one for tail part of Chol and liquid-ordered alkane mixture both in about $9:1$. Therefore, it is concluded that Chol and MePa molecules orient normal to the interface and closely packed in the C state.

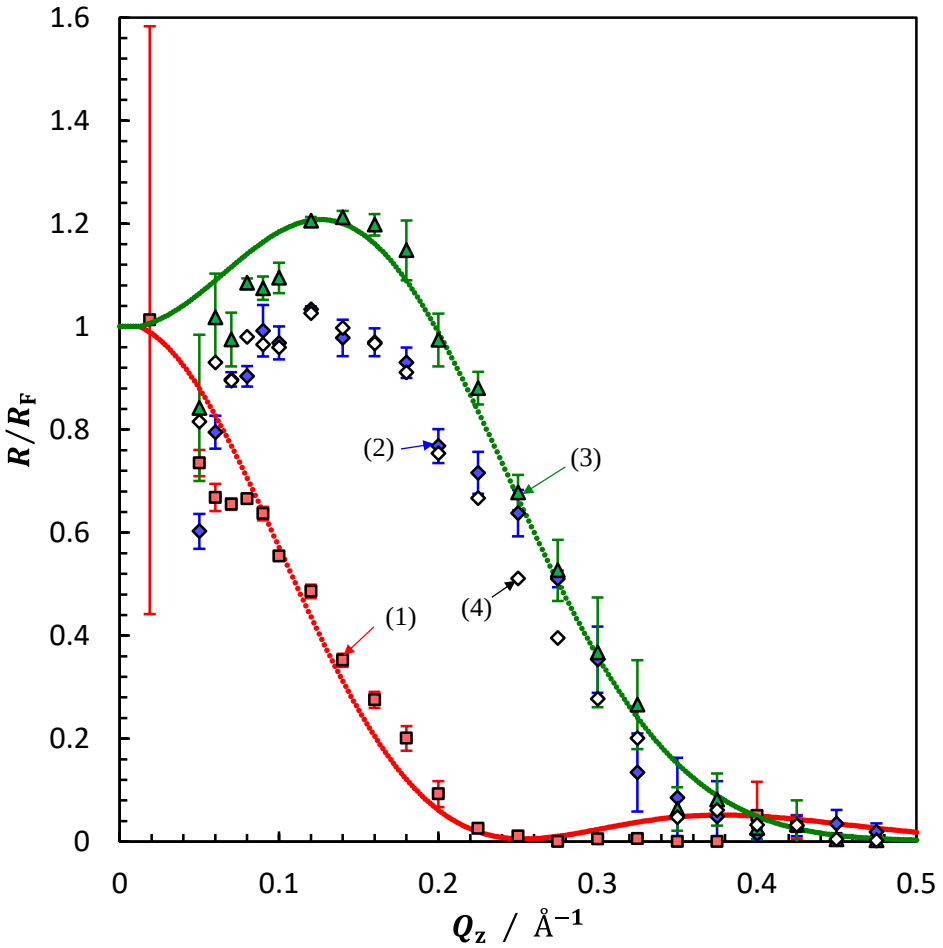

Figure 3-7-1. The R/R_F vs. Q_z plots under fixed $X_{\mathrm{Ch}} = 0.40$ at (1) $m = 1.5$, (2) 2.4, and (3) at 10.0 mmol kg^{-1}. The dotted lines represent the fitting curves by the slab model. The white diamond plots (4) were resulted from domain fitting by the coherent model with $C_{\mathrm{XR}} = 0.75$.

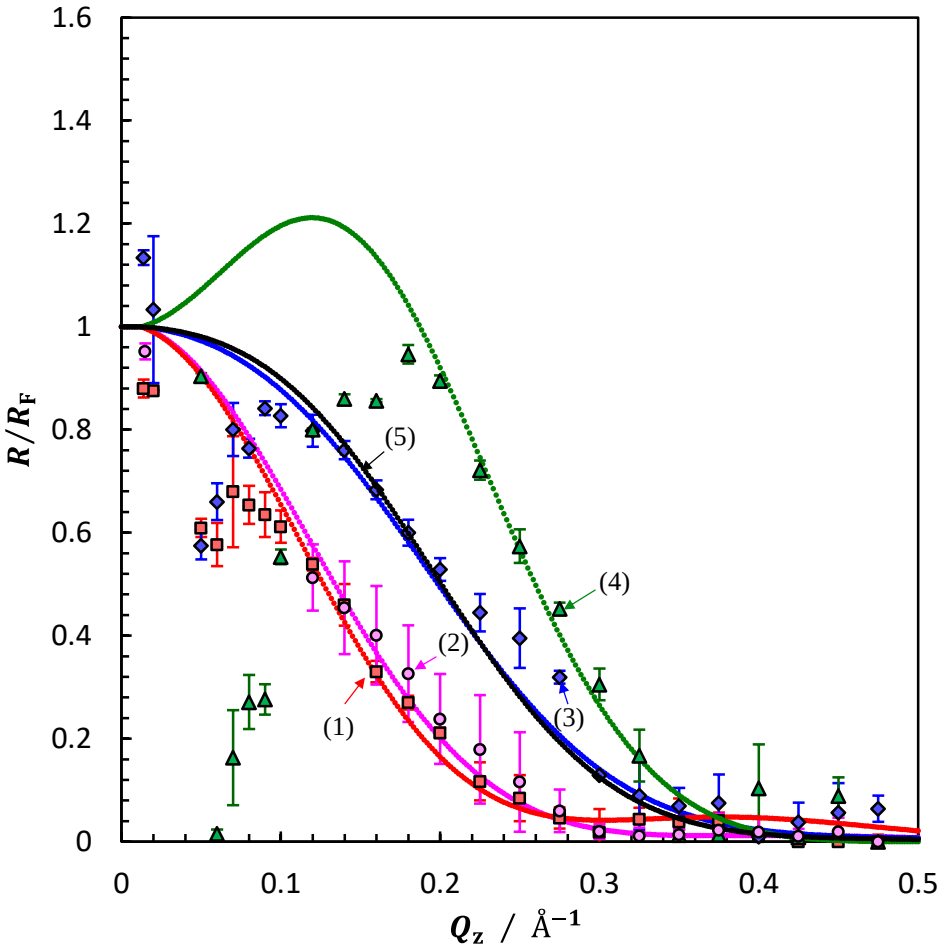

Figure 3-7-2. The R/R_F vs. Q_z plots under fixed $X_{\mathrm{Ch}} = 0.90$ at (1) $m = 0.4$, (2) 0.8, (3) 1.2, and (4) at 4.4 mmol kg^{-1}. The dotted lines except black one represent the fitting curves by the slab model. The black dotted line (5) was resulted from domain fitting by the incoherent model with $C_{\mathrm{XR}} = 0.42$. It is noted that the domain fitting was carried out using the fitting curves instead of corresponding plots because the plots have defects at low Q_z.

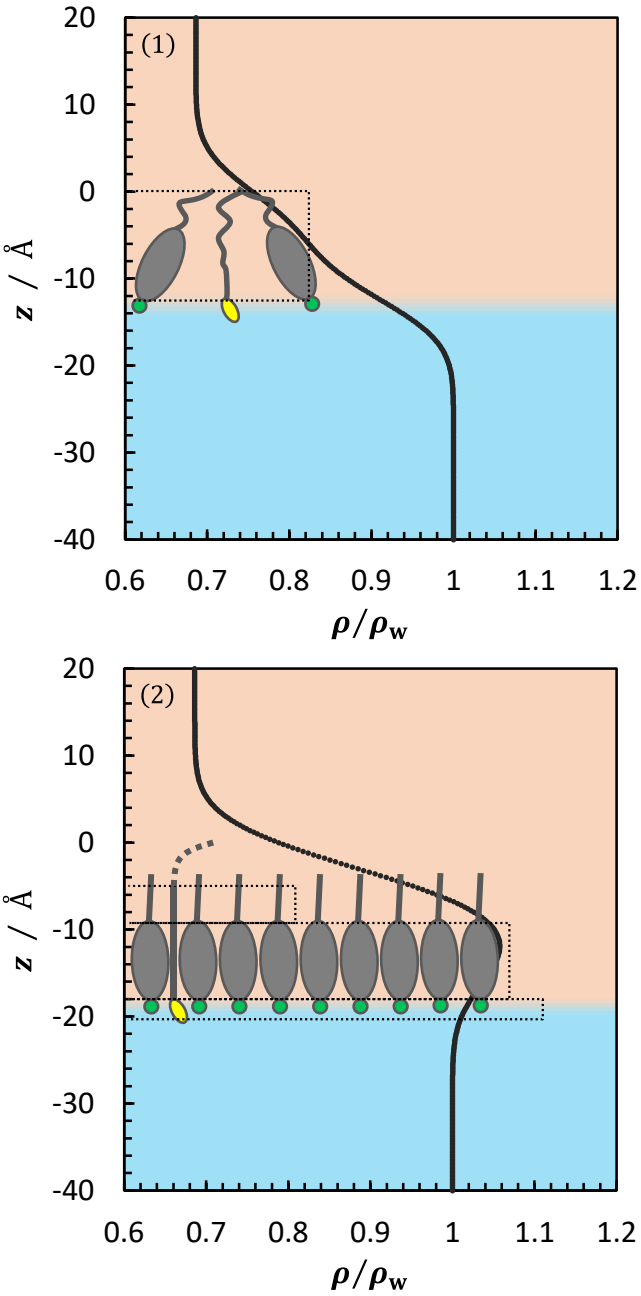

Figure 3-7-3. The electron density profiles normal to the interface under fixed $X_{\mathrm{Ch}} = 0.40$ at (1) $m = 1.5$ and (2) $10.0\,\mathrm{mmol\,kg^{-1}}$. The top part of hydrocarbon chain of MePa molecule was exhibited by the dotted line.

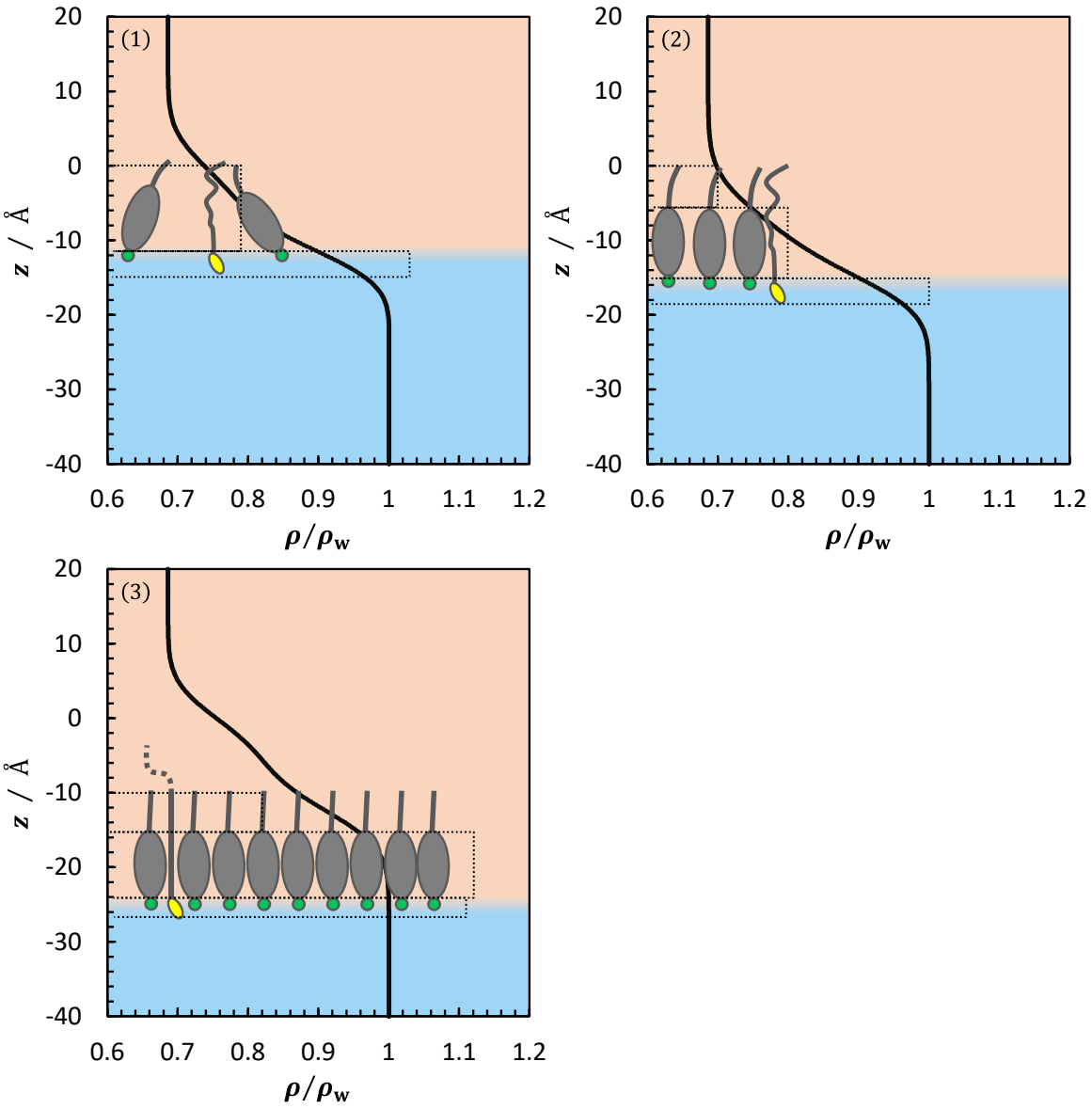

Figure 3-7-4. The electron density profiles normal to the interface under fixed $X_{\mathrm{Ch}} = 0.90$ at (1) $m = 0.4$, (2) 0.8, and (3) at 4.4 mmol kg^{-1}.

Table 3-1. The fitting parameters for the slab models. The ρ/ρ_{w} and σ (σ_{cap}) values calculated using Γ^{H},$X_{\mathrm{Ch}}^{\mathrm{H}}$, and γ were put into parentheses.

X_{Ch}	$\frac{m}{\mathrm{mmol\ kg^{-1}}}$	Film state	$X_{\mathrm{Ch}}^{\mathrm{H}}$	Slab 1			Slab 2 = Sterol + chain (+hexane)			Slab 3 = Tail + chain (+hexane)		
				$\frac{L_1}{\mathrm{Å}}$	ρ_1/ρ_{w}	$\frac{\sigma_1,\sigma_2}{\mathrm{Å^{-1}}}$	$\frac{L_2}{\mathrm{Å}}$	ρ_2/ρ_{w}	$\frac{\sigma_2,\sigma_3}{\mathrm{Å^{-1}}}$	$\frac{L_3}{\mathrm{Å}}$	ρ_3/ρ_{w}	$\frac{\sigma_3,\sigma_4}{\mathrm{Å^{-1}}}$
0.4	1.5	G	0.88	12.2	0.82 (0.89 ± 0.01)	4.0 (3.6 ± 0.1)						
	10.0	C	0.88	2.4	1.11 (1.11 ± 0.02)	4.0 (4.5 ± 0.2)	8.7	1.07 (1.09 ± 0.03)	4.0 (4.5 ± 0.2)	4.1	0.81 (0.82)	4.0 (4.5 ± 0.2)
0.9	0.4	G	0.90	3.6	1.03 (1.02)	4.0 (3.6 ± 0.1)	11.7	0.79 (0.79 ± 0.01)	4.0 (3.6 ± 0.1)			
	0.8	E	0.90	3.6	1.00 (1.05)	4.0 (3.6 ± 0.1)	9.2	0.80 (0.86 ± 0.02)	4.0 (3.6 ± 0.1)	5.6	0.70 (0.74)	4.0 (3.6 ± 0.1)
	4.4	C	0.90	2.6	1.11 (1.09 ± 0.02)	4.0 (4.5 ± 0.2)	8.8	1.12 (1.10 ± 0.02)	4.0 (4.5 ± 0.2)	5.3	0.82 (0.82)	4.0 (4.5 ± 0.2)

The $R/R_{\mathrm{F}}(Q_z)$ plots in the E state were fitted well by three slab model. It is realized that the L_1, L_2, and L_3 values are respectively similar to those obtained for the C state at $X_{\mathrm{Ch}} = 0.90$. It is noted that the ρ_2/ρ_{w} and ρ_3/ρ_{w} values are close respectively to that of slab constructed of sterol, liquid hydrocarbon and hexane (0.86 ± 0.02) and that of tail, liquid hydrocarbon and hexane (0.74). Thus, it is expected that hydrocarbon chain of MePa molecule is in liquid state and Chol one takes normal orientation to the interface.

The reflectivity in the C state at $m = 2.4$ ($X_{\mathrm{Ch}} = 0.40$) and at $m = 1.2$ ($X_{\mathrm{Ch}} = 0.90$) were tried to be fitted by the domain models because Γ^{H} is still increasing with m before saturated adsorption. The former was fitted well by coherent model in which the reflection amplitude of G state at $m = 1.5$ and that of C state at $m = 10.0\ \mathrm{mmol\ kg^{-1}}$ were employed as two references. Then we obtained the coverage of condensed phase $C_{\mathrm{XR}} = 0.75 \pm 0.1$ which gave interfacial densities of MePa and Chol as $\Gamma^{\mathrm{H}}_{\mathrm{Pa,XR}} = 0.36 \pm 0.04$ and $\Gamma^{\mathrm{H}}_{\mathrm{Ch,XR}} = 3.22 \pm 0.26\ \mu\mathrm{mol\ m^{-1}}$, respectively. These values are consistent with $\Gamma^{\mathrm{H}}_{\mathrm{Pa}}$ ($= 0.33$) and $\Gamma^{\mathrm{H}}_{\mathrm{Ch}}$ ($= 2.97\ \mu\mathrm{mol\ m^{-1}}$) ones obtained by interfacial tension data, as listed in Table 3-2. On the other hand, the latter was fitted well by incoherent model by using reflectivity of individual domains, R_1 of C domain at $m = 4.4$ and R_2 of E one at $m = 0.8\ \mathrm{mmol\ kg^{-1}}$, as references; $C_{\mathrm{XR}} = 0.42 \pm 0.1$ was obtained. The $\Gamma^{\mathrm{H}}_{\mathrm{Pa,XR}}$ and $\Gamma^{\mathrm{H}}_{\mathrm{Ch,XR}}$ values (0.31 ± 0.04 and 2.76 ± 0.30) are close to the $\Gamma^{\mathrm{H}}_{\mathrm{Pa}}$ and $\Gamma^{\mathrm{H}}_{\mathrm{Ch}}$ ones (0.39 ± 0.1 and 3.51 ± 0.09), respectively. Thus, we can say that the C film just above the G (or E) – C phase transition point is regarded to be a heterogeneous structure in which the G or E domain is surrounded by C region. It should be noted that both the coherent and incoherent models gave good fittings to the R/R_{F} plots and therefore the radii of domains in the MePa – Chol system are expected to be

Table 3-2. The fitting parameters for the domain models. $\Gamma^{\mathrm{H}}_{i,\mathrm{XR}}$ was calculated from eq. (2-23).

X_{Ch}	$\frac{m}{\mathrm{mmol\ kg^{-1}}}$	Film state	R_1	R_2	Model	C_{XR}	Γ^{H}_i / μmol m^{-2}	$\Gamma^{\mathrm{H}}_{i,\mathrm{XR}}$ / μmol m^{-2}
0.4	2.4	C	$X_{\mathrm{Ch}} = 0.4$ $m = 10.0$	$X_{\mathrm{Ch}} = 0.4$ $m = 1.5$	Coherent	0.75 ± 0.1	$\Gamma^{\mathrm{H}}_{\mathrm{Pa}} = 0.33 \pm 0.02$ $\Gamma^{\mathrm{H}}_{\mathrm{Ch}} = 2.97 \pm 0.08$	$\Gamma^{\mathrm{H}}_{\mathrm{Pa}} = 0.36 \pm 0.04$ $\Gamma^{\mathrm{H}}_{\mathrm{Ch}} = 3.22 \pm 0.26$
0.9	1.2	C	$X_{\mathrm{Ch}} = 0.9$ $m = 4.4$	$X_{\mathrm{Ch}} = 0.9$ $m = 0.8$	Incoherent	0.42 ± 0.1	$\Gamma^{\mathrm{H}}_{\mathrm{Pa}} = 0.39 \pm 0.1$ $\Gamma^{\mathrm{H}}_{\mathrm{Ch}} = 3.51 \pm 0.09$	$\Gamma^{\mathrm{H}}_{\mathrm{Pa}} = 0.31 \pm 0.04$ $\Gamma^{\mathrm{H}}_{\mathrm{Ch}} = 2.76 \pm 0.30$

close to the X-ray coherent length of ~ 5 μm. This will be further confirmed by BAM observation.

Domain Formation and Line Tension

Finally, let us consider the domain formation from the viewpoint of line tension. Figure 3-9 shows some typical BAM images observed in the C state just above the G (or E) – C phase transition point at several m and X_{Ch} listed in Table 3-3. A few μm circular dark domains are dispersed into a bright region. Counting size and number of domain provide the coverage of bright region as $C_{\mathrm{XR}} = 0.8 \sim 0.9$. According to the results of XR, it is reasonable to assign the bright and dark region to the C and G (or E) phases, respectively. Then the interfacial density of component i $\Gamma_{i,\mathrm{BAM}}^{\mathrm{H}}$ was calculated using C_{BAM}, $\Gamma_i^{\mathrm{H},\alpha}$ ($\alpha =$ G or E), and $\Gamma_i^{\mathrm{H,C}}$, and summarized together with Γ_i^{H} evaluated from the interfacial tension data in Table 3-3. $\Gamma_i^{\mathrm{H},\alpha}$ is the interfacial density of component i at the G (or E) – C phase transition point and $\Gamma_i^{\mathrm{H,C}}$ is that at high concentration with saturated adsorption. $\Gamma_{i,\mathrm{BAM}}^{\mathrm{H}}$ values are very close to Γ_i^{H} ones, confirming that the C film just above the phase transition is heterogeneous structure in which low density G (or E) domains are surrounded by high density C phase.

Here, it is noted that MePa molecule has a dipole pointing from water to hexane phase in its head group (~ 1.7 D)[8] and that in its terminal methyl group (0.4 D)[7]. These are quantitatively very close to the ones of Chol molecule, and thus, it is appropriate to use eq. $(2-21)$ to estimate τ_{el}. Then, the τ_0 and τ_{el} values calculated from eqs. $(2-21)$ and $(2-22)$ are plotted against $X_{\mathrm{Ch}}^{\mathrm{H}}$ in Figure 3-10, together with the mean radius R_{eq} determined as median in size distribution over 100 domains.

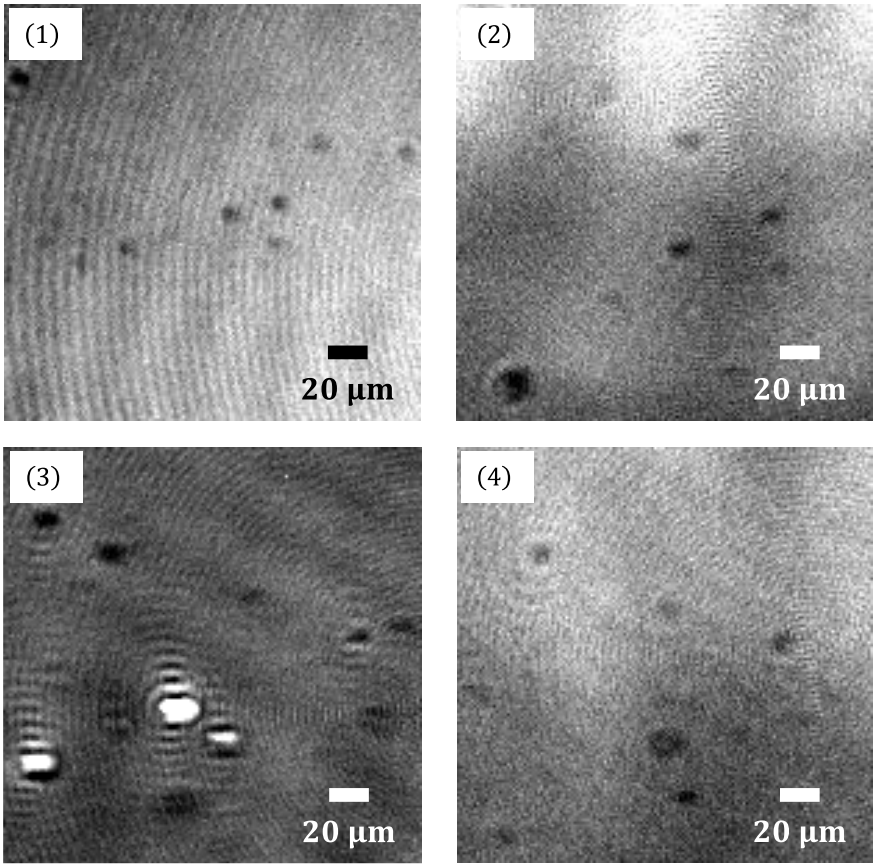

Figure 3-9. The BAM images of the adsorbed films observed at (1) $(m, X_{\mathrm{Ch}}) = (5.0, 0.21)$, (2) $(2.4, 0.40)$, (3) $(2.0, 0.61)$, and (4) at $(1.5, 0.79)$.

Table 3-3. The List of result of BAM. The $\Gamma^{\mathrm{H}}_{i,\mathrm{BAM}}$ value was calculated using $C_{\mathrm{BAM}} = 0.8{\sim}0.9$ from eq. (2-23).

X_{Ch}	$\frac{m}{\mathrm{mmol\ kg^{-1}}}$	Surrounding C domain	Dispersed α domain	Γ^{H}_{i} / μmol m^{-2}	$\Gamma^{\mathrm{H}}_{i,\mathrm{BAM}}$ / μmol m^{-2}
0.21	5.0	$\Gamma^{\mathrm{H}} = 4.3 \pm 0.1$	$\Gamma^{\mathrm{H}} = 1.4 \pm 0.1$	$\Gamma^{\mathrm{H}}_{\mathrm{Pa}} = 0.59 \pm 0.05$ $\Gamma^{\mathrm{H}}_{\mathrm{Ch}} = 3.32 \pm 0.26$	$\Gamma^{\mathrm{H}}_{\mathrm{Pa}} = 0.58 \pm 0.02$ $\Gamma^{\mathrm{H}}_{\mathrm{Ch}} = 3.29 \pm 0.12$
0.40	2.4	$\Gamma^{\mathrm{H}} = 4.3 \pm 0.1$	$\Gamma^{\mathrm{H}} = 1.5 \pm 0.1$	$\Gamma^{\mathrm{H}}_{\mathrm{Pa}} = 0.46 \pm 0.04$ $\Gamma^{\mathrm{H}}_{\mathrm{Ch}} = 3.34 \pm 0.26$	$\Gamma^{\mathrm{H}}_{\mathrm{Pa}} = 0.43 \pm 0.02$ $\Gamma^{\mathrm{H}}_{\mathrm{Ch}} = 3.41 \pm 0.12$
0.60	2.0	$\Gamma^{\mathrm{H}} = 4.3 \pm 0.1$	$\Gamma^{\mathrm{H}} = 1.5 \pm 0.1$	$\Gamma^{\mathrm{H}}_{\mathrm{Pa}} = 0.41 \pm 0.03$ $\Gamma^{\mathrm{H}}_{\mathrm{Ch}} = 3.29 \pm 0.27$	$\Gamma^{\mathrm{H}}_{\mathrm{Pa}} = 0.43 \pm 0.02$ $\Gamma^{\mathrm{H}}_{\mathrm{Ch}} = 3.45 \pm 0.12$
0.80	1.5	$\Gamma^{\mathrm{H}} = 4.4 \pm 0.1$	$\Gamma^{\mathrm{H}} = 2.0 \pm 0.1$	$\Gamma^{\mathrm{H}}_{\mathrm{Pa}} = 0.38 \pm 0.03$ $\Gamma^{\mathrm{H}}_{\mathrm{Ch}} = 3.42 \pm 0.27$	$\Gamma^{\mathrm{H}}_{\mathrm{Pa}} = 0.40 \pm 0.01$ $\Gamma^{\mathrm{H}}_{\mathrm{Ch}} = 3.56 \pm 0.10$

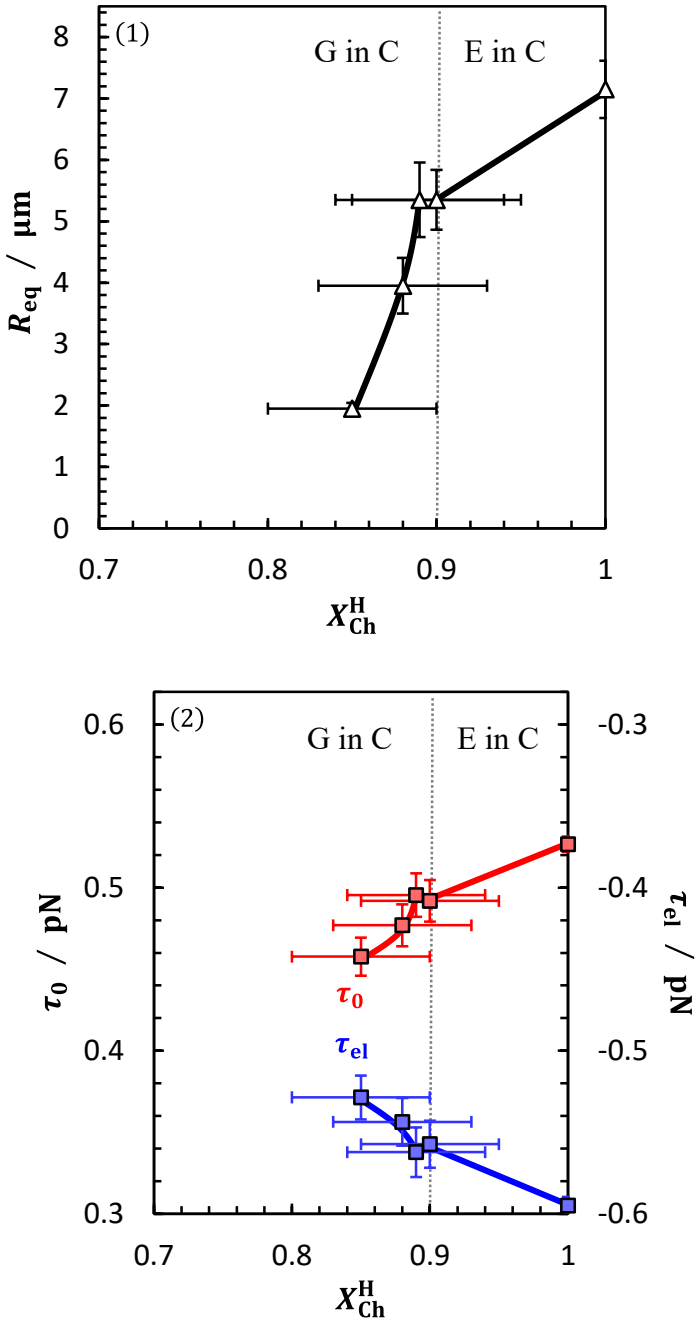

Figure 3-10. (1) The R_{eq} vs. X_{Ch}^{H} curve. (2) The τ_0 vs. X_{Ch}^{H} and τ_{el} vs. X_{Ch}^{H} curves. Below and above $X_{Ch}^{H} = 0.90$, the G and E domains are dispersed into the C phase region, respectively. This is also denoted by "E in C" and "G in C".

Now we will discuss the size of E domain surrounded by C phase. The R_{eq} value reduces from 7.2 ± 0.5 at $X_{\mathrm{Ch}}^{\mathrm{H}} = 1$ ($X_{\mathrm{Ch}} = 1$) to 5.4 ± 0.5 μm at 0.9 (0.8). The τ_0 value also decreases slightly while the τ_{el} one increases with decreasing $X_{\mathrm{Ch}}^{\mathrm{H}}$. The total interfacial density in E $\Gamma^{\mathrm{H,E}}$ and that in C phase $\Gamma^{\mathrm{H,C}}$ at $X_{\mathrm{Ch}}^{\mathrm{H}} = 0.90$ are almost equal to those at $X_{\mathrm{Ch}}^{\mathrm{H}} = 1$, respectively, suggesting that the difference of dipole density u^2 is independent of $X_{\mathrm{Ch}}^{\mathrm{H}}$. Thus, the decrease in R_{eq} is caused by the decrease in τ_0. Furthermore, taking into account that the mismatch length ΔL between hydrophobic parts of E and C films at $X_{\mathrm{Ch}}^{\mathrm{H}} = 0.9$ (~0.6 Å) is slightly smaller than that at $X_{\mathrm{Ch}}^{\mathrm{H}} = 1$ (~1.0 Å) (see Tables 3-1 and 2-1), the decrease in τ_0 value is probably due to the decrease in ΔL associated with mixing of MePa and Chol molecules at the interface.

The R_{eq} value of G domain changes from 5.4 ± 0.6 at $X_{\mathrm{Ch}}^{\mathrm{H}}$~0.89 ($X_{\mathrm{Ch}} = 0.61$) to 2.0 ± 0.1 μm at 0.85 ($X_{\mathrm{Ch}} = 0.21$), accompanying by the decrease in τ_0 and increase in τ_{el}. In this case, u^2 is an invariant within measured X_{Ch} region because both $\Gamma^{\mathrm{H,E}}$ and $\Gamma^{\mathrm{H,C}}$ do not change largely with $X_{\mathrm{Ch}}^{\mathrm{H}}$. Furthermore, the ΔL between hydrophobic parts of G and C films at $X_{\mathrm{Ch}}^{\mathrm{H}} = 0.88$ ($X_{\mathrm{Ch}} = 0.40$) is almost equal to that at $X_{\mathrm{Ch}}^{\mathrm{H}} = 0.9$ ($X_{\mathrm{Ch}} = 0.9$). Thus, the decrease in τ_0 at the G/C domain boundary seems to be related to the decrease in γ^{DS}.

Our experimental data suggest that the formation of hydrogen bonding is highly expected between hydrophilic groups of MePa and Chol molecules, and that the mixing of these molecules in the adsorbed film induces a loss of effective packing due to the difference in molecular structure, *i.e.*, cpp of the molecules. Thus, one of the possible explanations for reduction in τ_0 is a line adsorption of MePa at the G (or E)/C domain boundary, and reduce γ^{DS} by replacing the C domain/hexane contact by the hydrocarbon

chain of MePa/hexane one, such as a surfactant adsorbs at an interface, reducing the interfacial tension[3,18–21].

3-4. *Conclusions*

In this study, the molecular miscibility and domain formation was additionally examined in the adsorbed film of MePa and Chol mixture at the C6/W interface by interfacial tensiometry, XR, and BAM. The results are summarized as follows;

(i) Above $X_{\mathrm{Ch}} = 0.79$, the adsorbed film exhibited the phase transition from gaseous (G) to condensed (C) via expanded (E) states, and below this X_{Ch}, only G – C phase transition was recognized. In all states, the films were rich in Chol ($\mathrm{X}_{\mathrm{Ch}}^{\mathrm{H}} > 0.7$).

(ii) In the G film, Chol molecule took tilt orientation. In the E film, it became vertical to the interface whereas MePa one was in liquid state. In the C film, Chol and liquid-ordered MePa were densely packed with each other.

(iii) Just above the G (or E) – C phase transition point, the G or E domain formation in the C film was confirmed by both XR and BAM. The consistence of interfacial density calculated by each method suggested that the G or E domain was identical to the film just below the corresponding transition point and C one to the saturated C film, and that both coexisting domains were very rich in Chol molecules.

(iv) The R_{eq} of hole G or E domain reduced with decreasing X_{Ch}. Since the total interfacial density of each domain did not change largely with changing in X_{Ch}, u^2 was almost independent of X_{Ch} in this system. Thus, the decrease in R_{eq} was due to the decrease in $\tau_0 (= \Delta L \times \gamma^{\mathrm{DS}})$. Electron density profile of each film demonstrated the next relation;

$$\Delta L \text{ between E/C domains at } X_{\mathrm{Ch}} = 1 \ (X_{\mathrm{Ch}}^{\mathrm{H}} = 1)$$

$$> \Delta L \text{ between E/C domains at } X_{\mathrm{Ch}} = 0.9 \ (X_{\mathrm{Ch}}^{\mathrm{H}} = 0.9)$$

$$= \Delta L \text{ between G/C domains at } X_{\mathrm{Ch}} = 0.4 \ (X_{\mathrm{Ch}}^{\mathrm{H}} = 0.88)$$

Thus, the decrease in τ_0 of the E domain is probably due to the decrease in ΔL associated with mixing of MePa and Chol molecules at the interface, whereas the decrease in τ_0 of the G one is caused by the decrease in γ^{DS}. Considering that the hydrogen bonding between hydrophilic parts of MePa and Chol molecules attracts one another and the ineffective packing between their hydrophobic parts prevents from densely packing with each other, as indicated by $f_{\mathrm{Ch}}^{\mathrm{H,C}}$, MePa molecule was expected to adsorb at the domain boundary and to reduce γ^{DS} by replacing the C/hexane contact by hydrocarbon chain of MePa/hexane one.

3-5. ***References***

[1] M.C. Heinrich, I. Levental, H. Gelman, P.A. Janmey, T. Baumgart, *J. Phys. Chem. B*, 112, **2008**, 8063–8068.

[2] B.L. Stottrup, A.M. Heussler, T.A. Bibelnieks, *J. Phys. Chem. B*, **2007**, 11091–11094.

[3] A.A. Bischof, A. Mangiarotti, N. Wilke, *Soft Matter*, 11, **2015**, 2147–2156.

[4] D.W. Lee, Y. Min, P. Dhar, A. Ramachandran, J.N. Israelachvili, J. a Zasadzinski, *Proc. Natl. Acad. Sci. U. S. A.*, 108, **2011**, 9425–9430.

[5] S. Haldar, R.K. Kanaparthi, A. Samanta, A. Chattopadhyay, *Biophys. J.*, 102, **2012**, 1561–1569.

[6] Chem Bio3D Pro, Parkin Elmer Inc., Ver. 16.0.14.

[7] J.N. Israelachvili, Intermolecular and Surface Forces, 3rd ed., Academic Press, **2011**.

[8] E. Saiz, J.P. Hummel, P.J. Flory, M. Plavšić, *J. Phys. Chem.*, 85, **1981**, 3211–3215.

[9] J. Hénin, C. Chipot, *Chem. Phys. Lett.*, 425, **2006**, 329–335.

[10] J. Zidar, F. Merzel, M. Hodošček, K. Rebolj, K. Sepčić, P. Maček, D. Janežič, *J. Phys. Chem. B*, 113, **2009**, 15795–15802.

[11] J.P. Slotte, *Biochim. Biophys. Acta - Biomembr.*, 1858, **2016**, 304–310.

[12] N. Borochov, E.J. Wachtel, D. Bach, *Chem. Phys. Lipids*, 76, **1995**, 85–92.

[13] H. Sakamoto, A. Murao, Y. Hayami, *J. Inst. Image Inf. Telev. Eng.*, 56, **2002**, 1643–1650.

[14] M. Aratono, M. Villeneuve, T. Takiue, N. Ikeda, H. Iyota, *J. Colloid Interface Sci.*, 200, **1998**, 161–171.

[15] K. Motomura, *J. Colloid Interface Sci.*, 64, **1978**, 348–354.

[16] T. Takiue, T. Toyomasu, N. Ikeda, M. Aratono, *J. Phys. Chem. B*, 103, **1999**, 6547–6553.

[17] G. Weidemann, G. Brezesinski, D. Vollhardt, F. Bringezu, K. de Meijere, H. Möhwald, *J. Phys. Chem. B*, 102, **1998**, 148–153.

[18] K. Mitani, Y. Imai, T. Ina, K. Nitta, H. Tanida, T. Uruga, H. Matsubara, M. Aratono, T. Takiue, *J. Phys. Chem. B*, 119, **2015**, 12436–12445.

[19] T.R. Galimzyanov, A.S. Lyushnyak, V. V. Aleksandrova, L.A. Shilova, I.I. Mikhalyov, I.M. Molotkovskaya, S.A. Akimov, O. V. Batishchev, *Langmuir*, 33, **2017**, 3517-3524.

[20] S. Trabelsi, S. Zhang, T.R. Lee, D.K. Schwartz, *Phys. Rev. Lett*., 100, **2008**, 2–5.

[21] I. Sriram, B. Singhana, T.R. Lee, D.K. Schwartz, *Langmuir*, 28, **2012**, 16294–16299.

Chapter 4. Line Tensions in Ternary DSPC/DOPC/Chol and bSM/DOPC/Chol Bilayers

4-1. *Introduction*

In Chapters 2 and 3, the molecular miscibility and domain formation in the mixed adsorbed films of C14PC – Chol and MePa – Chol systems on the basis of phase diagram of adsorption, electron density profile, and BAM images captured in the heterogeneous condensed film close to the expanded – condensed phase transition point. Among them the evaluation of line tension τ by McConnell's theory[1,2] is limited to the pure component system and the mixed one consisted of the mixtures whose dipoles have similar moment to each other. This limitation makes it difficult to obtain an accurate τ value unless the parameters such as dipole moment and its direction are determined precisely[3–5], and therefore the direct measurement of τ is highly necessary to verify the mutual relation between the molecular miscibility inside and outside of domains and the domain formation including the morphology and distribution at interfaces.

Many researchers have devoted a lot of efforts to develop methods for τ measurement in both monolayer and bilayer. (i) Flicker spectroscopy is based on Fourier analysis on thermally fluctuating domain contour whose amplitude depends on τ[4,6–10]. (ii) Domain shape relaxation technique is based on the balance of τ and drag force during domain restores from deformed shape by perturbation to its equilibrium one[3,5,7,11]. (iii) Analyzing of domain size distribution in terms of 2-dimensional (2D) aggregate formation gives two contributions of line tension; τ_0 and τ_{el}[12]. Flicker spectroscopy has advantages to the others from the viewpoint of experimental procedure. One is that the method is applicable to measure τ in both monolayer and bilayer because this requires neither large number of domains nor the external perturbations to domains. The

other is that it can determine wide-ranged τ of the order of $0.1\sim1$ pN.

The line tension in Giant Unilamellar Vesicle (GUVs) bilayer is regarded to be essentially different with that in monolayer mainly because the molecular orientation at the domain boundary is different between them. According to the elastic theory of line tension in bilayer introduced by Kuzmin *et al.*[13], the thickness mismatch between liquid-ordered (Lo) and liquid-disordered (Ld) domains causes a hydrocarbon/water contact, giving tens of pN of line tension. To avoid this situation, however, molecules in the vicinity of domain boundary take tilt and splay conformation and alternatively cause an excess deformation energy τ_{elas} corresponding to the contact energy τ_0 in monolayer. The τ_{elas} value is supposed to be determined by thickness mismatch at the Lo/Ld boundary, mechanical properties such as bending and splay moduli of Lo and Ld domains, and spontaneous curvature[14–20]. The dipole – dipole repulsion τ_{el} in GUVs is essentially as same as that in monolayer, although the net τ_{el} value is much lower in the former than in the latter because dipoles generated in upper and lower leaflets face each other and thus should be canceled with each other[21]. Thus, the investigation on line tensions in both monolayer and bilayer systems provide useful information on the effect of line tension on domain formation and is helpful to understand the "raft" formation in biological membrane.

Thus, in this study, we tried to measure τ in GUVs of two ternary mixtures; (i) distearoyl phosphatidylcholine (DSPC)/dioleoyl phosphatidylcholine (DOPC)/Chol and (ii) brain sphingomyelin (bSM)/DOPC/Chol, by flicker spectroscopy. Fluctuating domain was recorded by fluorescence microscope (FM) and τ was determined by Fourier analysis on its contour spectrum. Then, the measured τ value was compared to that calculated by the elastic theory with the help of published structural and mechanical

parameters of Lo and Ld phases determined by small angle X-ray and neutron scatterings (SAXS and SANS)[14–20]. Furthermore, in the last section, appropriate method for the measurement of τ in the adsorbed film at the liquid/liquid interface is proposed.

4-2. *Experimental*

Materials

Chloroform and Methanol ((99.9% and 99.5% grade, Fisher Scientific) was used without further purification and water purified by Millipore Milli-Q system was used. distearoyl phosphatidylcholine (DSPC), brain sphingomyelin (bSM), and dioleoyl phosphatidylcholine (DOPC) were purchased from Avanti Polar Lipids (Alabaster, AL, USA). The concentration of stock solutions were determined to $< 1\,\%$ error by inorganic phosphate assay[22]. The purity of phospholipids was confirmed to be $> 99\,\%$ by Thin-Layer Chromatography (TLC), as shown in Figure 4-1. In this procedure, $\sim 20\ \mu l$ of lipid solution was spotted onto washed and heated unisil Silica gel plate (Analtech, Newark, DE, USA), and developed in chloroform/methanol/water mixture with $65:25:4$ (vol/vol/vol) . Cholesterol (Chol) was purchased from Nu Chek Prep (Elysian, MN, USA) and its concentration was measured by gravimetric procedures. The fluorescent dye; 1,10-didodecyl-3,3,30,30-tetramethylindocarbocyanine perchlorate (DiI) were purchased from Invitrogen (Carlsbad, CA). Both sucrose and D-glucose were purchased from VWR (Westchester, PA), and concentrations of their aqueous solutions were confirmed by an osmometer (Precision Systems Inc., Natick, MA).

GUVs Preparation

Giant Unilamellar Vesicle (GUVs) were prepared by electro-formation method[23,24]. First, thin lipid film was formed by spreading $200\ \mu l$ of chloroform solution containing 250 nmol of a lipid mixture including DiI at $0.2\ mmol\%$ onto indium tin oxide (ITO) coated glass (Delta Technologies, Stillwater, MN) which was warmed on hotplate at ~55℃, and removed solvent under vacuum for about 1 hour at ~ 40 mTorr. Then,

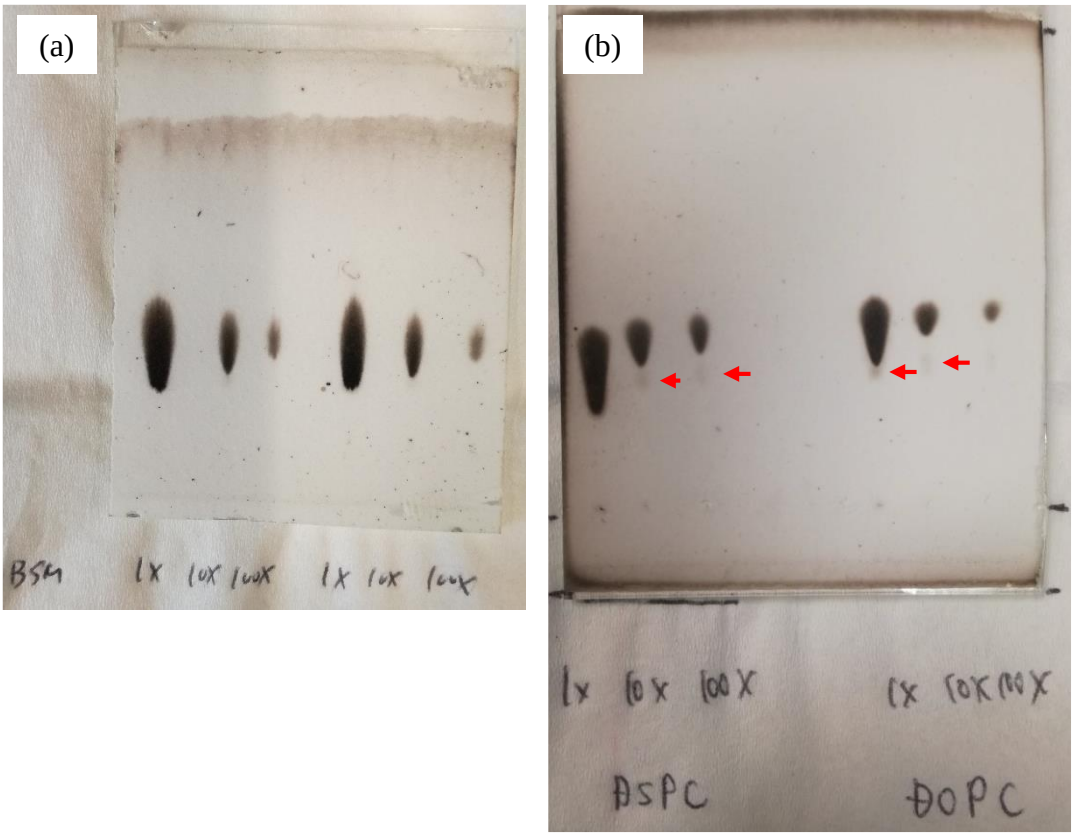

Figure 4-1. The results of TLC. The symbols "1 × ~100 ×" mean that the spotted solution is diluted 1~100 times with mixed solvent. (a) For bSM, there is no gray spot due to the existence of an impurity. (b) Both results for DSPC and DOPC exhibit very faint gray spot as indicated by arrow. However, judging from the contrast between black and gray spots, the purity of each stock solution was determined to be ＞ 99 %.

100 mM aqueous sucrose solution was filled in the space surrounded by O-ring sandwiched between two ITO glass plates, one of which was covered by lipid thin film. AC field (1 Vpp at 5 Hz) was applied to the sample for 2 hours at 55 ℃, followed by cooling to 23 ℃ over 12 hours. After that, the sample solution including lipid vesicle was pipetted into 100 mM glucose solution to settle GUVs to the bottom of a glass tube. Schematics of these procedures were shown in Figure 4-2.

Imaging of GUVs by Fluorescence Microscopy

Lo/Ld domain coexisting GUVs was observed at room temperature (20~22 ℃) by using wide-field fluorescence microscope, Eclipse Ti (Nikon Instruments, Melville, NY) equipped with 60x 1.2 NA water immersion objective and 1.5x intermediate magnifier. Domain images were recorded by using a Zyla VSC-01037 camera (Andor Technology, Belfast, UK). The pixel size of CCD camera is ~71 nm. In the image acquiring procedure, exposure time per frame was set to be 30 msec, and 500 consecutive frames were gained during 30 sec.

An isolated Lo (or Ld) domain with radius about 1.5~3 μm located on the top (or bottom) of a GUVs with radius larger than 25 μm was chosen to avoid an influence of GUV curvature on the domain size[6] and shape and to reduce the effect of inter-domain interaction on domain size[6,25]. Independence of domain radius in this range on line tension had verified by Usery *et al.*[6].

In order to obtain the image of the domain with suitable size for line tension measurement, domain size was controlled via heating and cooling procedures[6]. At a composition far from the critical point of Lo/Ld coexisting, many GUVs were completely phase separated into Lo and Ld phases like Janus particle. In this case, the vesicle solution

was heated at 45~48 ℃ for 0.5~10 min. to make GUVs have tiny domains, and then cooled to room temperature to promote domain growth. When stripe pattern domain was observed at a composition close to the critical point, the vesicle solution was also heated at 45~48 ℃ for 5~10 min. and then cooled to 0 ℃ for 5~60 sec.. These procedures were carried out several times until a suitable sized domain was observed.

Line Tension Measurement by Flicker Spectroscopy

Line tension was measured by fluid domain flicker spectroscopy developed by Esposito *et al.*[9]. First, thermally fluctuating domain boundary was extracted and the contour coordinate $R(\theta)$ was plotted against polar angle θ (Figures 4-3). Then, the $R(\theta)$ plots were decomposed into Fourier modes as below;

$$R(\theta) = R_0\left(1 + u_0 + \frac{1}{2}\sum\nolimits_{n\neq 0} u_n \exp(in\theta)\right), \qquad (4-1)$$

where $R_0 = \left(\sqrt{A/\pi}\right)$ is a radius of domain without fluctuation at area A and $|u_n|$ is Fourier coefficient of mode n. When probability of finding $|u_n|^2$ for mode n is Gaussian as shown in Figure 4-4 (a), next equation which connects line tension τ and u_n is given by

$$\langle|u_n|^2\rangle = \frac{2k_{\mathrm{B}}T}{\tau\pi R_0(n^2-1)}, \qquad (4-2)$$

where k_{B} is Boltzmann constant, T is temperature, and R_0 is average domain radius over sequent images. Thus, the τ value can be calculated by the slope of $\langle|u_n|^2\rangle$ vs. $1/(n^2-1)$ plots (Figure 4-4 (b)) or by substituting $\langle|u_n|^2\rangle$ into this equation.

Subset analysis was further performed to discard inadequate data which show the light-induced effect[26,27]. Artifacts such as dye cause irregular domain deformation, *i.e.*, fusion and abnormal fluctuation. 500 frames were divided into five sets of 100 ones,

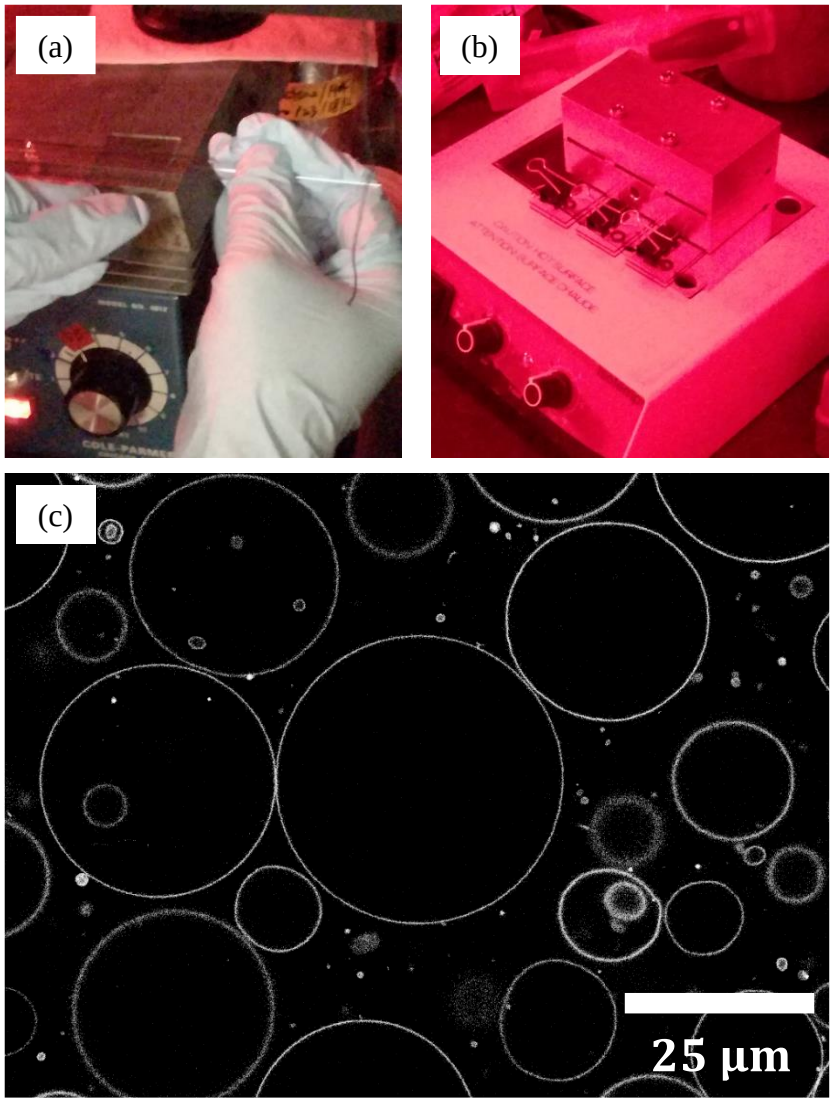

Figure 4-2. The procedure of GUVs Preparation. (a) Lipid solution was spread onto ITO glass on hotplate at ~55 ℃. (b) Setup of heating and application of AC field. The clip fastening two ITO glasses connects to AC field apparatus. (c) Typical GUVs image obtained as a result of this procedure.

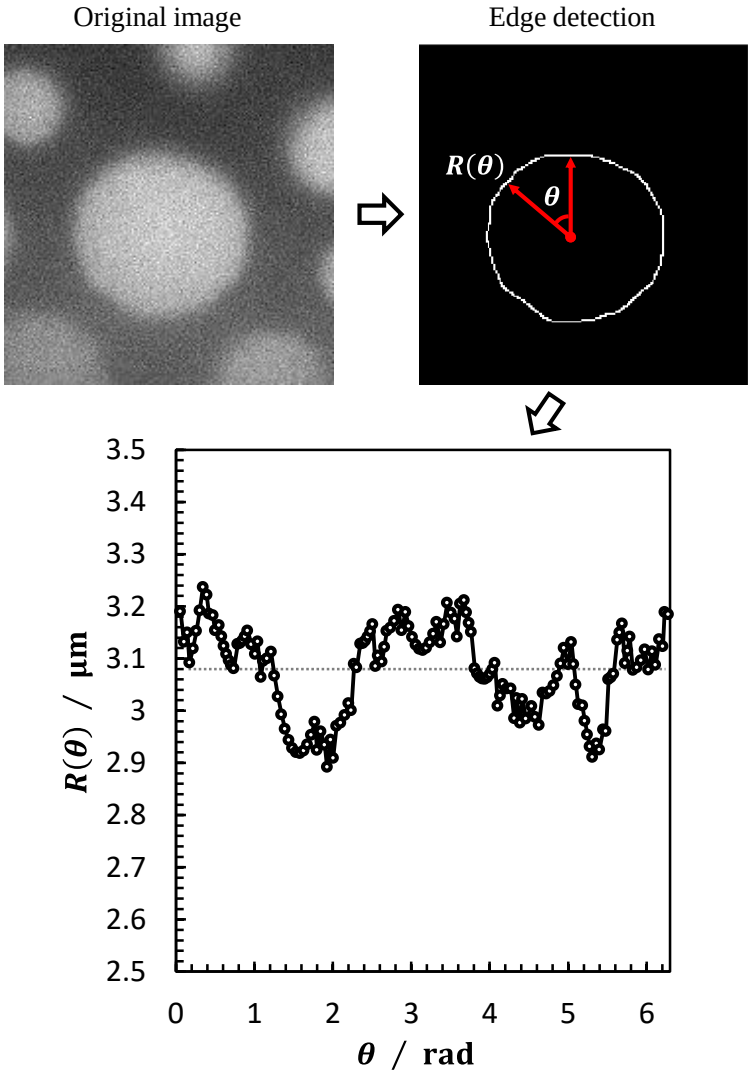

Figure 4-3. Sequent procedure of constructing contour plots. The data at DSPC/DOPC/Chol $= 0.475/0.30/0.225$ was shown here. Domain image was binarized and then domain contour are detected by Cenny's method. These image processing were performed using Matlab. The contour $R(\theta)$ plots gained by tracing an edge. Dotted line at $R(\theta) = 3.08$ μm indicates average R value over $\theta = 0{\sim}2\pi$ rad.

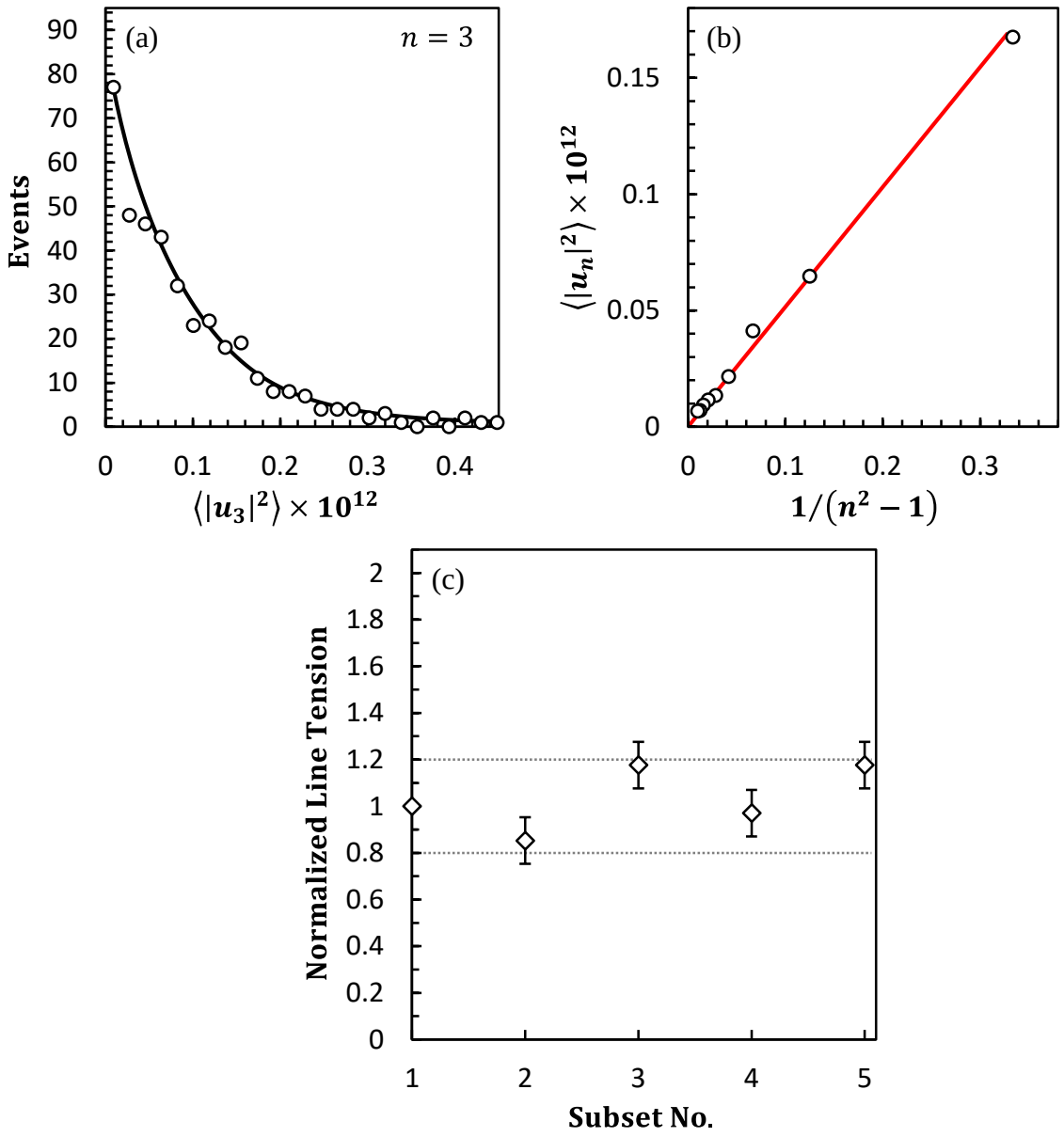

Figure 4-4. (a) Example of the event counts vs. $\langle|u_3|^2\rangle$ plots for mode $n = 3$. The plots were fitted by exponential decay. (b) The $\langle|u_3|^2\rangle$ vs. $1/(n^2-1)$ plots. The red slope drawn by least-squares method gave the τ value. (c) The subset analysis; all τ values normalized by that of the first subset are within 1 ± 0.2, indicating no or low light-induced effect on τ during a measurement.

in each of which line tension was normalized by the value of the first subset, and traced the changes with time from subset 1 to 5. Only data for which the line tension value at each subset was within 1 ± 0.2 was employed as the adequate one (Figure 4-4 (c)).

Phase Diagrams of Ternary Systems

Figure 4-5 shows the published phase diagrams of (a) DSPC/DOPC/Chol and (b) bSM/DOPC/Chol systems[18,28]. They were constructed by utilizing a signal emitted from fluorescent dye (donor) whose wavelength and intensity depend on the phase environment. The signal also correlates with the existence of another kinds of dye (acceptor) because of emission energy transfer from donor to acceptor (called FRET). When donor and acceptor dyes preferentially partition into different phases, the large distance between them reduces FRET efficiency, and when they exist into the same phase, the short distance enhances the efficiency. Thus, the phase boundary of Lo/Ld coexisting region can be characterized by tracing FRET at the lipid composition around the boundary.

In both phase diagrams, the tie line on the bottom of phase boundary (T1) is almost parallel to tangential line at critical point (blue line at stars). The others denoted by T2~T6 are also supposed to be parallel to them.

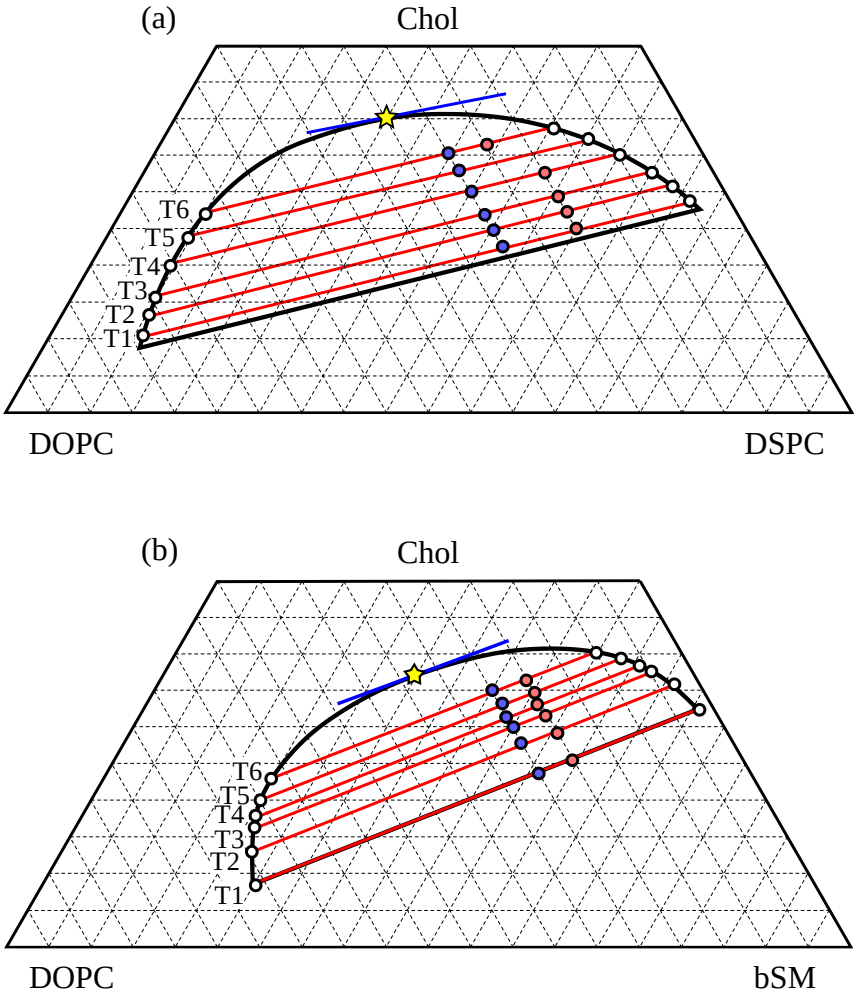

Figure 4-5. The phase diagrams of (a) DSPC/DOPC/Chol and (b) bSM/DOPC/Chol systems constructed by FRET methods[18,28]. The Star symbols indicate the critical point and the blue line is tangent. The red tie lines are denoted by T1~T6. The red and blue plots indicate the measured bilayer compositions.

4-3. ***Results and Discussion***

Figures 4-6 and 4-7 show the τ value vs. tie line No. plots for DSPC/DOPC/Chol and bSM/DOPC/Chol systems, respectively. For both systems, the τ values at different compositions on a tie line, for example blue and red dots on T1, agrees well with each other, confirming that the assumption on the tie lines mentioned above is reasonable. The value decreases with increasing tie line No., *i.e.*, as tie lines approach to critical point. When the tie line is closer to the critical point above T6, τ is less than 0.4 pN and the domains were disappeared. This agrees with the result by Usery *et al.*[6] that an abrupt decrease in domain size from microscopic to nanoscopic order occurs at about 0.3 pN, below which the dipole – dipole repulsion becomes effective to determine line tension. Thus, it is highly expected that the nanoscopic domain formation takes place in the Lo/Ld coexisting region close to the critical point.

In the elastic theory proposed by Kuzmin *et al.*[13], the line tension τ for symmetric bilayer is derived from elastic deformations of bilayer at around the domain boundary and is given by

$$\tau_{\text{elas}} = \frac{2\sqrt{B_{Lo}K_{Lo}B_{Ld}K_{Ld}}}{\sqrt{B_{Lo}K_{Lo}}+\sqrt{B_{Ld}K_{Ld}}}\frac{\Delta L^2}{L_0^2} - \frac{(J_{Lo}B_{Lo}-J_{Ld}B_{Ld})^2}{\sqrt{B_{Lo}K_{Lo}}+\sqrt{B_{Ld}K_{Ld}}}\ , \qquad (4-3)$$

where B and K are respectively bending and tilt moduli of monolayer, J is a monolayer spontaneous curvature, $\Delta L(=L_{Lo}-L_{Ld})$ is a monolayer thicknesses mismatch between Lo and Ld phases, and $L_0=(L_{Lo}+L_{Ld})/2$. First and second terms correspond to the elastic and curvature contributions, respectively. Using typical values of B, K, J, L_{Lo}, and L_{Ld}[14,15,17,29] (see table 4-1), τ values for DSPC/DOPC/Chol system were calculated and plotted by yellow triangle in Figure 4-6. The theoretical τ values are larger than the experimental ones, and thus it is required for quantitative

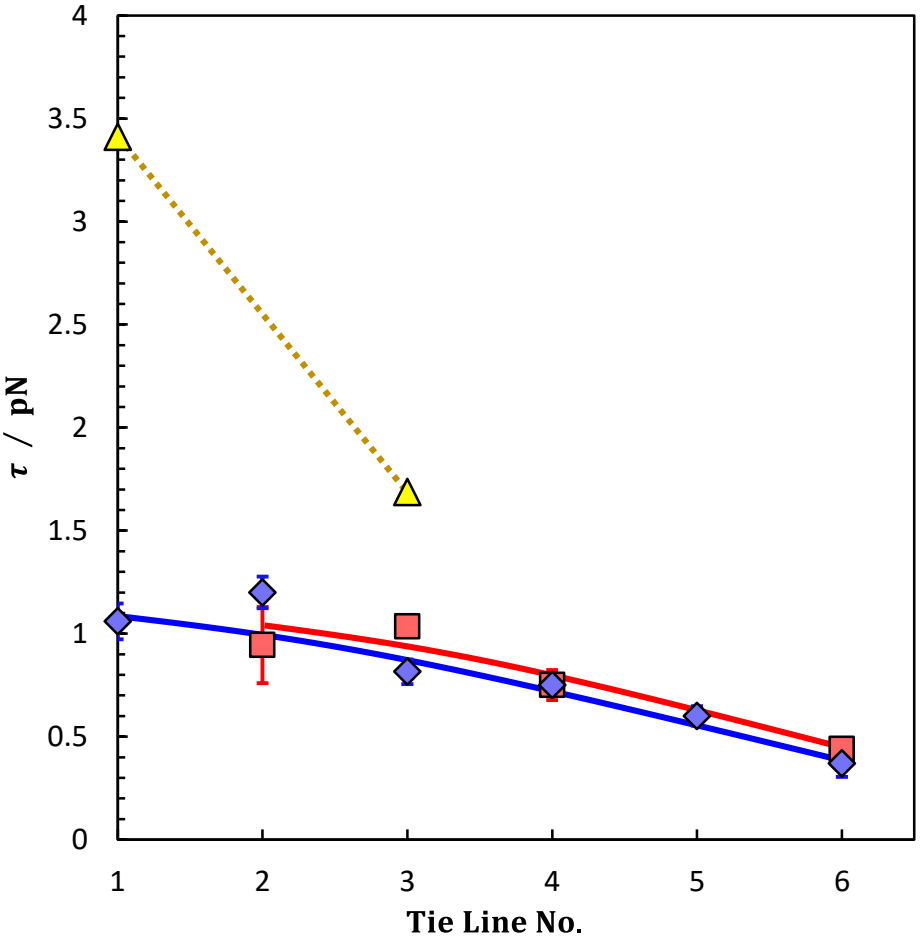

Figure 4-6. The experimental and theoretical τ values vs. tie line No. plots for DSPC/DOPC/Chol system. The red square plots were measured at fixed $X_{\mathrm{DSPC}} = 0.2$ except at $0.25/0.38/0.37$ on T6. The blue diamond ones were measured at fixed $X_{\mathrm{DSPC}} = 0.3$. The yellow triangle ones are calculated based on elastic theory.

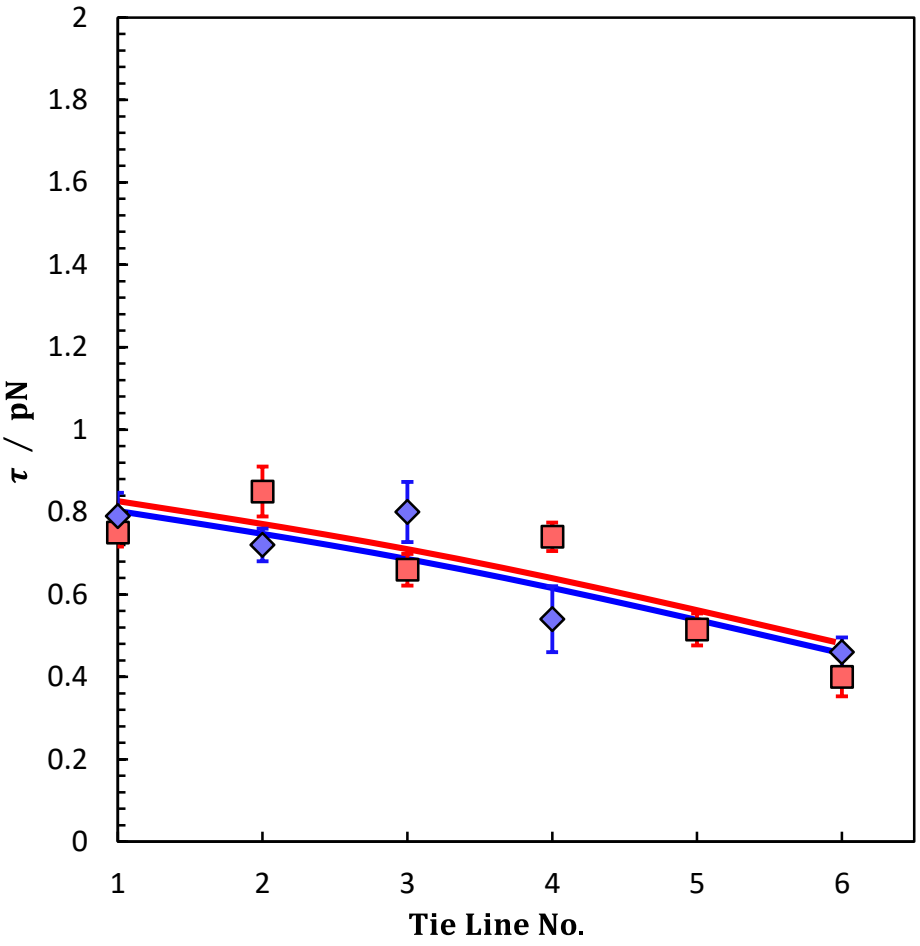

Figure 4-5-2. The experimental and theoretical τ values vs. tie line No. plots for bSM/DOPC/Chol system. The red square and blue triangle plots were measured at fixed $X_{\mathrm{bSM}} = 0.2$ and at fixed $X_{\mathrm{bSM}} = 0.25$.

discussion on the origin of τ as well as the dependence of τ on lipid molecular structure to improve on theory[29] and to acquire more accurate reference values for the calculation[15–17,30–32]. The dependence of J on monolayer composition has been proposed as $J = \sum_i X_{i,\alpha} J_{i0}$ [29], where J_{i0} is a spontaneous curvature of monolayer composed of component i in α state[17]. Furthermore, the decrease in ΔL as bilayer composition becomes closer to critical point has also quantified by using small angle X-ray scattering (SAXS) by Heftberger *et al.*[14]. In this study, both results were took into account for the calculation of τ. The values of the first and second terms are listed in Table 4-1. The results suggest that the ΔL is more dominant factor for the determination of τ than J and that the reduction of ΔL relates to the decrease in the τ value; our experiment is consistent with this calculation.

It is further noted that the τ value is larger for DSPC/DOPC/Chol than for bSM/DOPC/Chol system. The hydrocarbon chain of DSPC is longer than that of bSM by one carbon atom[34]; this difference ($\sim$2.5 Å) results in $\sim$4 pN of $\Delta\tau$. Thus, it is possible that the difference in τ is interpreted as subtle structural difference. Moreover, a similar result was obtained for dipalmitoyl phosphatidylcholine (DPPC)- and palmitoyl sphingomyelin (pSM)- containing vesicle by Kanda and Ueda of our group (data not shown). Taking note of that DPPC molecule is larger than pSM one, the thickness mismatch should affect appreciably the line tension as a predominant factor.

Table 4-1. The structural and compositional information on Lo and Ld phases. X_i; lipid composition of a domain[18], h; domain thickness[14], B and K; bending and tilt modulus[15], and J; spontaneous curvature of monolayer with Lo or Ld state calculated using $J_{\mathrm{DSPC}} = -0.01$, $J_{\mathrm{DOPC}} = -0.008$, and $J_{\mathrm{Chol}} = -0.044$ Å^{-1}[17,29]. The 1st and 2nd terms of eq. $(4-3)$ are also listed.

Tie line No.	Phase	X_{DSPC}	X_{DOPC}	X_{Chol}	h / Å	B/kT	K/kT Å^{-2}	J / Å^{-1}	1st term / pN	2nd term / pN
T1	Lo	0.67	0.05	0.28	24.9	50	0.9	−0.019	6.57	−3.16
	Ld	0.11	0.78	0.11	19.3	15	0.15	−0.012		
T4	Lo	0.55	0.1	0.35	24.6	50	0.9	−0.022	5.24	−3.71
	Ld	0.09	0.71	0.2	19.6	15	0.15	−0.015		

4-4. *Perspective*

Finally, let us consider the determination of line tension τ in adsorbed monolayer at the liquid/liquid interface such as those shown in Chapters 2 and 3. Flicker spectroscopy has already been performed to measure τ in Langmuir monolayer of lipid – Chol mixture at A/W surface by observing domain fluctuation by FM[4,10]. Considering that a domain lateral diffusion mainly caused by an interfacial convection occurs in both adsorbed and Langmuir monolayers, a domain fluctuation can be captured even in the adsorbed film at the liquid/liquid interface in principle. However, it is difficult to detect a domain contour with higher resolution than now because oil and aqueous solutions are enclosed with the cell large enough to evade meniscus and this restrains us from not only using higher power objective lens but also using FM. As suggested from eq. $(4-2)$ in addition to the result in this study, 100x objective lens is required in order to estimate τ on the order of 0.1 pN from tiny fluctuation by BAM. Thus, flicker spectroscopy does not seem to be applicable for determination of τ in the adsorbed film at the liquid/liquid interface.

For domain shape relaxation technique[3,11,33], τ can be estimated by measuring a speed of domain relaxation from deformed back to original equilibrium shape, since line tension working as restoring force is resisting the drag force during its speed is constant. An application of electric field to domain enables us to deform a domain existing on the liquid/liquid interface without any physical contacts. On the other hand, deformation of domain requires large domain or a large coverage. In Chapters 2 and 3, the coverage of dilute domain was found to be $0.05\sim0.2$. Thus, for applying this technique to the adsorbed monolayer adopted here, it is necessary to find a better condition where total interfacial density is lower and the coverage is larger than our results.

In the theory proposed by Lee *et al.*[12], a domain is regarded as 2D aggregate. Then, domain size distribution is fitted by distribution function for line tension and entropy, resulting in τ_0 and τ_{el} as fitting parameters. Only requirement for using this analysis is a large number of domains, suggesting that this can determine not only τ in the adsorbed monolayer in the O/W interface but also a wide-range τ value. However, note that τ_{el} is deal as well as the line tension theory proposed by McConell[2], *i.e.*, domain is assumed to be single-component system, and the net τ_{el} is gained.

4-5. *Conclusions*

In this study, for both DSPC/DOPC/Chol and bSM/DOPC/Chol systems, the contour fluctuation of domain on GUVs was observed by FM and τ was measured as a function of tie line No. cited from the published phase diagrams by flicker spectroscopy. The results and discussion are summarized as follow;

(i) First, it was confirmed that the measured τ values at different lipid compositions of GUVs on a tie line match to each other. For both DSPC- and bSM-containing systems, the τ value reduced as the GUVs composition gets closer to critical point and domain disappeared below 0.4 pN, indicating size transition of domain from microscopic to nanoscopic.

(ii) For DSPC/DOPC/Chol system, theoretical τ value was calculated by substituting the published data into the equation based on the elastic theory. Although the value was much larger than the measured one, the value also reduced as the GUVs composition gets closer to critical point. This indicates that a line tension is affected by molecular orientation and conformation inside and outside of domains, those are dependent on molecular miscibility.

(iii) Comparing the τ values between for DSPC- and for bSM-containing systems, the former was a little larger than the letter. Considering that ΔL is predominant factor for determination of τ value in the elastic theory and that DSPC is slightly longer than bSM molecules, the difference of τ is probably due to that DSPC-rich Lo domain is thicker than bSM-rich one.

(iv) Flicker spectroscopy does not seem to be applicable to measure τ in the adsorbed film at the liquid/liquid interface, technically. The fitting analysis on domain size distribution was proposed to be applicable instead of this method.

4-6. *References*

[1] H.M. McConnell, *Annu. Rev. Phys. Chem.*, 42, **1991**, 171–195.

[2] H.M. McConnell, V.T. Moy, *J. Phys. Chem.*, 92, **1988**, 4520–4525.

[3] A.A. Bischof, A. Mangiarotti, N. Wilke, *Soft Matter*, 11, **2015**, 2147–2156.

[4] M.C. Heinrich, I. Levental, H. Gelman, P.A. Janmey, T. Baumgart, *J. Phys. Chem. B*, 112, **2008**, 8063–8068.

[5] D.J. Benvegnu, H.M. McConnell, *J. Phys. Chem.*, 96, **1992**, 6820–6824.

[6] R.D. Usery, T.A. Enoki, S.P. Wickramasinghe, M.D. Weiner, W.C. Tsai, M.B. Kim, S. Wang, T.L. Torng, D.G. Ackerman, F.A. Heberle, J. Katsaras, G.W. Feigenson, *Biophys. J.*, 112, **2017**, 1431–1443.

[7] I. Sriram, D.K. Schwartz, *Surf. Sci. Rep.*, 67, **2012**, 143–159.

[8] S.L. Keller, A.R. Honerkamp-Smith, P. Cicuta, M.D. Collins, S.L. Veatch, M. den Nijs, M. Schick, *Biophys. J.*, 95, **2008**, 236–246.

[9] C. Esposito, A. Tian, S. Melamed, C. Johnson, S.Y. Tee, T. Baumgart, *Biophys. J.*, 93, **2007**, 3169–3181.

[10] B.L. Stottrup, A.M. Heussler, T.A. Bibelnieks, *J. Phys. Chem. B*, **2007**, 11091–11094.

[11] J.C. Alexander, A.J. Bernoff, E.K. Mann, J.A. Mann, J.R. Wintersmith, L. Zou, *J. Fluid Mech.*, 571, **2007**, 191–219.

[12] D.W. Lee, Y. Min, P. Dhar, A. Ramachandran, J.N. Israelachvili, J. a Zasadzinski, *Proc. Natl. Acad. Sci. U. S. A.*, 108, **2011**, 9425–9430.

[13] P.I. Kuzmin, S.A. Akimov, Y.A. Chizmadzhev, J. Zimmerberg, F.S. Cohen, *Biophys. J.*, 88, **2005**, 1120–1133.

[14] P. Heftberger, B. Kollmitzer, A.A. Rieder, H. Amenitsch, G. Pabst, *Biophys. J.*,

108, **2015**, 854–862.

[15] G. Khelashvili, B. Kollmitzer, P. Heftberger, G. Pabst, D. Harries, *J. Chem. Theory Comput.*, 9, **2013**, 3866–3871.

[16] F.A. Heberle, R.S. Petruzielo, J. Pan, P. Drazba, N. Kuc, *J. Am. Chem. Soc.*, 135, **2013**, 6853–6859.

[17] B. Kollmitzer, P. Heftberger, M. Rappolt, G. Pabst, *Soft Matter*, 9, **2013**, 10877–10884.

[18] T.M. Konyakhina, J. Wu, J.D. Mastroianni, F.A. Heberle, G.W. Feigenson, *Biochim. Biophys. Acta - Biomembr.*, 1828, **2013**, 2204–2214.

[19] A.C. Brown, S.P. Wrenn, *Langmuir*, 29, **2013**, 9832–9840.

[20] W. Helfrich, *Z. Naturforsch*, 28c, **1973**, 693–703.

[21] A. Travesset, *J. Chem. Phys.*, 125, **2006**, 084905.

[22] P.B. Kingsley, G.W. Feigenson, *Chem. Phys. Lipids*, 24, **1979**, 135–147.

[23] R. Shirakashi, K. Taniguchi, 日本機械学会論文集, 73, **2007**, 387.

[24] M. Angelova, S. Soleau, P. Meleard, *Trends Colloid Interface Sci. VI*, 89, **1992**, 127–131.

[25] E. Rufeil-Fiori, N. Wilke, A.J. Banchio, *Soft Matter*, 12, **2016**, 4769–4777.

[26] A.G. Ayuyan, F.S. Cohen, *Biophys. J.*, 91, **2006**, 2172–2183.

[27] N.F. Morales-Penningston, J. Wu, E.R. Farkas, S.L. Goh, T.M. Konyakhina, J.Y. Zheng, W.W. Webb, G.W. Feigenson, *Biochim. Biophys. Acta - Biomembr*., 1798, **2010**, 1324–1332.

[28] R.S. Petruzielo, F.A. Heberle, P. Drazba, J. Katsaras, G.W. Feigenson, *Biochim. Biophys. Acta - Biomembr.*, 1828, **2013**, 1302–1313.

[29] T.R. Galimzyanov, A.S. Lyushnyak, V.V. Aleksandrova, L.A. Shilova, I.I.

Mikhalyov, I.M. Molotkovskaya, S.A. Akimov, O. V. Batishchev, *Langmuir*, 33, **2017**, 3517-3524.

[30] R.M. Venable, A.J. Sodt, B. Rogaski, H. Rui, E. Hatcher, A.D. MacKerell, R.W. Pastor, J.B. Klauda, *Biophys. J.*, 107, **2014**, 134–145.

[31] J.V. Bleecker, P.A. Cox, R.N. Foster, J.P. Litz, M.C. Blosser, D.G. Castner, S.L. Keller, *J. Phys. Chem. B*, 120, **2016**, 2761–2770.

[32] J.V. Bleecker, P.A. Cox, S.L. Keller, *Biophys. J.*, 110, **2016**, 2305–2308.

[33] A.A. Bischof, N. Wilke, *Chem. Phys. Lipids*, 165, **2012**, 737–744.

[34] B. Terova, J.P. Slotte, T.K.M. Nyholm, *Biochim. Biophys. Acta - Biomembr.*, 1667, **2004**, 182-189.

Acknowledgements

I would like to express my greatest thanks to Professor Takanori Takiue for his kind and strict teaching throughout this study. He always gives first priority to let me mature as a person and as a scientist. I believe that I inherit his passionate and uncompromising attitudes toward science from him. Assistant Prof. Yosuke Imai has provided me wonderful time to discuss not only on my research but also basic and advanced subject of physical chemistry since he was Ph. D student. This time is one of what I love the most.

I also appreciate to Prof. Makoto Aratono, Prof. Michio Yamanaka, and associate Prof. Hiroki Matsubara for their special advices. Their rigorous and cutting edge opinions always let me notice new possibility for developing my research. In the experiment of X-ray reflectometry at SPring-8, Dr. Hajime Taninda, Kiyofumi Nitta, Toshiaki Ina, and Tomoya Uruga have paid a lot of efforts. We definitely cannot gain the cutting-edge results of XR at liquid/liquid interface without their technical supports. The study in Chapter 4 was worked in Laboratory of Prof. G. W. Feigenson of Cornell University (Ithaca, NY). He and his students took care of everything about me inside and outside of laboratory, and gave me very precise experience that changes me. Mr. Nobuaki Obayashi, Ryushi Fukuhara, Kenta Mitani, and my colleagues have given me special time and encouraged me. I am very glad and proud of being work with them.

This work was supported by the Research Fellow of Japan Society for the Promotion of Science (No. 17J09223). The experiment described in Chapter. 4 was performed at Cornell University with Pro. G. W. Feigenson. The X-ray reflectometry was carried out under the approval of the Japan Synchrotron Research institute (No. 2015A1519, 2016A1112, 2016B1383, 2017A1221, 2018A1250, and 2018B1421)